



# Antiprotozoal activity of compounds isolated from the root bark of *Ziziphus jujuba*

O. Sevik<sup>1</sup>, E. Hausmann<sup>1</sup>, S. Cretton<sup>1</sup>, M. Kaiser<sup>2</sup>, P. Christen<sup>1</sup>, M. Cuendet<sup>1</sup>

<sup>1</sup>School of Pharmaceutical Sciences, University of Geneva, Geneva, Switzerland

<sup>2</sup>Swiss Tropical and Public Health Institute, Basel, Switzerland

## INTRODUCTION

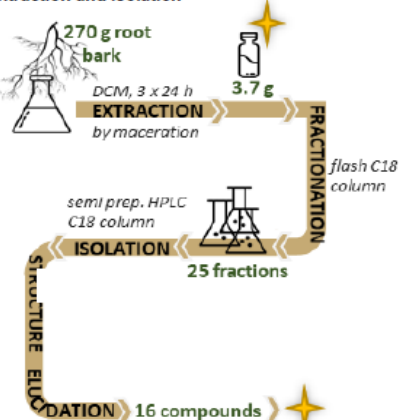
Human protozoal diseases such as malaria, sleeping sickness, Chagas disease and leishmaniasis remain important health problems, with significant morbidity and mortality, particularly in tropical countries. According to the WHO, approximately 80% of the African population uses traditional medicine for their health care.<sup>1</sup> *Ziziphus jujuba* Mill., commonly known as jujube, is traditionally used against diarrhea, ulcers, vomiting, indigestion, pulmonary ailments, dysentery and fever.<sup>2,3</sup>

## AIMS

As part of our ongoing research on the discovery of new antiprotozoal agents from West African plants, the dichloromethane extract of *Ziziphus jujuba* root bark was investigated.

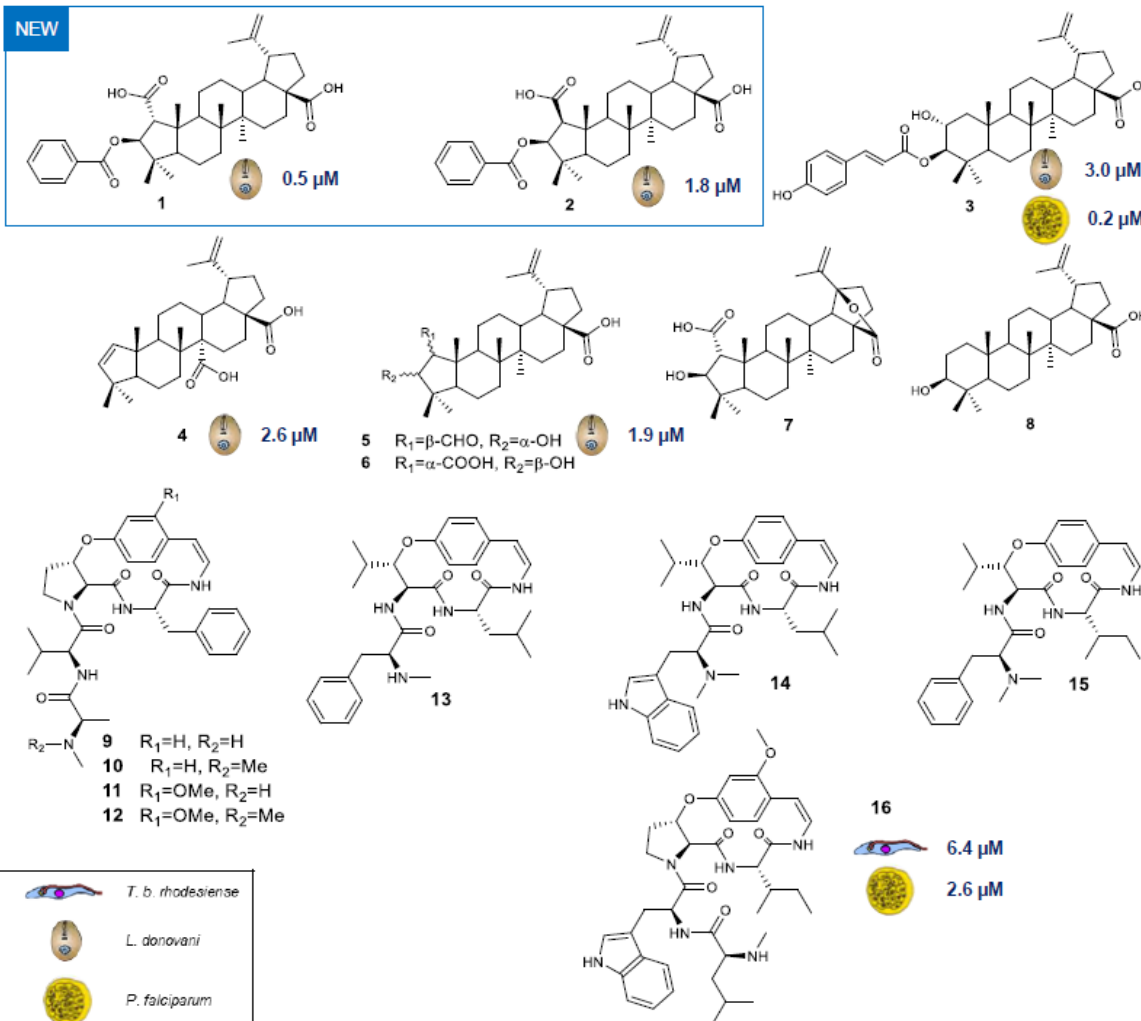
## METHODS

### Extraction and isolation



## RESULTS

NEW



## DISCUSSION & CONCLUSIONS

In a screening of Niger plants for antiprotozoal activity, the dichloromethane extract of *Z. jujuba* root bark exhibited inhibitory activities against *Trypanosoma cruzi* ( $\text{IC}_{50} = 7.4 \mu\text{g/mL}$ ), *Leishmania donovani* ( $\text{IC}_{50} = 2.7 \mu\text{g/mL}$ ), *Plasmodium falciparum* ( $\text{IC}_{50} = 1.7 \mu\text{g/mL}$ ), and *Trypanosoma brucei rhodesiense* ( $\text{IC}_{50} = 10.2 \mu\text{g/mL}$ ). Based on the screening results and the ethnopharmacological uses, *Z. jujuba* was selected for further investigation.

Eight cyclopeptide alkaloids and eight triterpenes were isolated. Among these, two compounds have not yet been described in the literature (1-2). The antiprotozoal activity and cytotoxicity was determined for fifteen of the compounds (1-7, 9-16). The  $\text{IC}_{50}$  value for active compounds is indicated on the figure. Compounds with  $\text{IC}_{50} > 10 \mu\text{M}$  were considered as inactive.

Among cyclopeptide alkaloids, 16 is the most active compound with  $\text{IC}_{50}$  values in the low  $\mu\text{M}$  against *T. b. rhodesiense* and *P. falciparum*. Among triterpenes, 1, 2, 3, 4 and 5 showed inhibitory activities against *L. donovani* ( $\text{IC}_{50} < 3 \mu\text{M}$ ) and *P. falciparum* ( $\text{IC}_{50} < 0.2 \mu\text{M}$ ). 1 exhibited the most potent antileishmanial activity ( $\text{IC}_{50} = 0.5 \mu\text{M}$ ). None of the compound showed cytotoxicity against rat skeletal myoblasts cells at  $30 \mu\text{M}$ . 1 and 2 will be tested in the intracellular form of *L. donovani* (amastigotes). Active compounds should be further tested to assess their possible use as antiprotozoal drugs.

## REFERENCES

- Abdullahi, A. A., Trends and challenges of traditional medicine in Africa. *Afr J Tradit Complement Altern Med* 2011, 8, 115-23.
- Dahiru, D.; Sini, J.; John-Africa, L., Antidiarrhoeal activity of *Ziziphus mauritiana* root extract in rodents. *Afr J Biotechnol* 2006, 5, 941-5.
- Liu, S.J.; Lv, Y.P.; Tang, Z.S., et al., *Ziziphus jujuba* Mill., a plant used as medicinal food: a review of its phytochemistry, pharmacology, quality control and future research. *Phytochem Rev* 2020, 1-35.

## CONTACT INFORMATION

ozlem.sevik@unige.ch

# Phytomedicines for mental diseases and the placental barrier: an *ex vivo* study\*

D. SPIESS<sup>1,2</sup>, V. F. ABEGG<sup>2</sup>, A. CHAUVEAU<sup>2</sup>, A. TREYER<sup>2</sup>, M. REINEHR<sup>3</sup>, M. OUFIR<sup>2</sup>, E. DUONG<sup>1</sup>, O. POTTERAT<sup>1</sup>, M. HAMGURGER<sup>2</sup> and A. P. SIMÕES-WÜST<sup>1</sup>

<sup>1</sup> Department of Obstetrics, University Hospital Zurich, 8091 Zurich, Switzerland  
<sup>2</sup> Pharmaceutical Biology, Department of Pharmaceutical Sciences, University of Basel, 4056 Basel, Switzerland  
<sup>3</sup> Department of Pathology and Molecular Pathology, University Hospital Zurich, 8091 Zurich, Switzerland

FN-SNF  
SWISS NATIONAL SCIENCE FOUNDATION

USZ  
Universitäts  
Spital Zürich

University of  
Zurich

University  
of Basel

SPhSD 2021

SAPhS  
Swiss Academy of  
Pharmaceutical  
Sciences

## INTRODUCTION



Non-psychotic mental disorders (NMDs), such as sleep disorders, restlessness, anxiety and mild depression are common issues during pregnancy and the postpartum period<sup>1</sup>. A recent prevalence estimate in Switzerland reported that 16.7% of perinatal women used mental healthcare<sup>2</sup>.

Treating NMDs during pregnancy with conventional medications has several drawbacks and expectant mothers often try to reduce their consumption<sup>3</sup>. Since an untreated NMD itself should be avoided, safe herbal preparations may be a treatment option. The perception of phytomedicines as being safe in pregnancy<sup>4</sup> is somewhat in contrast to the fact that studies on the safety of phytomedicines in pregnancy are essentially lacking.

## AIMS



The main aim of this work was to characterise the transplacental transfer of humulone, a characteristic and pharmacologically active compound in hops, and protopine, a major alkaloid in California poppy. The effects of humulone and protopine on the viability of placental tissue and on the production of placental hormones were also investigated.

## METHODS

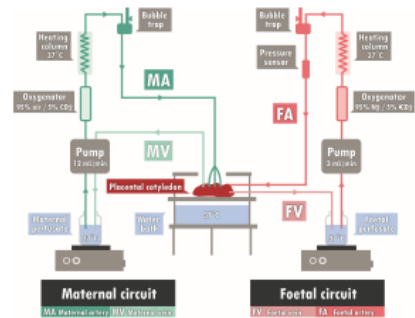


Figure 1. *Ex vivo* placental perfusion setup consisting of maternal and foetal circuit. Both perfusates are transported to the placental cotyledon (tubule) via arteries with the aid of peristaltic pumps. On the way to the placental cotyledon, the perfusates are gassed by oxygenators and freed from any air bubbles by bubble traps. Two veins return the perfusates to the corresponding reservoirs.

## RESULTS

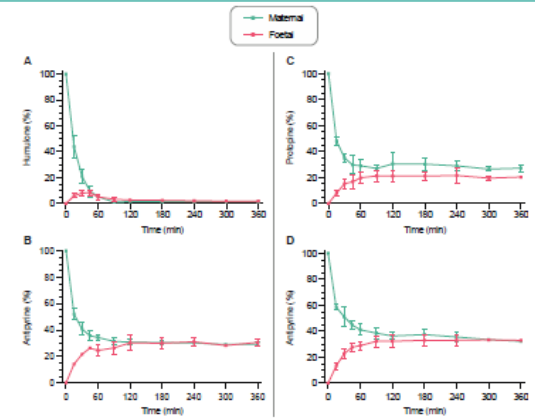


Figure 2. *Ex vivo* human placental perfusion profiles of humulone (A) and protopine (C) with corresponding connectivity control (antipyrine) transfers (B, D). Concentrations are expressed as a percentage (%) of initial analysed concentration in the maternal sample. All values are expressed as mean  $\pm$  SD of three independent experiments (except for humulone at t=300 and 360 min in which only two values are included).

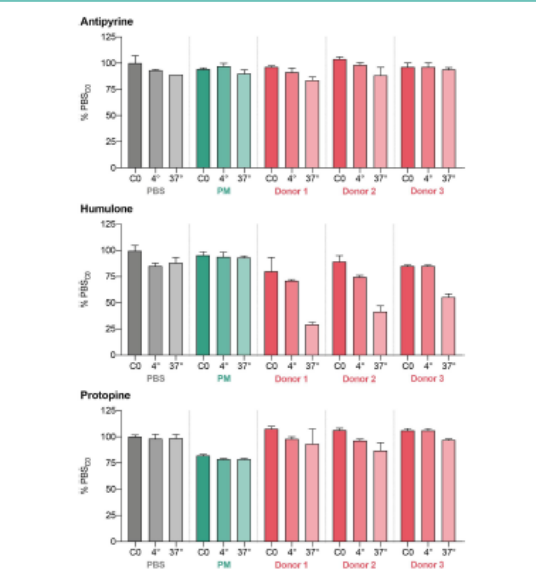
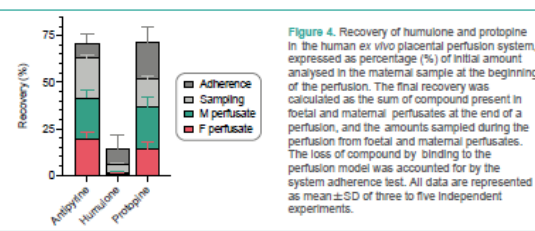
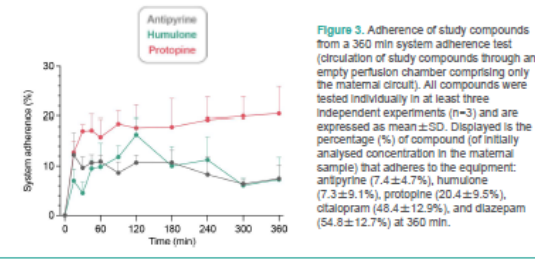


Figure 5. Stability data of antipyrine, humulone and protopine expressed as percentage (%) of the initial concentration (C0) in PBS. The stability test was performed for 360 min at two different temperatures (4°C and 37°C) and three different matrices (PBS, perfusion medium (PM), and placenta homogenates from three different donors). Samples were processed via solid phase extraction or protein precipitation prior to analysis. All data are represented as mean  $\pm$  SD.

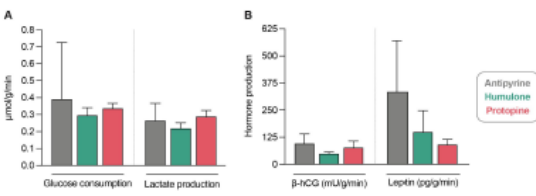


Figure 6. Assessment of tissue viability and functionality during the *ex vivo* human placental perfusion comparing the study compounds (humulone, protopine) with antipyrine from control perfusions. (A) Comparison of glucose consumption and lactate production. Displayed are the changes between beginning and end of the perfusion in foetal and maternal circuits. Normalized by the total perfusion time (min) and perfused cotyledon weight (g). (B) Comparison of beta-human chorionic gonadotropin (beta-hCG) and leptin tissue production. Displayed is the net release rate of placental hormones during the placental perfusion, normalized by the total perfusion time (min) and perfused cotyledon weight (g). All data are represented as mean  $\pm$  SD of three to five independent experiments.

## DISCUSSION & CONCLUSIONS

- Successful implementation of *ex vivo* human placental perfusion model testing phytochemicals.
- Humulone and protopine are differentially transported across placental barrier.
- Humulone concentrations rapidly decreased in the maternal circuit, but only a small portion of the compound appeared in the foetal circulation. Humulone did not significantly adsorb to the perfusion setup, nor did humulone accumulate in the membranes of the placental tissue. Moreover, the stability of humulone in presence of homogenate was much lower at 37°C compared to 4°C, indicating involvement of active processes. Our results point therefore to an active uptake into cells, and/or possible metabolism in the placenta.
- Protopine was rapidly transferred from the maternal to the foetal circuit, and no evidence for metabolism was found.
- Placental viability (glucose consumption, lactate production) and functionality (beta-hCG, leptin accumulation) were not detrimentally altered.
- For a further risk assessment of hops and California poppy additional phytochemicals in these plants have to be investigated, together with testing in additional models (e.g. *in vitro*).

The *ex vivo* placental perfusion model will now be used to measure the transplacental transport of relevant phytochemicals from other medicinal plants used for the treatment of mild NMDs in pregnancy.

## REFERENCES

<sup>1</sup> Spiess et al., *Planta Med* (accepted for publication)  
<sup>2</sup> Howard et al., *Lancet* 2014, 384: 1775-1788  
<sup>3</sup> Berger et al., *Swiss Med Wkly* 2017, 147: w14417  
<sup>4</sup> Randecker et al., *Swiss Med Wkly* (Op Ed) 2020  
<sup>5</sup> Schlicher et al., München: Urban & Fischer Verlag 2016  
<sup>6</sup> Manda et al., *Planta Med* 2016, 82: 551-558

## CONTACT INFORMATION

Deborah.Spiess@usz.ch



# Impact of *Petasites hybridus* extract Ze 339 on intestinal handling of histamine

SWISS  
PHARMA  
SCIENCE DAY  
2021



SAPhS  
Swiss Academy of  
Pharmaceutical  
Sciences

P - I - 3

L. Mettler<sup>1</sup>, K. Brecht Brüngger<sup>1</sup>, V. Butterweck<sup>2</sup>, H. Meyer zu Schwabedissen<sup>1</sup>

<sup>1</sup> Biopharmacy, Department Pharmaceutical Sciences, University of Basel, 4001 Basel, Switzerland

<sup>2</sup> Max Zeller & Söhne AG, Research and Development, Seeblickstrasse 4, 8590 Romanshorn, Switzerland



© 2021 Max Zeller Söhne AG

## INTRODUCTION

Histamine intolerance (HIT) is a common diagnosis in Western population with an estimated prevalence of 1% in a population [1]. In patients with HIT, exposure to exogenous histamine causes a broad spectrum of undesired symptoms such as rhinal congestion, dizziness, headache, tachycardia, hypotension, diarrhea, nausea, and flush. Food-derived histamine is degraded by intestinal diamine oxidase (DAO) and histamine-N-methyltransferase (HNMT), while the organic cation transporter 3 (OCT3) contributes to the transcellular flux of histamine. Anecdotal evidence suggests that intake of Ze 339 might also improve undesirable reactions of ingested histamine. In clinical studies it has been shown, that Ze 339, the lipophilic CO<sub>2</sub>-leaf extract of *Petasites hybridus* (Tesalin®), decreased histamine and leukotriene levels in nasal laryngeal fluids of patients with allergic rhinitis.

## AIM

In our current study we investigated the influence of Ze 339 on the key enzymes involved in intestinal handling of histamine, DAO, HNMT and OCT3.

## METHODS

For our studies we validated differentiated Caco-2 cells for the presence of DAO, HNMT and organic cation transporter 3 (OCT3; SLC22A3). We then investigated the effect of Ze 339 on mRNA and protein expression levels of the above-mentioned genes and proteins by real-time PCR and Western Blot analysis, respectively. We further tested the effect of Ze 339 on DAO release from Caco-2 cells polarized on permeable supports (Transwell®) and on DAO enzyme activity. We applied Caco-2 Transwell® transport studies to assess the influence of Ze 339 on the transcellular histamine flux. Findings on changes in transcellular flux were supplemented with transport studies using MDCKII cells stably overexpressing OCT3.

## RESULTS

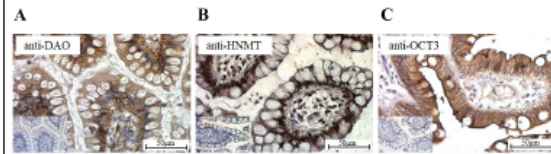


**Figure 1.** Detection of Diamine Oxidase (DAO), Histamine-N-Methyltransferase (HNMT) and the Organic Cation Transporter 3 (OCT3; SLC22A3) in intestine and differentiating Caco-2 cells. Immunohistochemical staining of DAO (A), HNMT (B), and OCT3 (C) in human ileum tissue. In controls (left corner of the respective image), the primary antibody was omitted. Bars indicate a size of 50 µm. DAO (D), HNMT (E) and OCT3 (F) mRNA expression in Caco-2 cells cultured for 7, 14 or 21 days. 18S served as endogenous control. Data are presented as mean relative mRNA expression normalized to the first time sample ± SD of three independent experiments, each performed in biological and technical replicates. (G) Detection of protein expression in Caco-2 cells harvested at the respective time points. Human adult small intestine homogenate served as control.

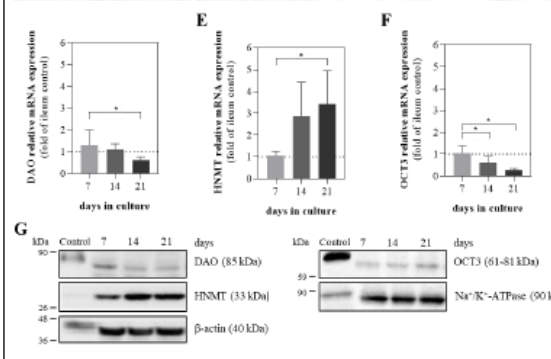


**Figure 2.** Influence of Ze 339 on mRNA and protein expression of DAO and HNMT in differentiated Caco-2 cells. Caco-2 cells, cultivated for 14 days prior to treatment, analyzed by real-time qPCR after 24 h or 48 h exposure to Ze 339 (0.1, 0.3 and 1.0 µg/mL). 18S served as endogenous control. Data are presented as mean ± SD of n=3 independent experiments, each performed in biological and technical replicates. Detection of DAO and HNMT protein expression in Caco-2 cells harvested after 24 h or 48 h treatment with histamine (150 µg/mL), heparin (10 USP U/mL), EGF (50 µg/mL) or Ze 339 (0.1, 0.3 and 1.0 µg/mL). For EGF, 10 µM and 10% fetal bovine serum albumin served as EGF control.

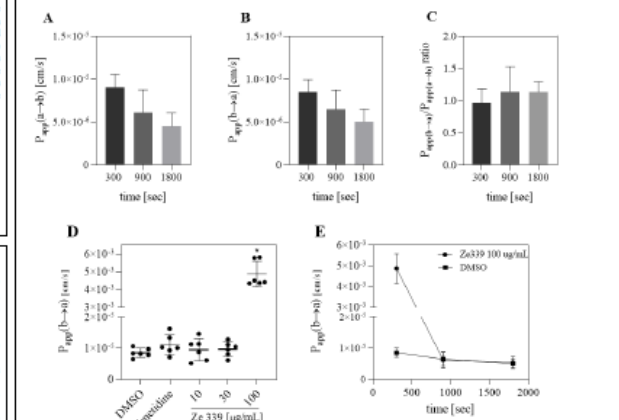
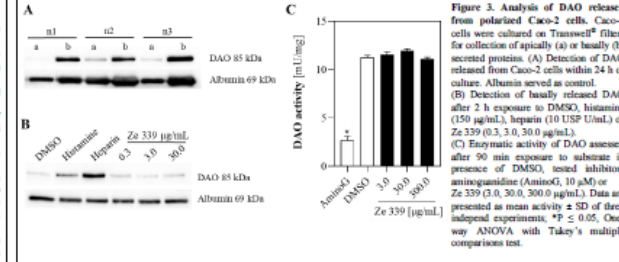
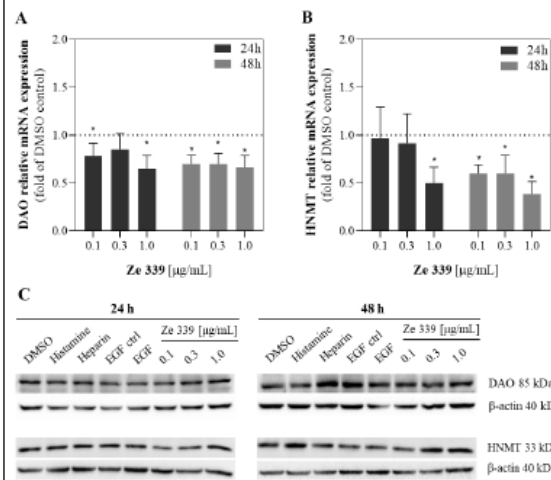
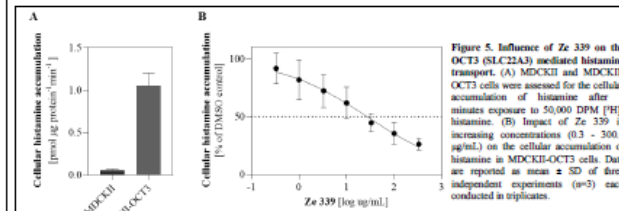


**Figure 5.** Influence of Ze 339 on the OCT3 (SLC22A3) mediated histamine transport. (A) MDCKII and MDCKII-OCT3 cells were assessed for the cellular accumulation of histamine after 2 minutes exposure to 50,000 DPM [3H]-histamine. (B) Impact of Ze 339 in increasing concentrations (0.3 - 300.0 µg/mL) on the cellular accumulation of histamine in MDCKII-OCT3 cells. Data are reported as mean ± SD of three independent experiments (n=3) each conducted in triplicates.



## DISCUSSION

Investigating the expression of DAO, HNMT and OCT3 in differentiating Caco-2 cells we observed good correlation between mRNA and protein expression levels. Whereas OCT3 and DAO showed maximal expression after 7 days followed by a steady decline, HNMT showed constant increase in expression over time. Thus, we selected 14 day of cultivation for all subsequent experiments on histamine handling. First, we tested the influence of Ze 339 on DAO and HNMT expression and observed a significant reduction in mRNA but not cellular protein content. Under basal conditions we observed a higher DAO protein content in the basolateral as compared to the apical compartment which is in line with previous reports [2]. When applying Ze 339, we observed no change in the amount of DAO protein released. Testing Ze 339 as a modifier of DAO activity did not reveal a significant effect either. Taken together, the modulatory effect of Ze 339 on DAO expression, release and activity and HNMT expression in differentiated Caco-2 cells is limited. In Caco-2 transepithelial transport experiments, we observed no active transport component for the transcellular transfer of histamine as neither the uptake nor the efflux ratio was greater than 1.5. However, in presence of high concentrations of Ze 339 we observed a high flux of histamine limited to the early phase of the experiment. From this finding, we concluded that Ze 339 might influence histamine transporters directly. Caco-2 cells express several transporters amongst others the uptake transporter OCT3 [3], which has been reported to transport monoamines such as histamine [4]. Using MDCKII cells overexpressing OCT3 we observed that Ze 339 inhibited histamine uptake in a dose-dependent manner. Therefore, Ze 339 might inhibit the apical cellular uptake leading to elevated levels of histamine detected in the apical compartment. Further research is necessary to clarify if the inhibition of OCT3-mediated histamine uptake by Ze 339 could play a role in the anecdotally reported improved symptoms of histamine intolerance in patients taking the extract.

## REFERENCES

- [1] Kovacova-Hanusova et al. 2015. Allerg. Immunopathol (Madr) 43(5)
- [2] D'Agostino, L et al. 1989. Gastroenterology 97(4)
- [3] Muller, J et al. 2005. Biochem Pharmacol 70(12)
- [4] Koepsell, H, et al 2007. Pharm Res 24(7)

## CONTACT INFORMATION

karin.brecht@unibas.ch



# Natural products targeting aberrant ERK/AKT signaling in human melanoma cell lines

L. DÜRR<sup>1</sup>, T. HELL<sup>1</sup>, G. BRADANINI<sup>1</sup>, M. DOBRZYNSKI<sup>2</sup>, A. MATTEI<sup>2</sup>, A. JOHN<sup>2</sup>, N. AUGSBURGER<sup>1</sup>, M. HAMBURGER<sup>1</sup>, O. PERTZ<sup>2</sup> and E. GARO<sup>1</sup>

<sup>1</sup> University of Basel, Division of Pharmaceutical Biology, Basel, Switzerland  
<sup>2</sup> University of Bern, Institute of Cell Biology, Bern, Switzerland

## INTRODUCTION

Targeted therapy against melanoma has been shown to generate fast clinical responses, but resistances occur quickly. Combination of inhibitors targeting enzymes in aberrant pathways already showed greater efficacy and increased median progression-free survival<sup>1</sup>. **Novel inhibitors targeting frequently aberrant proliferation signaling of the ERK and AKT pathways in melanoma are therefore urgently needed.**

To identify novel compounds, we combined our natural product (NP) lead discovery platform with an innovative high-content screening assay (HCS) that quantifies ERK/AKT signaling in melanoma cells.

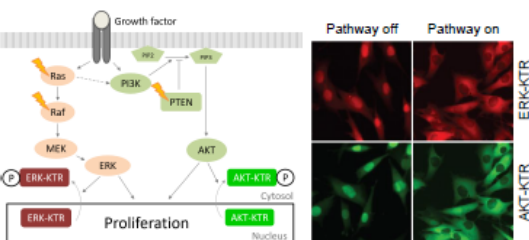
## AIMS

Finding new plant-derived AKT/ERK pathway inhibitors.

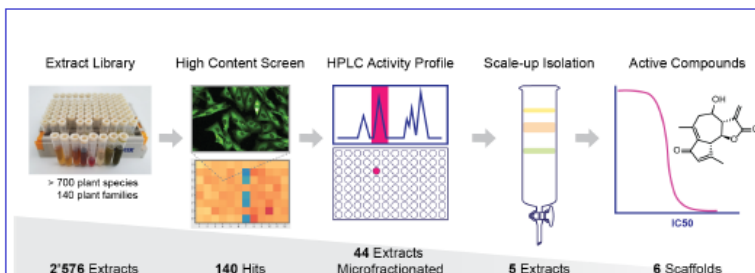
## METHODS

Kinase Translocation Reporter (KTR)-based biosensors are genetically encoded reporters which shuttle between the cytosol and nucleus upon phosphorylation<sup>2</sup>.

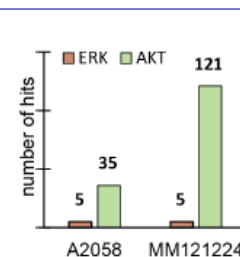
If ERK and AKT are inhibited the biosensors are located in the nucleus. Otherwise the phosphorylated biosensors are in the cytosol.



## RESULTS

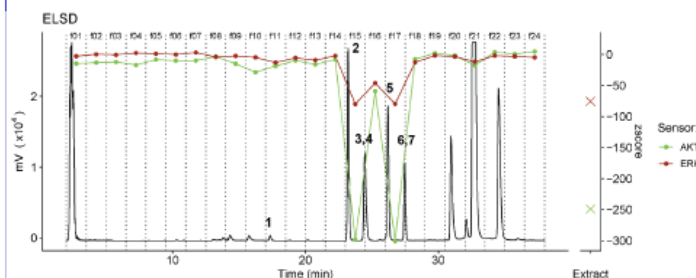


In order to screen our in-house library of 2576 extracts inhibiting AKT/ERK pathway, we developed a HCS assay, combining it with our activity profiling platform. This enabled us to efficiently dereplicate and select the most promising extracts. Scale-up of 5 extracts resulted in a structurally diverse set of compounds.



The hit rate on the AKT pathway was significantly higher than on the ERK pathway. This hit distribution indicates that the ERK pathway is more robust than the AKT pathway.

Active compounds were tracked with the help of HPLC activity profiling. The activity profile of *Arnica montana* radix PE extract is shown as an example.



600 µg of *A. montana* extract were injected on an analytical RP HPLC-MS system and fractionated with a method of 10-100% MeCN in 30 min. The HPLC-based activity profiling was obtained after testing all fractions in the HCS (AKT in green, ERK in red).

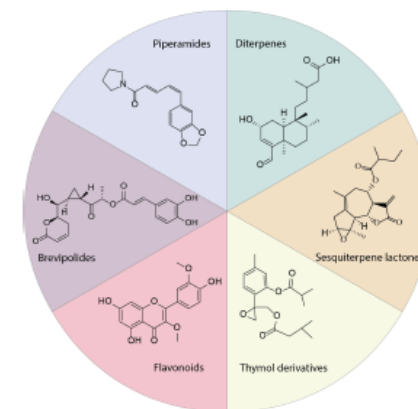
Fraction 15 and 17 display activity on both pathways.

Compound	R1	R2	R3
1	H	isobutyl	
2	isobutyl	isobutyl	
3	isobutyl	2-methylbutyl	
4	isobutyl	Isovaleryl	
5			isobutyl
6			2-methylbutyl
7			isovaleryl

Thymol derivatives were isolated with open silica gel columns, preparative and semi-preparative RP chromatography.

## DISCUSSION & CONCLUSIONS

- Establishment of a HCS with a state-of-the-art image-based bioassay, which enabled screening of our in-house extract library
- Efficient dereplication and selection of most promising extracts with the aid of HPLC activity profiles
- Discovery of a structurally diverse set of compounds



- Testing of pure compounds on-going
- Further work: target identification of active compounds

## REFERENCES

- [1] Grant A. McArthur, Front Oncol. 2015, 5:161
- [2] Maryu et al., Cell Structure and Function 2016; 41: 81–92

## CONTACT INFORMATION

Lara Dürr, Pharmaceutical Biology,  
Pharmazentrum, Universität Basel  
lara.duerr@unibas.ch







# Encapsulation of a combination of model microorganisms for fecal microbiota transplantation

A. RAKOTONIRINA<sup>1,2</sup> and E. ALLÉMAN<sup>1,2</sup>

<sup>1</sup> School of Pharmaceutical Sciences, University of Geneva, Geneva, Switzerland.

<sup>2</sup> Institute of Pharmaceutical Sciences of Western Switzerland, University of Geneva, Geneva, Switzerland



## INTRODUCTION

Research on the microbiome is expanding, and further host-microbiome interactions are continuously discovered. Recent research highlighted the correlation between the microbiome and several diseases. The methods used to modulate the microbiome are mostly probiotics, prebiotics and fecal microbiota transplantation (FMT). FMT is the administration of a filtrate of stools from a healthy donor into the gastrointestinal tract of a patient (1). Applying pharmaceutical technologies used for live bacteria formulation would help to produce a stable, standardized and efficient formulation for FMT (2,3).

## AIMS

The aim of this work is to formulate a complex mixture of microorganisms into microparticles with a high loading and without compromising the viability of the bacteria. We first developed the method using single model bacteria strains, then we combined them in a single formulation.

## CONCLUSIONS

This project successfully showed the encapsulation of single model strains and a mixture of them. Consistent particles from batch to batch were obtained in terms of appearance and mean particles size. A high-loading up to  $10^{15}$  and  $10^{17}$  CFU/g of dry product was successfully obtained for single strains and mixed strains, respectively. This corresponded to a viability of 40% and 60%, respectively, for flow cytometry. This method looks promising to achieve a high-loaded formulation of a designed mixture of microorganisms and an actual fecal mixture.

## REFERENCES

- 1) Cammarota G, Ianiro G, Tilg H, Rajlic-Stojanovic M, Kump P, Satokari R, et al. Gut. 66, 569-80 (2017).
- 2) Li S, Jiang W, Zheng C, Shao D, Liu Y, Huang S, et al. J Control Release. 327, 801-33 (2020).
- 3) Krasaekoopt W, Bhandari B, Deeth HC. LWT - Food Sci. Technol.. 39, 177-83 (2006).

## CONTACT

Mandimbimomena.Rakotonirina@unige.ch  
CMU, Rue Michel-Servet 1, 1206 Genève  
Office B08.2325.a ; Tel. +41 22 379 42 27



## RESULTS & DISCUSSION



Figure 1. Fresh particles loaded with bacteria



Figure 2. Lyophilized particles loaded with bacteria

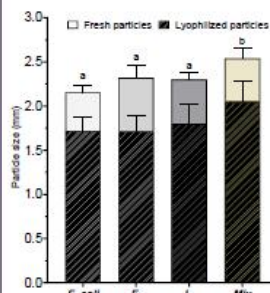


Figure 3. Particles size

The particles have the aspect of spherical and sturdy gel beads. The mean size is equivalent between all batches for each strain. There is a slight increase in size when all strains are mixed.

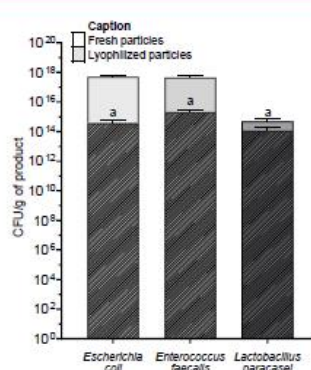


Figure 4. Viability by plate-counting of single model strains loaded in particles

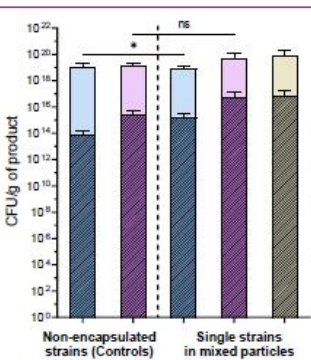


Figure 6. Viability by plate-counting of single strains loaded in mixed particles

The viability of the strains read by plate-counting is decreasing after lyophilization and it is strain-dependent. Up to  $10^{15}$  and  $10^{17}$  CFU/g of dry product were successfully obtained for single strains and mixed strains, respectively. We were successfully able to produce high-loaded particles both with single strains and a mixture of said strains.

The viability of the strains read by flow cytometry (LIVE/DEAD kit by Invitrogen™) is decreasing after lyophilization and it is strain-dependent, which confirms the results observed by plate-counting.

\*n=3±SD. Statistical analyses were performed as a two-way ANOVA followed by post-hoc analysis with Tukey's multiple comparison

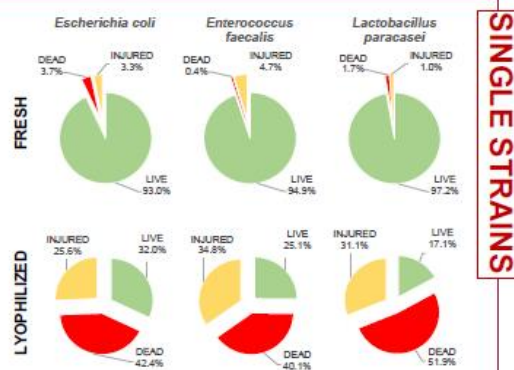


Figure 5. Viability by flow cytometry of single model strains loaded in particles

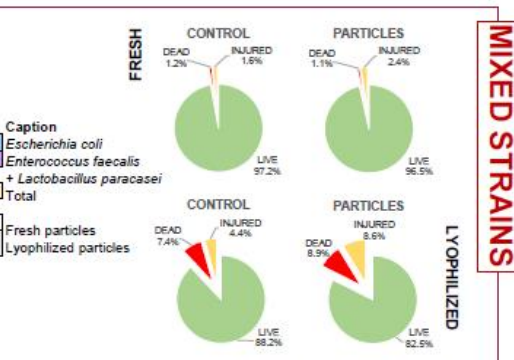


Figure 7. Viability by flow cytometry of mixed model strains loaded in particles

## METHOD

100  $\mu$ L concentrated bacteria  
900  $\mu$ L 2.5% alginate  
with 0.05% pyruvate  
and 10% trehalose

Syringe-pump  
VOL: 1 mL  
RATE: 5 mL/h

30 G needle

20 cm



0.10 M CaCl<sub>2</sub>  
solution

WASH with  
distilled water

LYOPHILIZATION

- ice condenser: -85°C
- pressure: 0.08-0.13 mBar
- time: overnight

PARTICLES  
CHARACTERIZATION

VIABILITY  
ASSESSMENT

MICROSCOPY

FLOW  
CYTOMETRY

PLATE  
COUNTING

# Drug Delivery by Amorphous Solid Dispersions: A Randomized Pharmacokinetic Study in Humans

A. SCHITTNY<sup>1,2,\*</sup>, S. WALDNER<sup>1,\*</sup>, U. DUTHALER<sup>2</sup>, A. VOROBYEV<sup>3</sup>, R. ABRAMOVICH<sup>3</sup>, S. KRÄHENBÜHL<sup>2</sup>, M. PUCHKOV<sup>1,\*</sup> and J. HUWYLER<sup>1,\*</sup>

<sup>1</sup>University of Basel, Basel, Switzerland | <sup>2</sup>University Hospital Basel and University of Basel, Basel, Switzerland | <sup>3</sup>Peoples' Friendship University of Russia (RUDN University), Moscow, Russia

\*These authors contributed equally to this work

## Aims

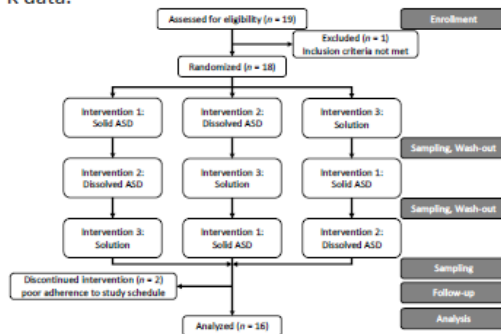
In this clinical study we aimed to investigate the **effects of a particle forming amorphous solid dispersion (ASD) on bioavailability in humans**, seeking insights in the complex **drug absorption mechanisms from ASDs** in a clinical setting.

## Study Design

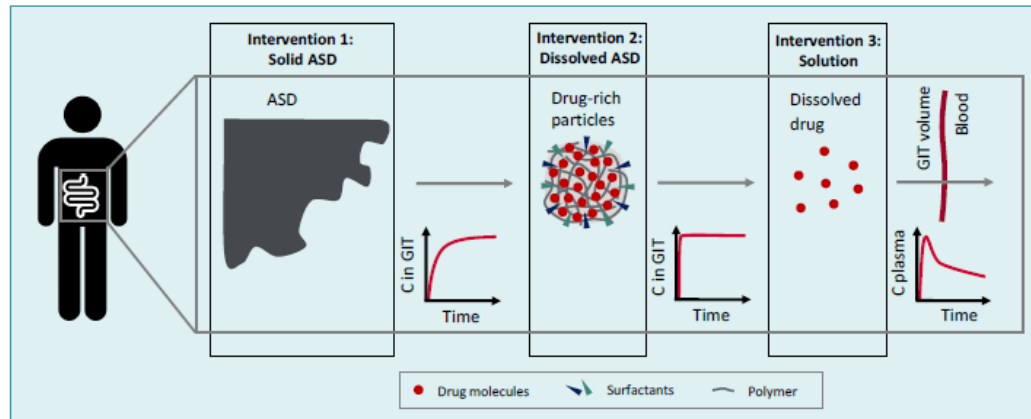
We conducted a randomized cross-over design open-label clinical study (NCT03886766) with 16 healthy male volunteers in an ambulatory setting, using micro-dosed efavirenz (EFV) as a model drug. Three interventions (oral ingestion) were performed in block-randomized order:

1. Solid ASD of EFV 50 mg
2. Dissolved ASD of EFV 50 mg (drug-rich particles)
3. Molecular solution of EFV 3 mg (non-ASD)

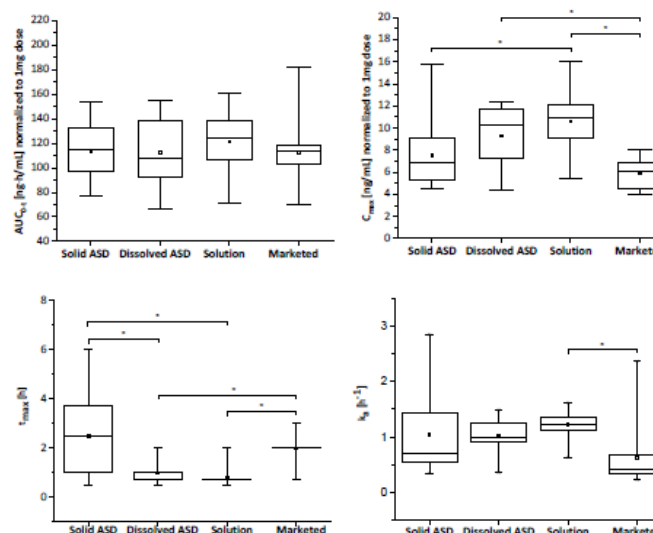
Endpoints were the pharmacokinetic profiles (EFV plasma concentration vs. time curves) and derived pharmacokinetic parameters thereof. Study results were also compared to existing data on a marketed formulation (Stocrin® 50 mg) in a non-cross-over design. Reverse PBPK-modeling was used to simulate the intestinal drug concentration based on measured PK data.



## Results



All interventions as well as the marketed formulation showed comparable areas under the curve  $AUC_{0-\infty}$  (scaled to dose). The solution showed the highest maximum concentration  $C_{max}$  and the shortest time to reach maximum concentration  $t_{max}$ , with a significant difference to both the solid ASD and the marketed formulation ( $p < 0.05$ ). The dissolved ASD showed a slower but comparable absorption compared to the solution. The results of the absorption constant  $k_a$  showed statistically significant differences between the liquid (dissolved ASD and solution) and the solid formulations (ASD and marketed formulation). Reverse PBPK-modeling indicated that the dissolved ASD in the human intestine behaved like a solution also at the higher dose.



## Conclusions

- Drug absorption from drug-rich particles, formed upon the dissolution of the ASD, was fast and complete in humans, underlining their potential as drug delivery system.
- A molecularly dissolved drug concentration beyond aqueous saturation concentration in the intestinal tract is indicated by the reverse PBPK model.
- The studied drug-rich particles from the ASD might prevent drug crystallization as well as permanent solubilization of drug into micelles.

## Background

Low oral bioavailability is a recurrent reason for drop-outs of poorly soluble drug candidates in preclinical and clinical stages of drug development, creating a need for reliable drug-delivery systems that can increase bioavailability. A promising candidate platform are amorphous solid dispersions (ASDs). In ASDs, the active pharmaceutical ingredient (API) is delivered in its amorphous state, which is stabilized by a solid polymer matrix. Upon dissolution, a complex system of drug-rich particles can evolve. While ASDs have been extensively investigated in vitro and in vivo and as well have been marketed in several cases, details on their behavior as a drug delivery platform in humans today are poorly investigated and understood.

## References

Schittny A et al., Pharmaceutics 2021, 13(3), 401

## Contact Information

Andreas Schittny: andreas.schittny@unibas.ch



# Translating thin film rehydration method for cationic liposome manufacture to a microfluidics system for a liposomal pDNA vaccine against SARS-CoV2

SWISS  
PHARMA  
SCIENCE DAY  
2021



UNIVERSITÉ  
DE GENÈVE  
P - II - 3  
SAPhS  
Swiss Academy of  
Pharmaceutical  
Sciences



ISPSO  
INSTITUT DES SCIENCES  
PHARMACIQUES  
DE SUISSE OCCIDENTALE

A. PELETTA<sup>1</sup>, E. PROMPETCHARA<sup>2,3</sup>, C. KETLOY<sup>2,3</sup>, G. BORCHARD<sup>1</sup>

<sup>1</sup>School of Pharmaceutical Sciences of Western Switzerland (ISPSO), University of Geneva, 1211 Geneva, Switzerland; <sup>2</sup>Dengue Vaccine Research Unit, Chula Vaccine Research Center (ChulaVRC), Faculty of Medicine and; <sup>3</sup>Department of Laboratory Medicine, Chulalongkorn University, Bangkok, 10330, Thailand

## INTRODUCTION

The sudden spread of SARS-CoV2 demands rapid development of therapeutics and prophylactic intervention in a short period of time. DNA vaccination is considered a potential strategy to meet the challenge. This technique holds two major disadvantages: poor immunogenicity and transfection of the target cell. Both require the development of effective delivery systems such as liposomes. New generation microfluidics devices are a great tool to overcome these problems.

## AIMS

- ✓ Formulation of DOTAP based liposomes for SARS-CoV2 protein S expressing DNA vaccine
- ✓ Translation of a thin film layer rehydration into a microfluidics preparation method using a NanoAssembler Ignite® (Precision Nanosystems)
- ✓ Characterization of the blank formulation and the lipoplexes
- ✓ Assessment of *in vitro* transfection efficiency using HEK293 cells

## METHODS

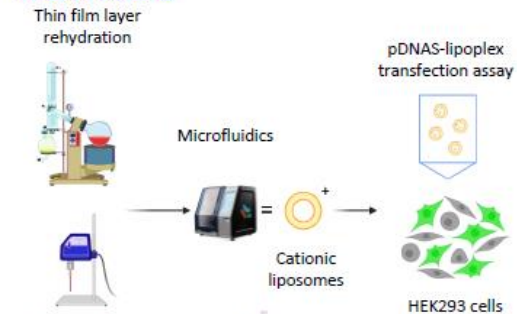
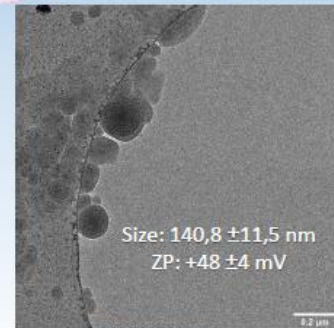


Fig.1: Visual schematization of the methods used. A thin film layer rehydration method for liposome production was translated into a microfluidics method. After DLS, TEM and Zeta-Potential characterization, lipoplexes were formed (see Fig.3) and characterized. In vitro transfection assays on HEK 293 cells were performed.

## RESULTS

### Microfluidics



### Thin film layer

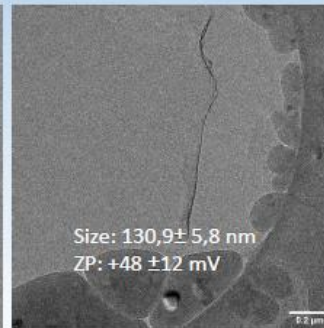


Fig.2: Characterization of blank liposomes produced by microfluidics or thin film layer rehydration. Results of TEM, DLS and Zeta-Potential

- ✓ Size and Zeta-Potential of the particles are comparable
- ✓ Cryo-TEM images show a multilamellar structure in particles manufactured by microfluidics and a unilamellar structure for particles manufactured by thin film method
- ✓ Complexation results are comparable for both methods
- ✓ 1:1 N/P ratio was selected for further *in vitro* studies

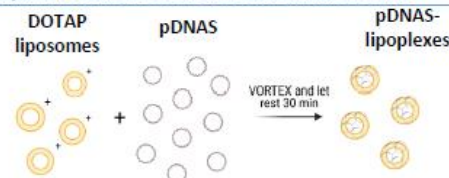


Fig 3: Method of preparation of lipoplexes

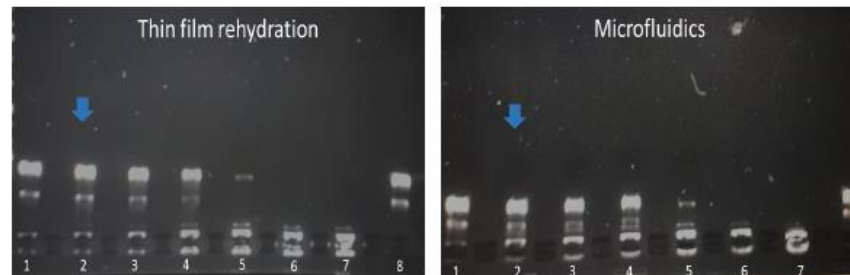


Fig 4: Electrophoretic mobility of lipoplexes at different N/P ratio. Different degrees of complexations are observed. A higher N/P ratio correspond to a more efficient complexation but an aggregated sample.

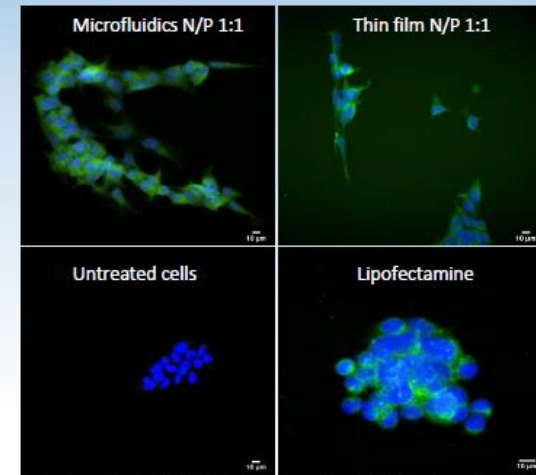


Fig 5: Intracellular SARS-CoV-2 S protein expression. HEK293 cells were transfected with pDNAS as nanoplexes at a N/P ratio of 1:1. Untreated cells are used as negative control and Lipofectamine complexed with pDNAS as positive control. Green = S protein, Blue = nucleus. Images were obtained by confocal laser scanning microscopy.

## DISCUSSION & CONCLUSIONS

- ✓ Liposomes manufactured by microfluidics method seems comparable in characteristics with thin film rehydration method manufactured liposomes
- ✓ Main structural difference is observed by Cryo-TEM images where lamellarity of the liposomes appears to be different
- ✓ *In vivo* immunogenicity studies in ICR mice are planned to confirm antibody production and T cell activation by the liposomes manufactured by both methods

### N/P ratio

1	0.25:1
2	1:1
3	5:1
4	10:1
5	25:1
6	50:1
7	100:1
8	pDNAS

## REFERENCES

1. Coronaviridae Study Group of ICTV. The species Severe acute respiratory syndrome-related coronavirus: classifying 2019-nCoV and naming it SARS-CoV-2. *Nature Microbiology*. 2020;5(4):536.
2. Flingai S, Czerwinski M, Goodman J, Kudchodkar SB, Muthumani K, Weiner DB. Synthetic DNA vaccines: improved vaccine potency by electroporation and co-delivered genetic adjuvants. *Frontiers in Immunology*. 2013;4:354.
3. Khan KH. DNA vaccines: roles against diseases. *Germs*. 2013;3(1):26.
4. Forbes N, Hussain MT, Briuglia ML, Edwards DP, Ter Horst JH, Zita N, et al. Rapid and scale-independent microfluidic manufacture of liposomes entrapping protein incorporating in-line purification and at-line size monitoring. *International journal of pharmaceuticals*. 2019;356:68-81.

## CONTACT INFORMATION

Allegra.Peletta@unige.ch



# Efficient colonic drug delivery

## Novel tablet formulation with double control concept

SWISS  
PHARMA  
SCIENCE DAY  
2021



P - II - 4

SAPhS  
Swiss Academy of  
Pharmaceutical  
Sciences

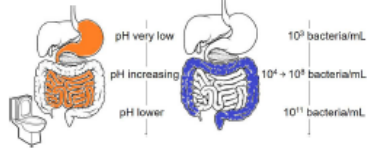
V. DOGGWILER<sup>1,2</sup>, M. LANZ<sup>1</sup>, G. LIPPS<sup>1</sup>, G. IMANIDIS<sup>1,2</sup>

<sup>1</sup> University of Applied Sciences and Arts Northwestern Switzerland, Institute of Pharma Technology, Muttenz, Switzerland

<sup>2</sup> University of Basel, Department of Pharmaceutical Sciences, Basel, Switzerland

### INTRODUCTION

Targeted colonic delivery: necessary for the local treatment of inflammatory bowel diseases  
Available tablets: only one control concept (mainly pH) – too early or late release.



### AIMS

New oral formulation  
- for targeted colonic delivery  
- with double drug release control

1. pH-sensitive coating  
- prevents drug release in the upper gastrointestinal tract
2. Xyloglucan matrix  
- prevents drug release before entry into the large intestine  
- is cleaved by enzymes in the colonic microbiome.

### METHODS

Fluid-bed granulation:  
33% API, 7% PVP K30, 60% xyloglucan  
Tableting: 200 mg dose; either 5-ASA or caffeine  
Coating: Eudragit® FS 30 D  
dissolution rate increased at pH > 6.8  
Dissolution testing (USP 2):  
Gastrointestinal tract simulation  
- Stomach: 900 mL HCl 0.1 M  
- Upper small intestine: 900 mL phosphate buffer pH 6.5  
- Lower small intestine: 900 mL phosphate buffer pH 6.8  
- Large intestine: 200 mL phosphate buffer pH 6.8, with varying xyloglucanase amounts  
Measurement of API release and xyloglucan matrix degradation

### RESULTS

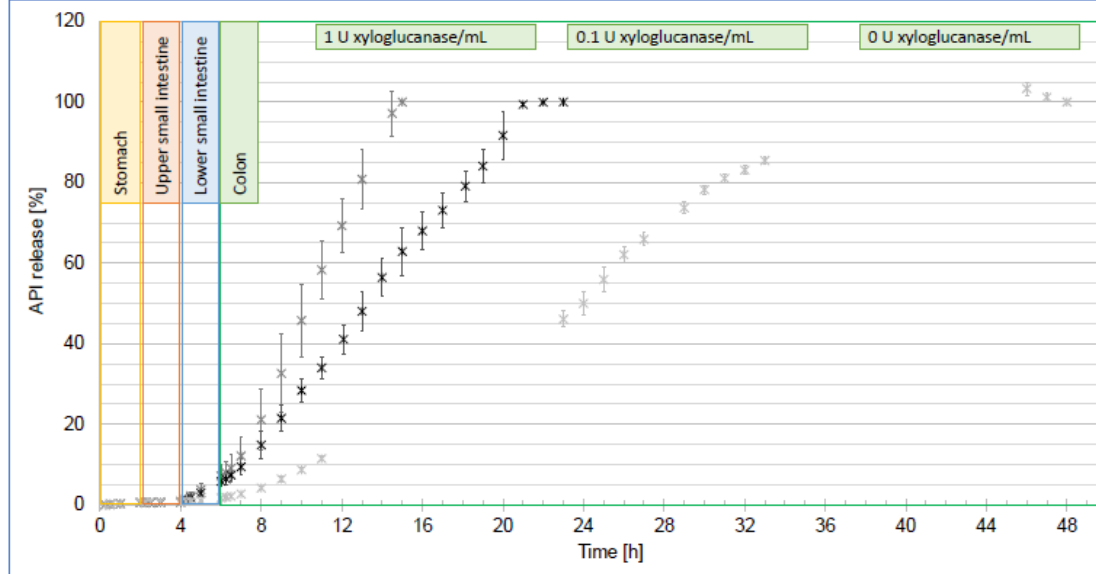


Fig. 1: Dissolution profiles of coated Xyloglucan-5-ASA tablets at three different enzyme levels in the final dissolution medium (1 U/mL: dark grey, 0.1 U/mL: black, 0 U/mL: light grey).

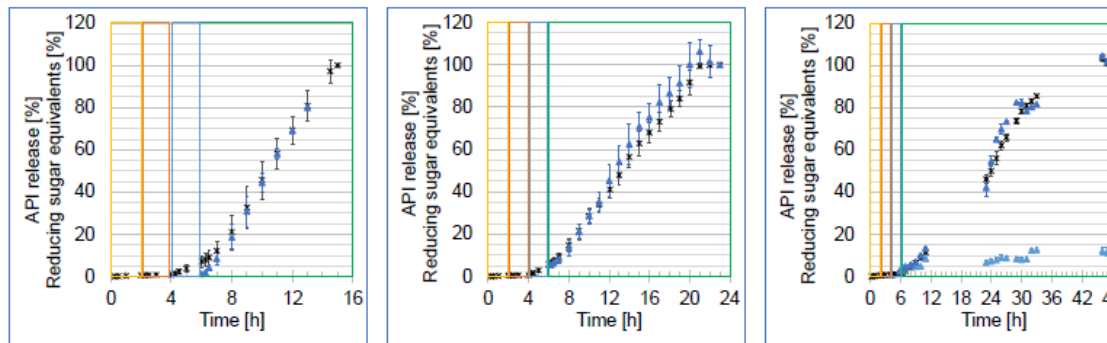


Fig. 2: Release profiles of both API (black) and reducing sugar equivalents (blue) from coated Xyloglucan-5-ASA tablets at three different enzyme levels in the final dissolution medium (left: 1 U/mL, middle: 0.1 U/mL, right: 0 U/mL).

### DISCUSSION & CONCLUSIONS

The applied double control concept led to efficient and selective colonic drug release.

1. pH-sensitive coating:  
- Release control in the upper gastrointestinal tract
2. Xyloglucan matrix:  
- Release control in the lower small intestine  
- <10% API released before entry in the large intestine  
- Enzymatic matrix degradation in the colon.  
The higher the enzyme concentration, the faster the drug release

Under physiological conditions with  
- 0.5 U xyloglucanase per g feces<sup>[1]</sup> and  
- 20 h colonic transit<sup>[2]</sup>  
complete dose release is realistic!

Outlook:

- *in vivo* evaluation of the formulation in landrace pigs
- Investigation of drug release mechanisms

### REFERENCES

- [1] Y. Tuncil et al., "Delayed utilization of some fast-fermenting soluble dietary fibers by human gut microbiota when presented in a mixture," J. Funct. Foods, vol. 32, pp. 347–357, 2017.
- [2] A. Abuhelwa, D. Foster, and R. Upton, "A quantitative review and meta-models of the variability and factors affecting oral drug absorption - part II: Gastrointestinal transit time," AAPS J., vol. 18, no. 5, pp. 1322–1333, 2016

### ACKNOWLEDGEMENTS

Valeria Paredes  
for reducing sugar measurements  
SNF BRIDGE  
for project funding

### CONTACT INFORMATION

Corresponding author: Prof. Dr. Georgios Imanidis  
georgios.imanidis@fnw.ch  
+41 61 228 56 36



# Characterization of immunocomplexes

SWISS  
PHARMA  
SCIENCE DAY  
2021



UNIVERSITÉ  
DE GENÈVE  
P - II - 5  
SAPhS  
Swiss Academy of  
Pharmaceutical  
Sciences  
ISPSO

M. Petrovic<sup>1,2</sup>, G. Borchard<sup>1,2</sup>, \*O. Jordan<sup>1,2</sup>

<sup>1</sup> Institute of Pharmaceutical Sciences of Western Switzerland (ISPSO), Section of Pharmaceutical Sciences, University of Geneva, 1 rue Michel Servet, Geneva, Switzerland

<sup>2</sup> Section of Pharmaceutical Sciences, University of Geneva, 1 rue Michel Servet, Geneva, Switzerland

\*corresponding author

## INTRODUCTION

2'3'cGAMP activates stimulator of interferon genes (STING) pathway which results in overexpression of type I interferons on antigen presenting cells (APC), that promotes CD8+ T cell priming against tumor-associated antigens. In order to transfect APCs within tumor microenvironment, there is a need for a carrier for a negatively charged cGAMP prone to degradation by hydrolases from the blood.

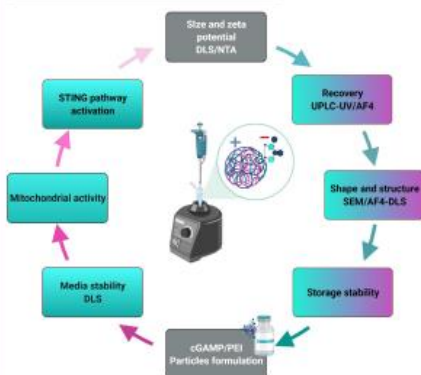
## AIMS

To form nanocomplexes (NCs) with cGAMP and its carrier polyethylenimine 25 kDa (linPEI25), which will finally enable delivery of cGAMP intracellularly and activate STING pathway. The aim of this work is to challenge the state-of-the-art physicochemical characterization techniques towards the design of efficient NCs for tumor immunotherapy.

## METHODS

NCs were prepared based on the ionic gelation method in milliQ water or PBS. CDN (2'3'cGAMP) was added dropwise to linPEI25 at 0.01 mg/ml under vortexing. Linear PEI 25 kDa was tested as a drug carrier, at two different cGAMP loadings - N/P ratios of 1/1 and 2/1. Tested conditions were linPEI25 (empty complexes) and 1/1 and 2/1 NCs (loaded complexes)

Several parameters were optimized:



Scheme 1. Physicochemical characterization of NCs

## RESULTS AND DISCUSSION

### SIZE

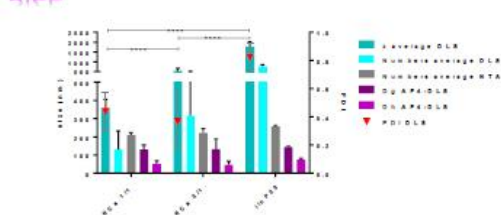


Figure 1. DLS (z-average and numbers), NTA and AF4-UV-MALS-DLS (Dg and Dh) comparison of empty and loaded NCs graphical and table representation

- Based on DLS and AF4-DLS nanocomplexes sizes, 1/1 and 2/1 NCs were smaller than linPEI25 ( $p < 0.0001$ ).
- DLS (Numbers) and NTA number-averaged size were comparable
- In contrast, there was significant difference between z-average by DLS and Dh calculated by AF4-DLS. This can be due selected population which was eluted and separated by AF4.

### SHAPE

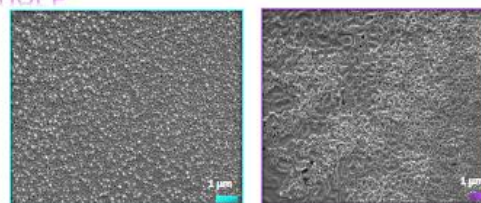


Figure 3. SEM: 1/1 (left) and 2/1 (right) NCs in water. Scale 1  $\mu$ m.

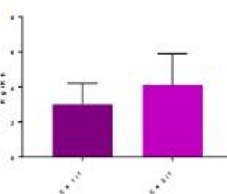


Figure 4. AF4-DLS, shape factor Rg/Rh of NCs in water

- NCs corresponded to elongated structures based on the shape factor (Fig 4.), while their structure observed by SEM resembled gels (Fig 3).
- In case of 2/1 NCs we observed more gelified and rigid structure,
- NCs may form rod-like structures capable of crosslinking.

### ZETA POTENTIAL

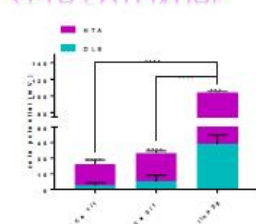


Figure 2. DLS and NTA zeta potential of NCs in water

NCs at 1/1 and 2/1 ratio had significantly lower zeta potential compared to linPEI25 alone, suggesting that adding negatively charged cGAMP, neutralizes PEI ( $p < 0.0001$ ,  $n=3$ ). Zeta potential for the 2/1 ratio ( $7.7 \pm 6$  mV) was twice higher compared to 1/1 ratio ( $4 \pm 2.3$  mV) as expected for a complete complexation. This difference is confirmed by NTA measurements, although with higher zeta potential values. ( $p < 0.0001$ ,  $n=3$ ) (sup 1. b)).

### cGAMP LOADING



Figure 5. EE% and Rcf of NCs in PBS

cGAMP encapsulation efficiency (EE - UPLC/UV) are without significant difference compared to Recovery (Rcf AF4-UV) having a value around 60-70%.

## CONCLUSIONS

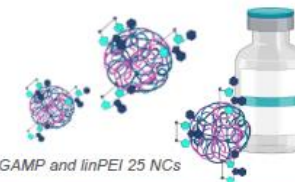
In-depth complementary characterization techniques indicated that cGAMP was successfully complexed with PEI

Specifically, NCs are smaller and have lower zeta potential than empty linPEI25 (orthogonal techniques used: DLS, NTA, AF4-MALS-DLS for size and DLS, NTA for zeta potential). Moreover, particles have significantly lower zeta potential compared to linPEI25.

Shape obtained by SEM and AF4-DLS shape factor  $>2$  suggests elongated rod-like structure, which is preferred for the phagocytosis having the similar shape as a bacteria.

In conclusion, LinPEI25 and cGAMP are forming elongated scaffolds and eventually nanogels, being complexed as shown by size, zeta potential, shape and drug loading measurements (60-70%).

Based on the next steps and biological assays it still remains to decide on the ratio out of the two tested.



Scheme 2. cGAMP and linPEI 25 NCs

## REFERENCES

- [1] Barber GN. STING: infection, inflammation and cancer. Nat Rev Immunol. 2015;15(12):760-70
- [2] Li T, Cheng H, Yuan H, Xu Q, Shu C, Zhang Y, et al. Antitumor Activity of cGAMP via Stimulation of cGAS-cGAMP-STING-IRF3 Mediated Innate Immune Response. Scientific reports. 2016;6:19049
- [3] Pandey AP, Sawant KK. Polyethylenimine: A versatile, multifunctional non-viral vector for nucleic acid delivery. Materials science & engineering C, Materials for biological applications. 2016;68:904-18.

## CONTACT INFORMATION

Marija.petrovic@unige.ch.



# Zebrafish embryo (*Danio rerio*) as an *in vivo* vertebrate model to study renal function

J.S. BOLTEN<sup>1</sup>, A. PRATSINIS<sup>1</sup>, C.L. ALTER<sup>1</sup>, G. FRICKER<sup>2,3</sup>, J. HUWYLER<sup>2,3</sup>

<sup>1</sup> Division of Pharmaceutical Technology, University of Basel, Basel, Switzerland  
<sup>2</sup> Division of Pharmacy and Molecular Biotechnology, University of Heidelberg, Heidelberg, Germany  
<sup>3</sup> Mount Desert Island Biological Laboratory, Maine, USA

## INTRODUCTION

The study of renal function remains a challenge. *In vitro* cell-based assays do not cover renal functions such as glomerular filtration and tubular reabsorption. *In vivo* studies often rely on experimentation with higher vertebrates, are expensive, and do not always provide mechanistic insights at a cellular level. In view of these limitations, there is a high unmet need for cost-effective and animal experiment reducing *in vivo* test systems that include mechanistic studies and allow a translation to higher vertebrates such as humans. The zebrafish embryo (ZFE) pronephric kidney shares high similarity with the anatomy of nephrons in higher vertebrates. Thus, they are not considered as an animal.

## AIMS

The aim is to use ZFE as an *in vivo* vertebrate model to study glomerular filtration, ABC/SLC mediated drug transport and folate receptor 1-mediated tubular reabsorption. We assessed whether 3 to 4 days old ZFE have a fully functional pronephron.

## METHODS

- Fluorescent labelling, purification and hydrodynamic size determination of polymers using Fluorescent Correlation Spectroscopy (FCS)
- Transgenic zebrafish lines expressing GFP/mCherry in specific organs (e.g. endothelial cells, glomerulus, parts of proximal tubules)
- I.v.* injections of fluorescent model compounds and non-fluorescent inhibitors into living zebrafish embryos (3-4 days old)
- Confocal microscopy of tail and nephron region

## RESULTS

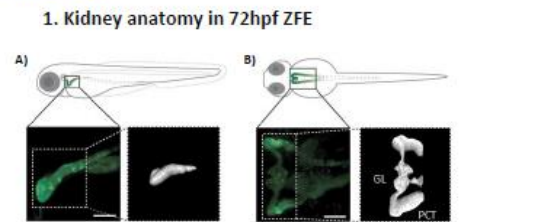


Fig. 1: Anatomical localization of the kidney in 72hours post-fertilized (hpf) ZFE. (A) Lateral and (B) ventral projection of a 72hpf tg(wt1b:eGFP) zebrafish embryo (ZFE) expressing GFP in the proximal convoluted tubule (PCT) and glomerulus (GL). Scale bar = 50µm.

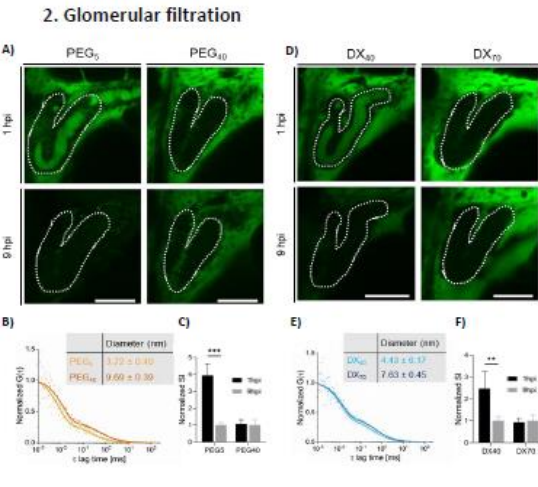


Fig. 2: Glomerular filtration in 96hpf ZFE. (A/D) Qualitative assessment of polyethyleneglycol/dextran (PEG/DX, green signal) within the proximal tubule lumen 1 and 9 hours post-injection (hpi). PCT marked with white dotted lines. (B/E) Hydrodynamic diameter of PEG/DX polymer with molecular weight of 5-70kDa determined by fluorescent correlation spectroscopy. (C/F) Quantitative assessment of luminal PEG/DX signal compared to corresponding 9hpi values. Values are means ± SD, n=5. \*\*p<0.005, \*\*\*p<0.0005. Scale bars = 50µm. Signal intensity (SI).

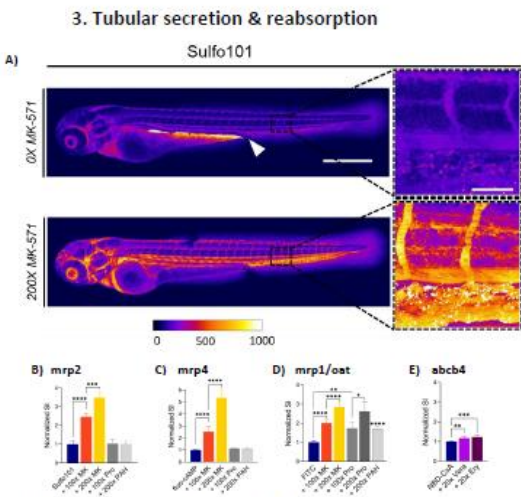


Fig. 4: Renal secretion of fluorescent substrates of drug transporters. (A) Confocal microscopy analysis of 72hpf ZFE 1hpi i.v. injection of Sulfo101 in presence of increasing concentrations of the mrp inhibitor MK-571. White arrow: GI tract and cloaca. Scale bar = 500µm. Magnified sections of the tail region vasculature are shown. High signal intensity: red to white colors. Scale bar = 50µm. (B-E) Quantitative analysis of transporter substrates within dorsal artery in the presence and absence (blue bar) of x-fold excess of inhibitor in 72hpf ZFE. Pro (probenecid), MK (MK-571), PAH (p-aminohippurate), Vera (verapamil), Ery (erythromycin), FITC (fluorescein), NBD-CsA (fluorescent cyclosporine A). Values are means ± SD, n=5. \*p<0.05, \*\*p<0.005, \*\*\*p<0.0005, \*\*\*\*p<0.0001.

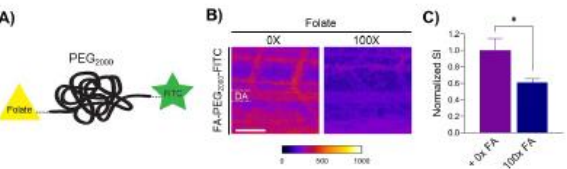


Fig. 3: Reabsorption of folate in the distal tubule. (A) Folate receptor 1 (folr1) mediated renal reabsorption was studied using a folate (FA) conjugate, modified with PEG (molecular weight 2000 Da) and the fluorescent dye FITC. (B) Confocal microscopy image of the tail region of 72hpf ZFE 1hpi of the fluorescent labeled FA derivative in presence and absence of a 100-fold excess of native folate. (C) Quantitative evaluation of signal in DA in (B). Signals were compared to control (no inhibitor). Values are means ± SD, n=5. \*p<0.0001. Scale bars = 50µm.

## DISCUSSION & CONCLUSIONS

We could show that relevant kidney processes (e.g., GF, renal secretion & folate reabsorption) are functional in 3-4 days old ZFE.

- Glomerular filtration:
  - has a similar cut-off of 4.4-7.6nm as observed in humans and rats (1)
  - Filtration properties based rather on hydrodynamic diameter than molecular weight
- ABC/SLC mediated renal drug transport:
  - Homologue ABC/SLC transporters in ZFE genome detected (2)
  - No hepatic metabolism in 3-4 days old ZFE (3)
  - Reliable detection of fluorescent substrates in blood vessels in the presence/absence of inhibitors using confocal microscopy
- Folr1 mediated tubular reabsorption:
  - Cave: concentration of fluorescent substrate is 0.1mM; excess of correlating inhibitors must not be toxic
  - Fluorescent FA construct is glomerular filtrated and reabsorbed into the blood stream via folr1 (4)
- Conclusion & Extrapolation:
  - Drug transporter processes show high similarity to *in vitro* and *ex vivo* (Killifish) transport assay
- As an application, ZFE represents a useful *in vivo* vertebrate model to study drug transport and drug-drug interactions

## REFERENCES

- (1) Soo Choi et al. 2007, Nat Biotechnol./ Tencer J et al, 1998, Kidney Inter.
- (2) Luckenbach et al. 2014, Comp Biochem Physiol Part C Toxicol Pharmacol
- (3) Chu et al. 2009, Ahepatik Baltim Md
- (4) Jones. et al. 2017, Gene Expr Patterns

## CONTACT INFORMATION

jan.bolten@unibas.ch







# Artificial intelligence in the analysis of time-resolved (4D) micro-computed tomography data

S. WALDNER<sup>1</sup>, J. HUWYLER<sup>1</sup> and M. PUCHKOV<sup>1</sup>  
<sup>1</sup>Division of Pharmaceutical Technology, University of Basel, 4056 Basel

## DATA ACQUISITION

**Paul Scherrer Institute**  
Swiss Light Source (SLS) Synchrotron

- 4D  $\mu$ CT image acquisition of disintegrating mini-tablets
- 64 different tablet formulations according to design of experiment
- 1 to 10 scans per second for up to 30 seconds
- 23 TB of raw projection data
- Reconstruction quadruples size, only done as needed

4D projection raw data

## IMAGE RECONSTRUCTION

4D reconstructed data

- Custom raw data reconstruction software
- Written in Python and CUDA-C++
- Runs massively parallelized on GPUs

## AIMS

We provide tools to further mechanistic understanding of tablet disintegration. To this end we generate a large dataset of segmented time-resolved micro-computed tomography images to provide a unique direct insight into the disintegration process. We apply artificial intelligence in the form of deep learning computer vision to overcome the challenges posed by this approach.

## COMPUTATION

- Software runs on the sciCORE high-performance computing facility
- Data storage handled by sciCORE
- No interactive access, uses SLURM queueing system

## OUTCOME

- 4D- $\mu$ CT approach provides direct insight into tablet disintegration
- Deep learning needs to be applied for image segmentation due to the variability in image quality

## IMAGE SEGMENTATION

Deep learning  
TensorFlow

Convolution & Pooling  
Deconvolution & skip concatenation  
Skip connection  
Convolution kernel [3x3x3]

- Image segmentation using 3-dimensional UNet convolutional neural net architecture
- Algorithm trains autonomously on a large sample dataset
- Realization in Tensorflow and Python
- Runs parallelized on GPUs
- Training dataset generated in Ilastik using supervised machine learning

## CONCLUSION

Our approach demonstrates the power of deep learning when it is applied in a suitable setting. Due to the non-linearly separable nature of the data, the convolutional neural network outperforms traditional image segmentation approaches and is able to process massive amounts of data without user intervention. Dynamic micro-computed tomography gives unprecedented insights into tablet dissolution but offers unique challenges with data management and image analysis. A dedicated high power computation facility and the use of deep learning artificial intelligence are employed to tackle these challenges.

# Thermoresponsive hyaluronan-based hydrogels for formulation of standardized transplants in tendon regenerative medicine

A. Porcello<sup>1,2</sup>, A. Laurent<sup>3,4</sup>, N. Hirt-Burri<sup>4</sup>, P. Abdel-Sayed<sup>4</sup>, C. Scaletta<sup>4</sup>, A. de Buys Roessingh<sup>5</sup>, W. Raffoul<sup>4</sup>, L.A. Applegate<sup>4,6,7</sup>, O. Jordan<sup>1,2</sup> and E. Allémann<sup>1,2</sup>

<sup>1</sup> School of Pharmaceutical Sciences, University of Geneva, Geneva, Switzerland.

<sup>2</sup> Institute of Pharmaceutical Sciences of Western Switzerland, University of Geneva, Geneva, Switzerland.

<sup>3</sup> Research Department, LAM Biotechnologies SA, Épalinges, Switzerland.

<sup>4</sup> Musculoskeletal Medicine Department, Lausanne University Hospital, University of Lausanne, Lausanne, Switzerland.

<sup>5</sup> Department of Pediatric Surgery, Lausanne University Hospital, University of Lausanne, Lausanne, Switzerland.

<sup>6</sup> Center for Applied Biotechnology and Molecular Medicine, University of Zurich, Zurich, Switzerland.

<sup>7</sup> Oxford OSCAR Suzhou Center, Oxford University, Suzhou 215123, Jiangsu, China.

## INTRODUCTION

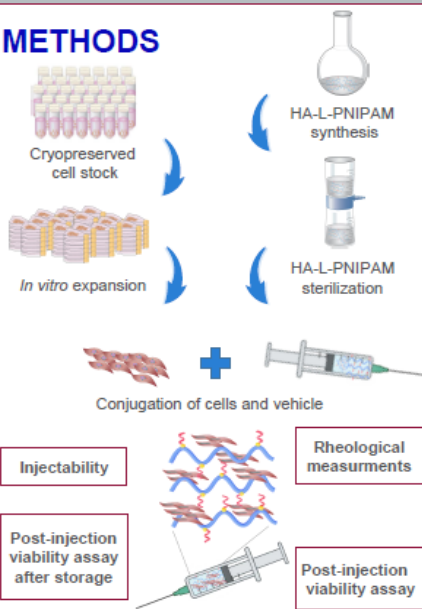
Thermoresponsive hyaluronan-based hydrogels enable facilitated injection of products developing high viscosity values *in situ* and thus present potential for delivery of therapeutic cellular materials in specific regenerative medicine applications [1].

Cultured human fetal progenitor tenocytes (hFPT) have been identified as potentially optimal therapeutic cell sources for manufacture of homologous therapeutic standardized transplants [2].

## AIMS

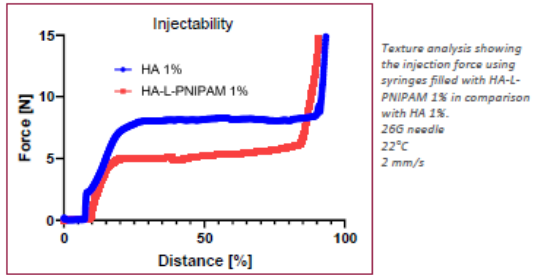
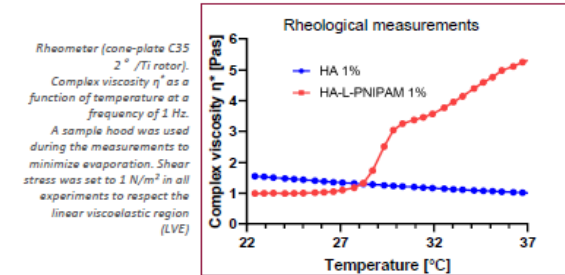
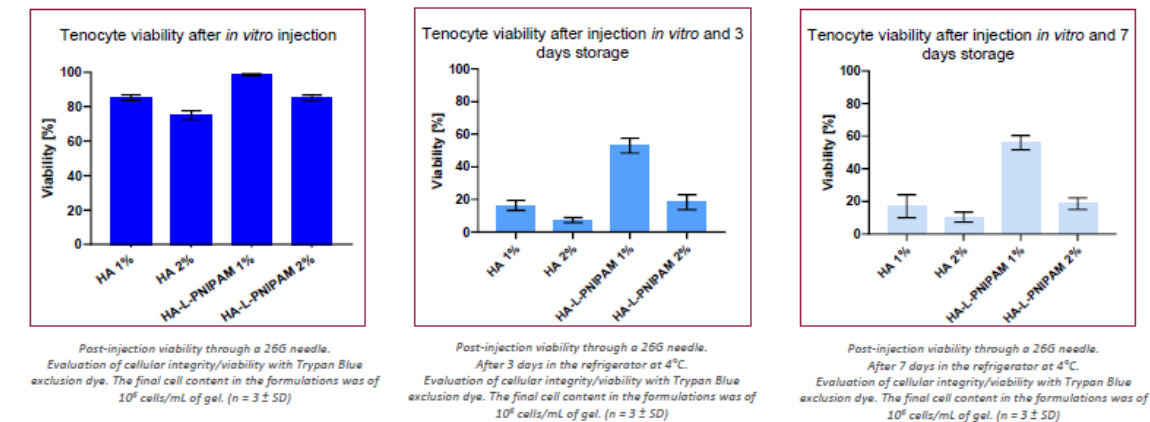
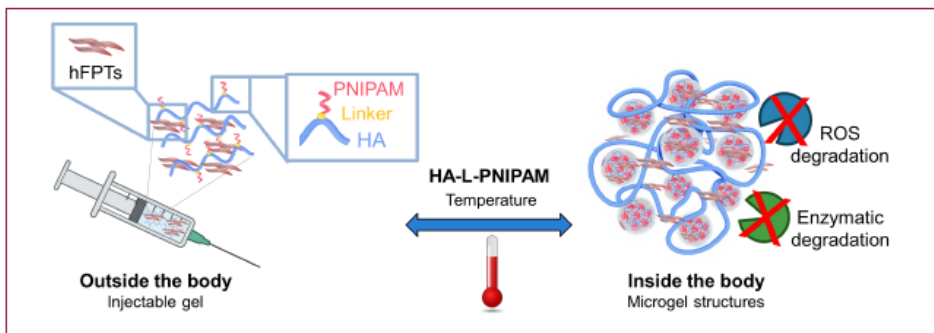
The objective of the present study is to validate the combination of product prototypes, composed of viable hFPTs and thermoresponsive hyaluronan-based hydrogels named HA-L-PNIPAM.

## METHODS



## RESULTS

Graphical representation of the combination product prototype composed of viable hFPTs and the thermoresponsive hyaluronan-based hydrogel which is easily injected at room temperature and has the ability to form microgel structures at body temperature. These structures confer resistance to enzymatic and oxidative degradation [1].



## DISCUSSION & CONCLUSIONS

Post-injection tenocyte viability assay  
HA-L-PNIPAM formulations outperformed linear hyaluronic acid (HA) formulations in terms of maintenance of cellular integrity/viability after extrusion through 26G needles.

Post-injection tenocyte viability assay after storage  
HA-L-PNIPAM formulations showed better post-injection viability after a storage of 3 and 7 days of the combination formulation at 4°C.

Rheological measurements  
Below the lower critical solution temperature (LCST), HA-L-PNIPAM showed lower viscosity properties, and higher over the LCST. HA-L-PNIPAM showed unique temperature-dependent properties leading to facilitated injection and cell-supportive viscoelastic properties.

Injectability  
HA-L-PNIPAM required less injection force than HA.

Conclusion  
The thermosensitive viscous behaviour of the hydrogel during the injection may play a major role in the preservation of cell viability. HA-L-PNIPAM provides the required highly viscous matrix for the cells at 37°C. This study provides the technical basis for further formulation optimization in translational musculoskeletal regenerative medicine, with specific focus set on hand tendon disorder management.

## REFERENCES

- [1] Maudens, P.; Meyer S.; Seemayer, C.A.; Jordan, O and Allémann, E. Nanoscale (2018). 1845-54.
- [2] Grognez, A.; Scaletta, C.; Farron, A.; Pioletti, D.P.; Raffoul, W and Applegate, L.A. Cell Medicine (2016). 87-97.

## CONTACT INFORMATION





# Mesoporous Silica Particles as Drug Delivery System offering prolonged drug release

L. Müller, S. Wegmann, S. Gallagher, D. Brühwiler, S. Lehmann  
 Institute of Chemistry and Biotechnology, Zürich University of Applied Sciences, 8820 Wädenswil

## INTRODUCTION

Mesoporous silica particles (MSP) are inorganic nanoparticles and have gained great popularity pharmaceutical science over recent years. Due to their controllable and uniform pore sizes, flexible surface functionalization, significant biocompatibility, biodegradability and lack of toxicity, they are of high interest as carriers for a targeted drug delivery.

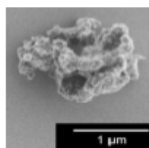


Figure 1: irregular MCM-41 under the scanning electron microscope.

## RESULTS

### Loading Efficiency

For the control of loading efficiency by functionalization, three different concentrations of APTES were used for the functionalization. Subsequently, equal amounts of fluorescein free acid were added to the differently functionalized MSPs. By UHPLC analysis, the content of FFA in the loaded MCM-41 was detected (Figure 2). The measurement showed a linear correlation between the APTES concentration and loading efficiency of FFA (mg/g MSP) ( $R^2=0.992$ ).

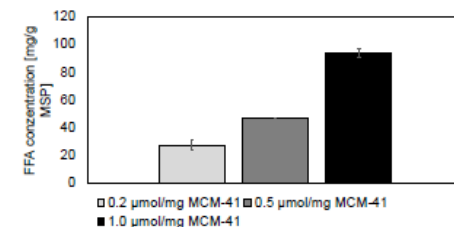


Figure 2: Loading efficiency for the different APTES concentrations (0.2, 0.5, 1.0 µmol/mg MCM-41). The error bars indicate the standard deviation.



Figure 3: Pictures of the MCM-41 loaded with fluorescein. Left: 0.2 µmol/mg MCM-41, middle: 0.5 µmol/mg MCM-41, right: 1.0 µmol/mg MCM-41.

### Control of the drug release profile

The drug release profile of MCM-41, functionalized with APTES and loaded with ibuprofen, in powder or tableted form is shown in Figure 4. The release of ibuprofen from drug-loaded MCM-41 in powder form occurred within 1 hour. Tableting of MCM-41 resulted in sustained ibuprofen release for up to 50 hours, in agreement with earlier reports in the literature [3]. The performed proof of concept study showed, that the IBU-loaded MSPs, which were coated with HEMA displayed a prolonged release of IBU over several days in organic solvents as shown in Figure 5. Figure 6 shows the coated MSP under the scanning electron microscope.

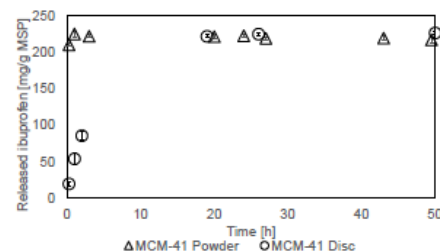


Figure 4: Drug release profile of tableted MCM-41 discs and MCM-41 powder. The error bars indicate the standard deviation.

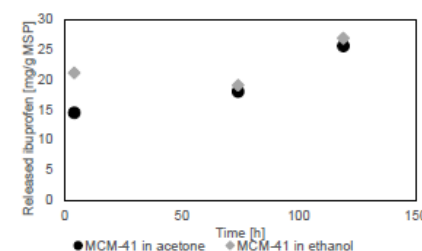


Figure 5: Drug release profile of HEMA coated MCM-41 in ethanol and acetone.

## DISCUSSION

Based on the experiments with the model drug fluorescein free acid, it was demonstrated that the loading efficiency can be enhanced by increasing the APTES concentration. According to the results, the loading efficiency at the tested concentration was linearly related to the degree of functionalization. The functionalization of the MCM-41 was intended to achieve a sustained release of ibuprofen. However, this could not be observed for powdered MCM-41. Only tableting of the functionalized and IBU-loaded MCM-41 led to a prolonged release of 50 hours. It can be assumed that the sustained release is related to the smaller surface area of the MCM-41 as tablets, preventing fast dissolution. Additionally, in a proof of concept experiment it was demonstrated that a sustained drug release from MSPs can be achieved through MSP polymer coating.

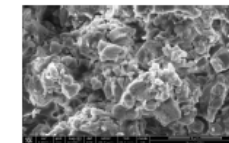


Figure 6: The HEMA-coated and IBU-loaded MCM-41 under the scanning electron microscope.

## OUTLOOK

For further experiments, a biodegradable polymer such as Poly (lactic-co-glycolic acid) should be chosen, where the drug release kinetics are controlled through the degradation time of the polymer.

## REFERENCES

- [1] Ritter, H., Nieminen, M., Karpinen, M., Brühwiler, D., 2009. A comparative study of the functionalization of mesoporous silica MCM-41 by deposition of 3-aminopropyltrimethoxysilane from toluene and from the vapor phase. *Microporous and Mesoporous Materials* 121, 79–83.
- [2] Ritter, H., Ramm, J.H., Brühwiler, D., 2010. Influence of the Structural Properties of Mesoporous Silica on the Adsorption of Guest Molecules. *Materials* 3, 4500–4509. <https://doi.org/10.3390/ma3084500>
- [3] Manzano, M., Aina, V., Areán, C.O., Balas, F., Cauda, V., Colilla, M., Delgado, M.R., Vallet-Regí, M., 2008. Studies on MCM-41 mesoporous silica for drug delivery: Effect of particle morphology and amine functionalization. *Chemical Engineering Journal, Porous Inorganic Materials for Biomedical Applications* 137, 30–37.

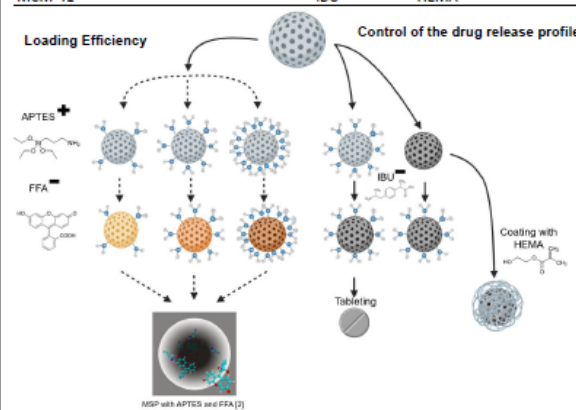
## CONTACT INFORMATION

B.Sc. Laila Müller, [muellai@students.zhaw.ch](mailto:muellai@students.zhaw.ch)  
 Department of Pharmaceutical Technology and Pharmacology  
 Einsiedlerstrasse 31, 8820 Wädenswil

## METHODS

MCM-41 with 3.8 nm pore size were prepared according to the procedure of Ritter et al. [1]. The experimental design is shown in the following flowchart. MSPs were functionalized with 3-aminopropyltriethoxysilanes (APTES) and loaded with fluorescein free acid (FFA, yellow) or ibuprofen (IBU, dark gray). In addition, the loaded MSP were pressed into discs, or coated with 2-hydroxyethyl methacrylate (HEMA).

MSP	Functionalization	Drug	Polymer Coating
MCM-41	APTES	FFA	-
MCM-41	APTES	IBU	-
MCM-41	-	IBU	HEMA





# Electrospun poly(L-lactide-co-ε-caprolactone) (PLCL) fibres loaded with Mesoporous Silica Particles to prevent bacterial biofilms on medical implants

D. ZUKOVIĆ<sup>1</sup>, S. WEGMANN<sup>1</sup>, A. SCHMID<sup>1</sup>, D. BRÜHWILER<sup>1</sup>, S. LEHMANN<sup>1</sup>

<sup>1</sup> Zurich University of Applied Sciences ZHAW, 8820 Wädenswil, Zurich, Switzerland

## INTRODUCTION

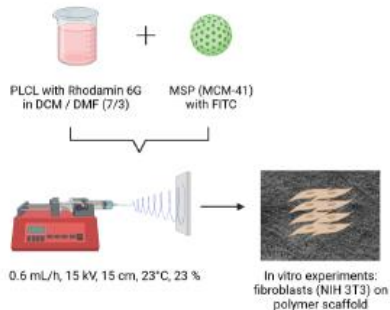
Implant innovation represents a very essential area in the field of medical research. One of the complications associated with medical implants are bacterial infections, which can lead to systemic inflammation. The adhesion of bacteria on the implant surface, which is faster than adhesion of host cells like fibroblast, leads to a successive formation of several bacterial layers in a so-called biofilm. By forming a protective matrix, biofilms prevent penetration of antibiotics and complicate the antibiotic treatment. Current research efforts thus focus on novel implant coatings and wraps preventing biofilm formation.

## AIMS

The aim of this study was the development of a novel antibacterial implant wrap, based on a scaffold of poly(L-lactide-co-ε-caprolactone) (PLCL) polymer fibres, fabricated by electrospinning and containing mesoporous silica particles (MSPs) as drug carriers for prolonged release of antibiotics. Here, we established a suitable electrospinning protocol to produce the scaffolds, characterized them by scanning electron microscopy (SEM) regarding fiber properties and MSPs incorporation and assessed their biocompatibility.

## METHODS

The procedure for the manufacturing of the fibres of this study is illustrated below:



## RESULTS

The development of the electrospinning parameters ensured a suitable quality of the polymer fibres (A). Observing the morphology, the fibers showed an average diameter of 0.5-1.2  $\mu\text{m}$ . The integration of the MSPs inside the PLCL fibres (B) showed large agglomerations (2.4  $\mu\text{m}$ ), which likely represent the MSPs.

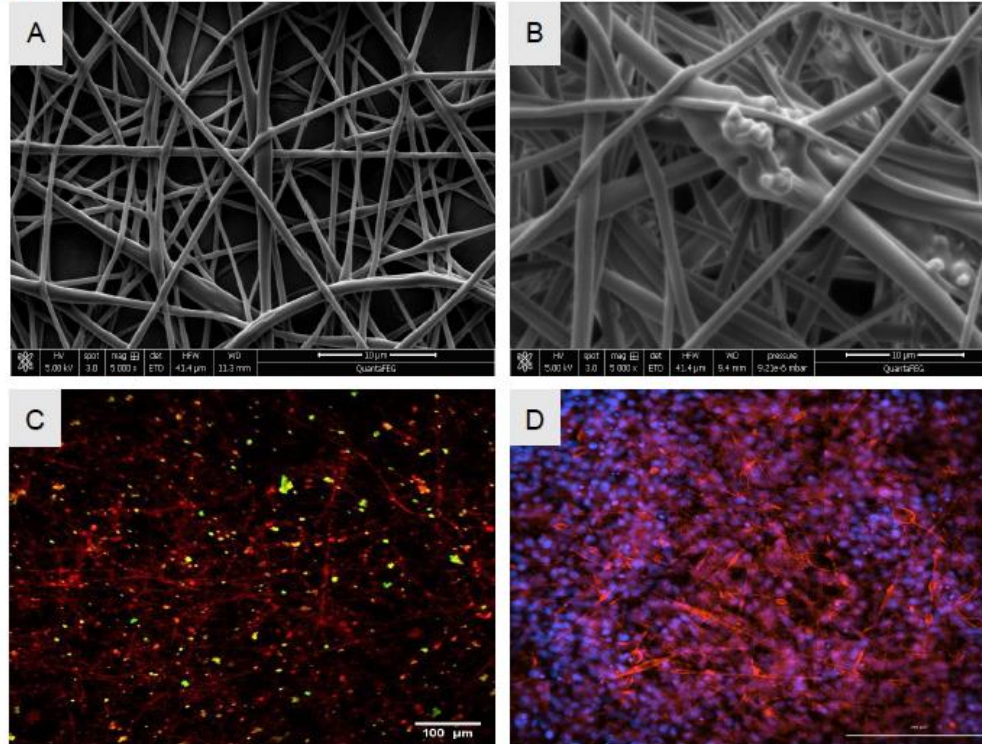
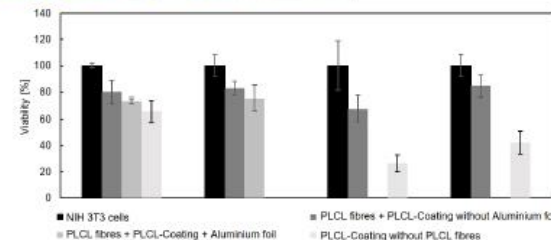


Figure 1: SEM images of fibres using electrospinning after 10 minutes (A) and MSPs agglomerations in the scaffold (B). The pictures were taken with a 5'000x magnification.

Figure 2: PLCL fibres with the integration of MSPs on the left (C) and the polymer scaffold with NIH 3T3 cells on the right (D). This images were taken with a 20x magnification.

According to the SEM images, the MSPs could be incorporated in the PLCL fibres. However, this finding could not be fully confirmed via fluorescence microscopy: a major part of green labeled MSPs lied outside the fibers labeled in red (C). In the *in vitro* experiments the fibroblasts (NIH 3T3) invaded the polymer scaffold and showed good overall viability (D).



## DISCUSSION

The structure and shape of the electrospun polymer fibers are consistent with several literature reports for example Z. Li & Wang, 2013 [1] and confirm successful implementation of the method. Incorporation of MSPs the agglomerations cause an undesired enlargement of the fibers. Therefore, an improved distribution of the individual MSPs is needed. The *in vitro* experiments suggest cell attachment to the polymer scaffold. Cell proliferation within the scaffolds was comparable to previous studies like Kwon & Matsuda, 2005 [2].

## CONCLUSIONS

In conclusion, the potential of electrospinning was shown to be suitable to produce fiber scaffolds for implant wraps. The integration of the MSPs was achieved but requires further optimization. The migration of fibroblasts in the scaffolds needs to be further analyzed. An example could be the expansion of the scaffold to produce more space for the cells.

## REFERENCES

- [1] Li, Z., & Wang, C. (2013). One-Dimensional nanostructures: Electrospinning Technique and Unique Nanofibers. Springer-Verlag. [2] Kwon, I. K., & Matsuda, T. (2005). Co-Electrospun Nanofiber Fabrics of Poly( L -lactide- co -ε-caprolactone) with Type I Collagen or Heparin. Biomacromolecules, 6 (4), 2096–2105.
- [2] Kwon, I. K., & Matsuda, T. (2005). Co-Electrospun Nanofiber Fabrics of Poly( L -lactide- co -ε-caprolactone) with Type I Collagen or Heparin. Biomacromolecules, 6(4), 2096–2105.

## CONTACT INFORMATION

B. Sc. Dženneta Zuković,  
zukovdze@students.zhaw.ch  
Department of Pharmaceutical Technology and  
Pharmacology  
Einsiedlerstrasse 31, 8820 Wädenswil



# Influence of manufacturing parameters during high-pressure homogenization on oxidation products in parenteral lipid emulsions

S. LEHNER<sup>1</sup>, G. HOLTZHAUER<sup>1</sup>, A. HERBST<sup>1</sup>, J. RADONJIC<sup>1</sup>, T. VILVALINKAM<sup>1</sup>, E. LUCCHINETTI<sup>2</sup>, G. ROGLER<sup>3</sup>, M. HERSBERGER<sup>4</sup>, M. ZAUGG<sup>2,5</sup>, S.D. KRÄMER<sup>1</sup>

<sup>1</sup>Biopharmacy, Institute of Pharmaceutical Sciences, Department of Chemistry and Applied Biosciences, ETH Zürich, Zürich, Switzerland

<sup>2</sup>Department of Anesthesiology and Pain Medicine and Cardiovascular Research Centre, University of Alberta, Edmonton, Canada

<sup>3</sup>Division of Gastroenterology and Hepatology, University Hospital Zurich, Zurich, Switzerland

<sup>4</sup>Division of Clinical Chemistry and Biochemistry, University Children's Hospital Zurich, Zurich, Switzerland

<sup>5</sup>Department of Pharmacology, University of Alberta, Edmonton, Canada

SWISS  
PHARMA  
SCIENCE DAY  
2021



ETH zürich

## INTRODUCTION & AIM

Triglycerides contained in lipid emulsions (LE) are susceptible to oxidation. Exposure to high temperature and process pressure as well as atmospheric oxygen during the manufacturing of emulsions can deteriorate the quality by oxidation of double bonds. LEs are produced by high-pressure homogenization. The use of a backpressure module during homogenization alleviates the pressure drop from the process pressure up to 2000 bar back to atmospheric pressure at the outlet. Different cooling systems are used to compensate for the development of heat during compression of the emulsion.

Our aim was to examine the influence of the installation of a backpressure module and two different cooling systems on the formation of oxidation products in lipid emulsions.

## METHOD

LEs containing either 20% soybean or 10% fish oil were homogenized for six cycles at a process pressure of 22 kpsi, using the Dyhydromatics HL60 high-pressure homogenizer (HPH). To investigate the effect of the backpressure module, as well as the cooling system, the droplet size was measured and the primary and secondary oxidation products of the LE were quantified with established assays namely the modified ferrous oxidation xylenol orange assay [1] and the thiobarbituric acid reactivity assay [2]. The assays were adapted to work with minimal sample amount and optimized for high throughput in a microplate reader setup. The results of the produced LEs were compared to readings from three commercially available reference emulsions, determined with the same assays.

Tab. 1: Dimensions of cooling systems

Studied cooling systems	
Long	21 cm length, 7 cm diameter, 27 coil windings
Small	5 cm length, 4 cm diameter, 7 coil windings



Fig. 1: Disassembled small cooling coil with 7 coil windings

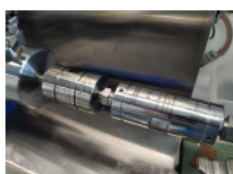


Fig. 2: HPH with installed reaction chamber and backpressure module

## RESULTS

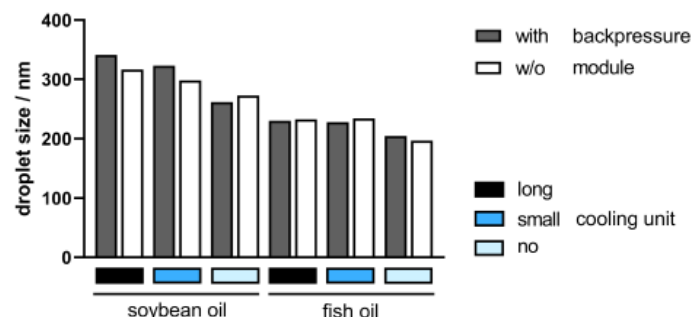


Fig. 3: Comparison of droplet sizes of different emulsions manufactured using the backpressure module and without it (n=1)

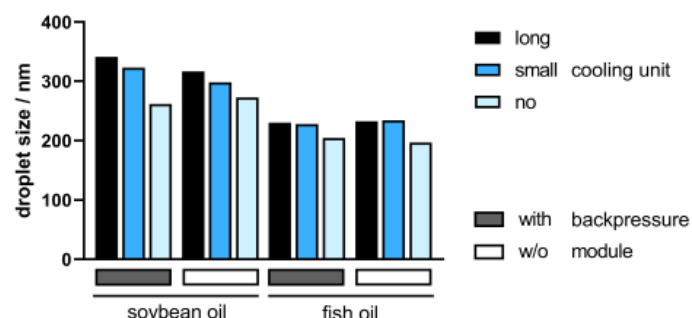


Fig. 5: Droplet size of the emulsions as a function of the used cooling system (n=1; same data as in Fig. 3 but rearranged for easier visual comparison)

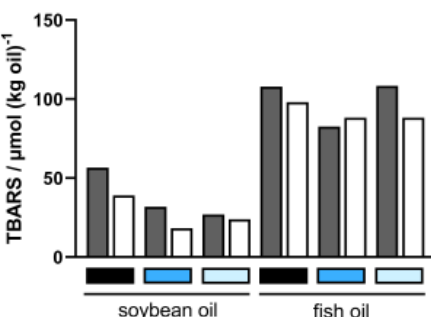


Fig. 4: Secondary oxidation products (measured by TBARS assay) of autoclaved emulsions to investigate the effect of the backpressure module on oxidation (n=1)

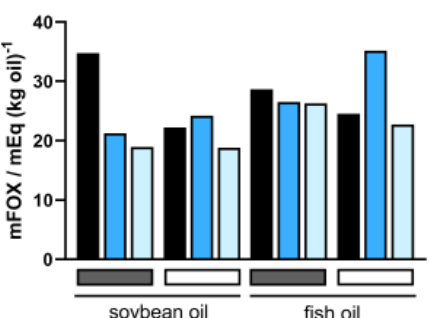


Fig. 6: Influence of the cooling system on primary oxidation products of emulsions right after manufacturing (n=1)

## RESULTS & DISCUSSION

The HL60 HPH is by default not equipped with a backpressure module and only with a small cooling unit. From larger scale devices the potential benefit of extending the cooling unit as well as alleviating the pressure drop was known. The design of these preliminary experiments allows us to draw first conclusions although each combination of conditions was investigated only once so far.

### Droplet size:

In general, droplets of emulsions with fish oil were smaller in size than droplets of emulsions with soybean oil, due to the lower oil content, but independent of the use of the backpressure module. A trend towards smaller droplets when omitting any cooling was detected.

### Oxidation products:

While the levels of primary oxidation products were not significantly different between the emulsions with soybean and fish oil ( $p > 0.05$ ), the levels of secondary oxidation products were significantly higher ( $p < 0.01$ ) for fish-oil containing emulsions, independent of the experimental conditions. Due to the high degree in unsaturation fish oil is prone to oxidation. The levels of primary and secondary oxidation products in soybean oil-based emulsions were within the range of commercially available reference emulsions.

### Influence of backpressure and cooling:

Any effect of the backpressure module or cooling unit during the homogenization would be marginal compared to the influence of the oil source. We are currently comparing these results for primary and secondary oxidation products to the levels before homogenization to address the effect of the homogenization process itself.

## REFERENCES

- [1] Dermiş S, Can S, Doru B. Spectrosc Lett 2012; 45: 359-365
- [2] Alamed J, McClements DJ, Decker EA. Food Chem 2006; 95: 585-590

## ACKNOWLEDGEMENT

This project is funded by a Sinergia team grant by the Swiss National Science Foundation SNF (project CRSII5\_177225).



## CONTACT INFORMATION

S. LEHNER: selehne@ethz.ch  
G. HOLTZHAUER: gregoryh@ethz.ch

## CONCLUSION

Backpressure and cooling during the high-pressure homogenization had marginal effects on primary and secondary oxidation products of the lipid emulsions. A trend towards smaller droplet sizes when omitting the cooling unit was detected. The main difference in droplet size and secondary oxidation products were assigned to the type of oil in the emulsion. Droplet size was smaller and secondary oxidation product levels were higher when fish oil was used instead of soybean oil. We are currently investigating the effect of the high-pressure homogenization itself on the oxidation of the lipids. Generally, no striking benefit of upgrading the standard HL60 setup with installation of a backpressure module or extending the cooling unit was found.



# Colonic Capsules for Bacterial Suspensions

P - II - 12



**SAPhS**  
Swiss Academy of  
Pharmaceutical  
Sciences

SPHSD 2021

## Introduction

The human microbiome comprises archaea, yeasts, fungi, viruses and other eucaryotic colonizers and a large community of aerobic and anaerobic bacteria composed of at least 500-1000 different species. [1]

It modulates the metabolism of the host and the barrier function of the gut epithelium, induces immunological functions as well as the suppression of pathogens. [2]

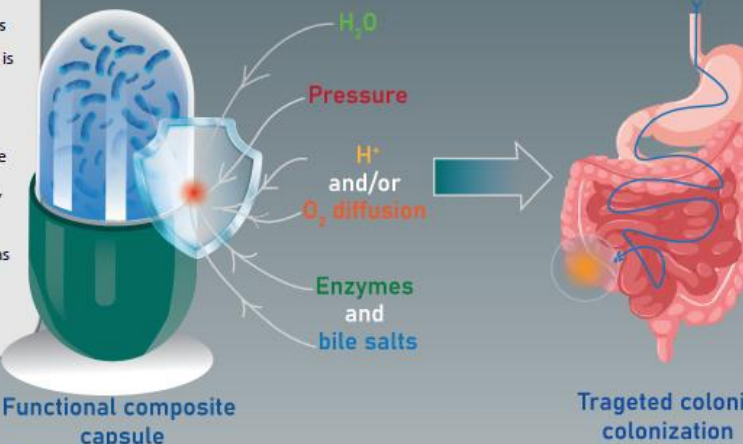
While promising, the administration of "therapeutic" bacteria in a dry state with classical dosage forms (e.g. enteric-coated capsules and tablets), leads to a significant loss of survival, requiring high doses to obtain a therapeutic effect. [3]

## Aim

Engineering a capsule capable of delivering orally aqueous suspensions of microorganisms to avoid the drying step, which is associated in loss of survival.

This capsule made of composite materials will protect bacteria, against the low stomach pH, enzymes and bile salts as well as oxygen in case of anaerobic strains.

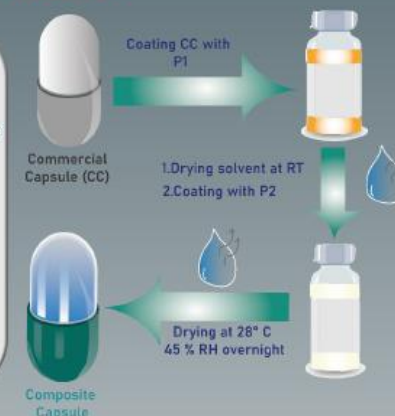
Live bacteria in aqueous suspension



## Methods

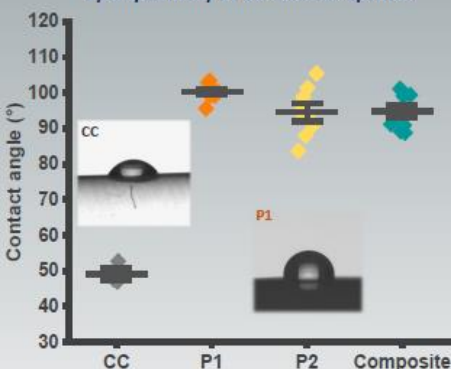
HPMC capsules were dip-coated with various cellulose derivatives (P1) and methacrylic acid copolymers (Eudragit S100) (P2) mixed with hydrophobic plasticizers, to render them more hydrophobic and pH-sensitive.

Those layers were characterized with respect of their thickness as well as their hydrophobicity.



## Results and Discussion

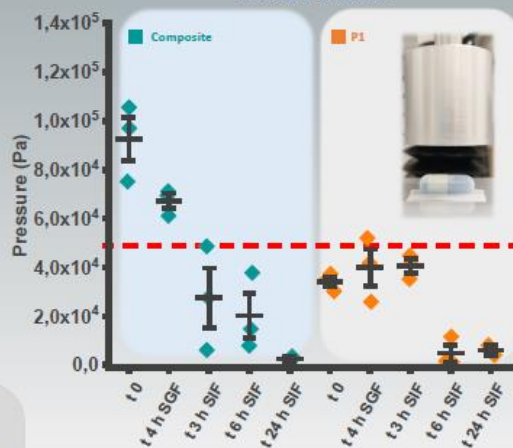
### Hydrophobicity of the coated capsules



Commercial capsules (CC) are hydrophilic ( $CA \leq 50^\circ$ ) while the capsules coated with P1 and P2 as well as the composite are more hydrophobic ( $CA \geq 90^\circ$ ).

The composite coating allows the introduction of an aqueous medium in the capsule without inducing its quick dissolution.

### Pressure at break



t0: Time when the capsule is filled with aqueous medium

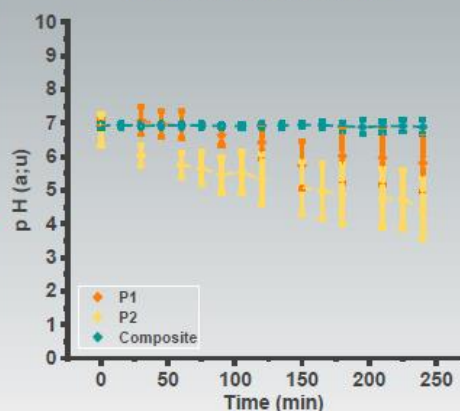
tx: Time the capsule was subjected to disintegration test in the corresponding fluid

SGF: Simulated gastric fluid pH = 1

SIF: Simulated intestinal fluid pH = 6.8

The composite capsule should sustain the pressure in the stomach ( $P > 5.10^4$  Pa) and the small intestine ( $P > 2.10^4$  Pa) based on the results from compression tests.

### H<sup>+</sup> diffusion inside the capsule



The composite capsule prevents the acidification of the loaded fluid when incubated for 4 h in SGF.

P1 and P2 alone cannot maintain a neutral pH inside the capsules.

### Disintegration of the composite capsule



Disintegration tests confirmed that the composite system should keep its content during the transit in the gastrointestinal tract. Release will occur when the capsules pressure at break drops below  $2.10^4$  Pa (after 6 h in SIF).

## Conclusion and Outlook

Stable composite capsules that contain aqueous suspensions were successfully engineered.



O<sub>2</sub> diffusion is the next property to be assessed.

## References

- [1] 10.1126/science.1080029
- [2] 10.1038/ni.2847
- [3] 10.1111/1751-7915.12880





C. Becker<sup>1,2</sup>, L. Eggenschwiler<sup>3</sup>, S.S. Jick<sup>4</sup> and C.R. Meier<sup>1,2,4</sup>

<sup>1</sup>Basel Pharmacoepidemiology Unit, Division of Clinical Pharmacy and Epidemiology, Department of Pharmaceutical Sciences, University of Basel, 4003 Basel, Switzerland

<sup>2</sup>Hospital Pharmacy, University Hospital Basel, 4056 Basel, Switzerland

<sup>3</sup>Department of Ophthalmology, University Hospital Basel, 4003 Basel, Switzerland

<sup>4</sup>Boston Collaborative Drug Surveillance Program, Boston University School of Public Health, 02421 Lexington, Massachusetts, USA

## INTRODUCTION

Previous research suggests a link between cataract and Alzheimer's disease (AD), as postulated by one observational study [1].

## AIMS

To analyse the incidence of AD in patients with or without cataract

## METHODS

**Study design:**  
Retrospective cohort study

**Source population:**  
Patients registered with the UK-based Clinical Practice Research Datalink (CPRD) aged  $\geq 40$  years

**Study period:** Jan 1995 to Dec 2019

**Exposed cohort:**  
Patients with a first-time cataract (diagnosis or cataract extraction)

**Comparison cohort:**  
Random sample of general population, matched 1:1 to each patient from the exposed cohort on age, sex, general practitioner, date of cataract recording

**Exclusion criteria:**  
Diagnosis of vascular or other dementias at any time or anti-AD medication before cohort entry

**Outcome definition:**  
Diagnosis (Dx) of AD,  $\geq 1$  prescriptions (Rx) for an anti-AD drug, the 1<sup>st</sup> Dx and 1<sup>st</sup> Rx should be within 6 months

**Statistical analysis:**  
Follow-up and assessment of person-time at risk (person-years, py) as well as number of events in each cohort. Calculation of incidence rates (IR) and incidence rate ratios (IRR) with 95% confidence intervals (CI)

**Sensitivity analyses:**  
a) Outcome as previously plus individuals with a diagnosis of 'unspecified dementia' and  $\geq 2$  Rx for anti-AD drugs  
b) Outcome as in a) plus individuals with a diagnosis of AD and one of the following: specific dementia test, referral to an AD specialist, assessment based on neuroimaging techniques,  $\geq 2$  recorded dementia symptoms

## RESULTS

We identified 403'564 patients with a 1<sup>st</sup>-time cataract and an equal amount of cataract free individuals.  
Figure 1 shows the selection process of the cataract cohort.

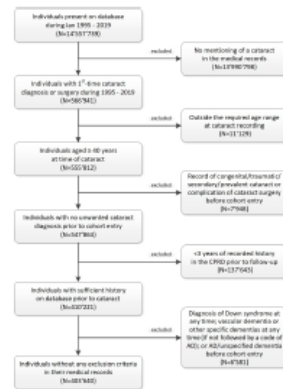


Figure 1. Number of included patients with cataract after application of the exclusion criteria

During follow-up, we identified 5'932 cataract patients with AD as well as 5'944 AD cases among the comparisons.  
The incidence of AD was slightly lower in individuals with a previous cataract and the results for the two sexes differed only slightly (Figure 2).  
However, patients with a previous cataract aged  $>79$  years had a lower incidence of AD compared with individuals of the same age but no recording of a cataract (IRR 0.75, 95% CI 0.72-0.78, Figure 3).  
The results of the sensitivity analyses remained unchanged.

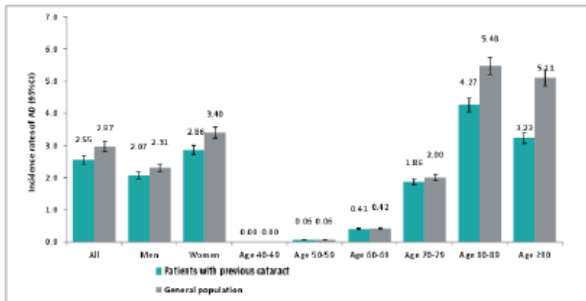


Figure 2. Incidence rates of AD in individuals with a previous cataract and in controls without a recording of a cataract

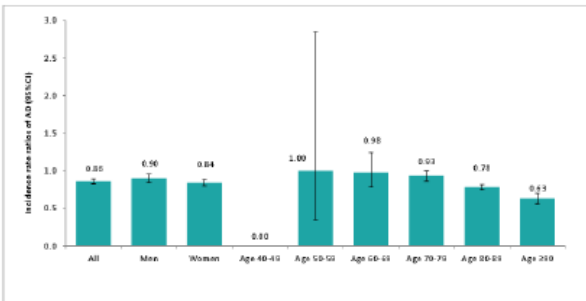


Figure 3. Incidence rate ratios of AD in individuals with a previous cataract compared to controls without a recording of a cataract

## DISCUSSION & CONCLUSIONS

In contrast to a previous study, we did not observe an increased risk of AD in patients with cataract compared to the general population.

## REFERENCES

Lai SW et al. Cataract may be a non-memory feature of Alzheimer's disease in older people. Eur J Epidemiol 2014;29(6):405-9

## CONTACT INFORMATION

Claudia.Becker@usb.ch

# Changes in Serum Creatinine during and after Pregnancy in a Cohort of Women with or without pre-existing Chronic Kidney Disease

C. Marxer<sup>1,2</sup>, K. Hagberg<sup>1,2</sup>, J. Paik<sup>1,2</sup>, M. Zhuo<sup>1,2</sup>, R. Desai<sup>1,2</sup>, S. Jick<sup>1,2</sup>, C. Meier<sup>1,2</sup>, and J. Spoendlin<sup>1,2</sup>

<sup>1</sup> Hospital Pharmacy, University Hospital Basel, Basel, Switzerland; <sup>2</sup> Basel Pharmacoepidemiology Unit, Division of Clinical Pharmacy and Epidemiology, Department of Pharmaceutical Sciences, University of Basel, Basel, Switzerland; <sup>3</sup> Boston Collaborative Drug Surveillance Program, Lexington, MA, United States; <sup>4</sup> Division of Pharmacoepidemiology and Pharmacoeconomics, Department of Medicine, Brigham and Women's Hospital, Harvard Medical School, Boston, MA, United States; <sup>5</sup> Renal Division, Department of Medicine, Brigham and Women's Hospital, Harvard Medical School, Boston, MA, United States; <sup>6</sup> Renal Division, Department of Medicine, Beth Israel Deaconess Medical Center, Harvard Medical School, Boston, MA, United States; <sup>7</sup> Boston University School of Public Health, Boston, MA, United States

SWISS  
PHARMA  
SCIENCE DAY  
2021



P - III - 2

SAPhS  
Swiss Academy of  
Pharmaceutical  
Sciences

## INTRODUCTION

It has been suggested that kidneys of women with chronic kidney disease (CKD) may not sufficiently adapt to physiological changes during pregnancy, but evidence is sparse.[1-4]

## AIMS

The objective of this study was to describe pregnant women with or without CKD in terms of demographics, comorbidities, and changes in serum creatinine levels over the course of pregnancy and until one year after delivery.

## METHODS

### Data source

- Clinical Practice Research Datalink (CPRD) GOLD
- UK-based longitudinal primary care database
- Information: drug prescriptions, diagnoses, demographics, certain life-style factors, lab results, referrals to and diagnoses from secondary care

### Study design: Descriptive study

Study period: 1.1.2000 – 31.12.2019

**Study population:** All pregnancies of women aged 18-55 years with a singleton live-birth (extraction of pregnancies by Read codes indicating delivery). Definitions are shown in Figure 1.

### Inclusion criteria:

- ≥ 2 serum creatinine (SCr) values during the total study period (see Figure 1)
- ≥ 1 SCr value during baseline or trimester 1

**Exclusion criteria:** Pregnancy during baseline or post-pregnancy period; dialysis, kidney transplantation, HIV or drug abuse any time before end of study period; acute kidney disease during study period

### Last menstrual period (estimated):

- Recorded date of LMP (recorded Read code within 310 days before delivery date\*)
- Delivery date\* - 245 days (if preterm delivery recording within 90 days before or after delivery date)
- Otherwise, LMP was delivery date\* - 280 days

\*delivery date = date of first recorded Read code for a delivery during any time period of 134 days

**Categorization of pre-existing CKD:** Estimated based on mean eGFR (CKD-EPI formula) in baseline and trimester 1 (pre-existing CKD is defined as mean eGFR < 90 ml/min/1.73m<sup>2</sup>):

- Moderate-severe CKD (eGFR < 60 ml/min/1.73m<sup>2</sup>)
- Mild CKD (eGFR 60-90 ml/min/1.73m<sup>2</sup>)
- No CKD (eGFR ≥ 90 ml/min/1.73m<sup>2</sup>)

**Statistical analysis:** We calculated the percentage change of period (definition: see Figure 1) mean SCr levels after each period and determined the mean difference of SCr between baseline and post-pregnancy period in all groups separately.

## RESULTS

**Characterization of the study population:** We extracted 3'492'634 pregnancies resulting in live-birth, of which 40'888 pregnancies (38'968 women) met all inclusion and exclusion criteria (Table 1).

### Change in serum creatinine levels (Figure 2):

- We observed the greatest decline in SCr in trimester 1 and 2 in all three groups (moderate-severe CKD: -15.2%, mild CKD: -21.9%, no CKD: -25.4%).
- The greatest increase in SCr levels was observed between trimester 3 and post-pregnancy period 1 in pregnancies with mild and without CKD, and between trimester 2 and trimester 3 in pregnancies with moderate-severe CKD.
- The difference in mean SCr levels [μmol/L] between baseline and post-pregnancy period was +1.6 in pregnancies with moderate-severe CKD, -5.6 in pregnancies with mild CKD, and 0.0 in pregnancies without CKD.

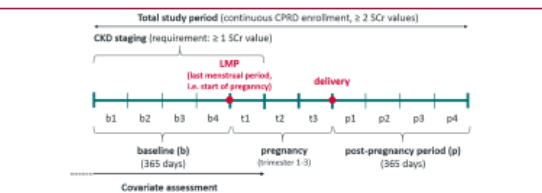


Figure 1: Graphical illustration of time periods of one pregnancy (1 period = 93.3 days, i.e. 1 period has the length of one trimester)

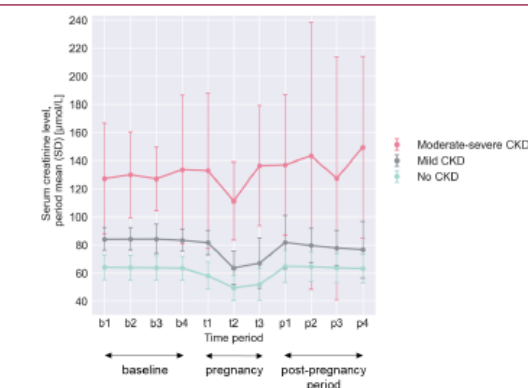


Figure 2: Period mean serum creatinine levels (SD) in baseline (b1-b4), trimester 1-3 (t1-t3), and in post-pregnancy period (p1-p4) by severity of CKD

Table 1: Renal filtration parameters and baseline characteristics of the study population by severity of CKD

	No CKD (eGFR ≥ 90 ml/min/1.73m <sup>2</sup> )	Mild CKD (eGFR 60-90 ml/min/1.73m <sup>2</sup> )	Moderate-severe CKD (eGFR < 60 ml/min/1.73m <sup>2</sup> )
Age at delivery [years], median [IQR]	30.0 [26.0,34.0]	33.0 [29.0,37.0]	33.5 [30.0,37.8]
Renal filtration:			
eGFR [ml/min/1.73m <sup>2</sup> ] in baseline/trimester 1, mean (SD)	112.9 (13.2)	81.4 (8.7)	50.2 (10.3)
SCr [μmol/L] in baseline/trimester 1, mean (SD)	62.3 (9.3)	83.5 (8.8)	130.3 (42.1)
N SCr values in total study period	97'562	17'332	761
N SCr values per pregnancy in baseline/trimester 1, median [IQR]	1 [1, 2]	1 [1, 2]	1 [1, 2]
N SCr values per pregnancy in total study period, median [IQR]	2 [2, 3]	2 [2, 3]	3 [2, 5]
Comorbidities:			
Overweight or obesity	11352 (32.9)	2074 (33.2)	57 (37.0)
Pre-existing diabetes	3468 (10.1)	593 (9.5)	23 (14.9)
Pre-existing hypertension	6455 (18.7)	1373 (22.0)	71 (46.1)
Systemic autoimmune disorder*	664 (1.9)	136 (2.2)	5 (3.2)
Immune-mediated kidney disease*	202 (0.6)	53 (0.8)	5 (3.5)
Non-immune-mediated kidney disease*	114 (0.3)	53 (0.8)	22 (15.5)

Values are the number (%) unless indicated otherwise.

\* Systemic lupus erythematoses and/or rheumatoid arthritis or other inflammatory polyarthropathies and/or Sjögren syndrome or Sicca syndrome and/or dermatomyositis or polymyositis and/or systemic sclerosis and/or other connective tissue disease

\* Chronic glomerulonephritis and/or vasculitis and/or hemolytic uremic syndrome

\* Cystic kidney disease and/or other miscellaneous other non-immune-mediated renal disease

## DISCUSSION & CONCLUSIONS

- All three CKD severity groups share similar trends of SCr levels during pregnancy (decline between trimester 1 and 2 in all groups, but most in women with moderate-severe CKD), but SCr levels increased in post-pregnancy period in women with moderate-severe CKD while the other two groups did not.
- SCr levels in women without CKD return to baseline after delivery. In women with moderate-severe CKD, SCr levels were higher after delivery compared to baseline, which may indicate a permanent damage of kidneys after pregnancy.
- Sample size in the moderate-severe CKD group was small and results have to be interpreted carefully.
- This study highlights the need to carefully monitor renal function during pregnancy in women with pre-existing CKD, especially in the case of severe renal impairment.

## REFERENCES

- Kendrick J, Sharma S, Holmen J, Palit S, Nuccio E CM. Kidney Disease and Maternal and Fetal Outcomes in Pregnancy. Am J Kidney Dis. 2015;25(3):289–313.
- Bharti J, Vatsa R, Singhal S, Roy KK, Kumar S, Perumal V, et al. Pregnancy with chronic kidney disease: maternal and fetal outcome. Eur J Obstet Gynecol Reprod Biol [Internet]. 2016;204:83–7.
- Harel Z, McArthur E, Hladunewich M, Dirk JS, Wald R, Garg AX, et al. Serum Creatinine Levels Before, During, and after Pregnancy. JAMA - J Am Med Assoc. 2019;321(2):205–7.
- Imbasciati E, Gregorini G, Cabiddu G, Gammato L, Ambrosio G, Del Giudice A, et al. Pregnancy in CKD Stages 3 to 5: Fetal and Maternal Outcomes. Am J Kidney Dis. 2007;49(6):753–62.

## CONTACT INFORMATION

caroleanna.marxer@usb.ch



# Patient Groups in Rheumatoid Arthritis Identified by Deep Learning Respond Differently to Biologic or Targeted Synthetic disease modifying antirheumatic drugs

M. Kalweit<sup>1</sup>, A.M. Burden<sup>2</sup>, T. Hügler<sup>3</sup>, T. Burkard<sup>2</sup>

<sup>1</sup> *Neuroinformatics Lab, University of Freiburg, 79085 Freiburg, Germany*  
<sup>2</sup> *ETH Zurich, Department of Chemistry and Applied Biosciences, Zurich, 8093 Zurich, Switzerland*  
<sup>3</sup> *Department of Rheumatology, Lausanne University Hospital, and University of Lausanne, 1011 Lausanne, Switzerland*

## INTRODUCTION

Cycling of biologic or targeted synthetic disease modifying antirheumatic drugs (b/tsDMARDs) in rheumatoid arthritis (RA) patients due to non-response is a problem preventing and delaying disease control.

## AIMS

To assess and validate treatment response of b/tsDMARDs among RA patients groups identified by deep learning.

## METHODS

**Data source and study period:** Swiss Clinical Quality Validation Programme in Rheumatic Diseases (SCQM) [1999 and 2018]  
**Study design:** cohort study  
**Study population:** RA patients with first-time b/tsDMARD use (cohort entry) and a record of a disease activity measurement using 28 joints and erythrocyte sedimentation rate (DAS28-esr)  $\geq 0$  months before cohort entry  
**Features:** demographics, life-style factors, clinical information (e.g. sex, seropositivity, pain level, number of tender joints), other medication (i.e. conventional synthetic [cs] DMARDs)  
**Clustering:** At cohort entry, we clustered patients several times using a deep embedded clustering in combination with an adaptive deep adaptive neural network (Figure 1) to create 3, 4, and 5 clusters with 2 different specifications (i.e. a total of 24 clusters).

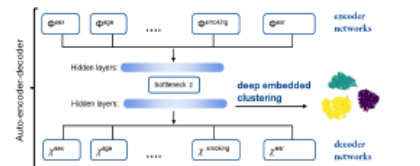


**Figure 1.** Scheme of the adaptive deep neural network architecture. AnyNet-Autoencoder with deep embedded clustering. The features can either be numerical or categorical. The latent bottleneck representation  $z$  is a low-dimensional vector representing the patient. The encoder layer consists of 1024 hidden dimensions, the decoder layer of 64 hidden dimensions.

**Outcomes:** Within 15 months after cohort entry, we assessed b/tsDMARD stop due to non response, and separately a  $\geq 20\%$  reduction in DAS28-esr as a proxy for treatment response  
**Data analysis:** We described patient characteristics overall and visually inspected each cluster. Because findings resulting from individual clusters are not robust and each cluster was similar in patient characteristics to at least one other cluster, we grouped clusters according to most distinct patient characteristics  
We assessed comparative effectiveness of b/tsDMARDs using Cox proportional hazard regression in each cluster estimating hazard ratios (HR) with 95% confidence intervals (CI). Because findings from individual clusters may be chance findings, we compared results among clusters belonging to the same group  
Stratification is the preferred method to validate comparative effectiveness results obtained in clusters because it makes results applicable to clinical practice by using fewer patient characteristics. Therefore, we validated results through stratified analyses according to most distinctive patient characteristics of each group of clusters (i.e. the grouping characteristics)

## RESULTS

- Clusters comprised between 362 and 1481 patients per cluster among 3516 unique patients. Overall, at their first b/tsDMARD use, patients had a mean age of 55 years and 76% were women. Median RA duration of patients was 6 years, 66% were rheumatoid factor positive, mean DAS28-esr was 4.3, and 77% of patients concomitantly used at least 1 csDMARD.
- Figure 2 depicts a 2D latent representation of clusters and suggests a very good clustering (data points within a cluster are close together and all clusters are equally spread around the center)
- Most distinct patient characteristics between clusters – given visual inspection – were sex, seropositivity, individual csDMARD use, prednisone use, measures of RA activity and pain, and RA duration. These features were used to group clusters manually into 5 distinct cluster groups:

**1<sup>st</sup> group:** Clusters of patients with highest frequencies of individual csDMARD and prednisone use and a tendency towards seropositivity and no family history of rheumatic diseases. Clusters in this group yielded a good response to tocilizumab (significant HRs of 2.55-2.67, depending on the cluster). In stratified analyses for validation purposes (see Table 1), among 728 patients with at least two csDMARDs and use of prednisone, we confirmed the good response to tocilizumab with an age and sex adjusted HR of 5.46 (95% CI 1.76-16.94) when compared to adalimumab. Furthermore, we observed a significant good response to golimumab and tofacitinib, and an increased risk of non-response to golimumab.  
**2<sup>nd</sup> group:** Clusters of men with highest frequency of smoking and mean body mass index. Clusters in this group yielded a good response to tocilizumab (significant HRs of 6.78-8.54, depending on the cluster). In stratified analyses (see Table 2), among 837 men, the good response to tocilizumab was confirmed with an age adjusted HR of 8.44 (95% CI 3.43-20.74). Moreover, we observed a significant good response to golimumab and tofacitinib, but also a significant non response to golimumab.  
**3<sup>rd</sup> group:** Clusters of seronegative patients with lowest frequency of prednisone use and a tendency towards a higher proportion of women. Clusters in this group yielded a high risk of non-response with golimumab (significant HRs of 2.10-2.53, depending on the clusters). In stratified analyses for validation purposes, among 590 seronegative patients without use of prednisone, an increased risk of non-response with golimumab was not confirmed (age and sex adjusted HR of 1.98, 95% CI 0.64-4.19). However, in a more specific population containing only women (n=459) [see Table 3], we observed a significant result of non-response with golimumab (age adjusted HR of 2.30, 95% CI 1.03-5.40).

**4<sup>th</sup> group:** Clusters of seropositive patients with a high disease burden/duration and a tendency towards a higher proportion of women. Clusters in this group yielded a high risk of non-response with golimumab (significant HRs of 2.45-4.54, depending on the clusters). In stratified analyses for validation purposes (see Table 4), among 717 patients with seropositivity and high disease burden/duration, we confirmed a high risk of non-response with golimumab with an age and sex adjusted HR of 3.75 (95% CI 1.54-9.12)  
**5<sup>th</sup> group:** Clusters of patients with low disease burden and a tendency towards seropositivity and a higher proportion of women. Clusters in this group yielded a good response to golimumab (significant HRs of 2.56-3.15, depending on the cluster) and tocilizumab (significant HRs of 3.30-4.43, depending on the cluster). In stratified analyses for validation purposes (see Table 5), among both 2486 patients with low disease burden, we confirmed a good response to golimumab with an age and sex adjusted HR of 2.72 (95% CI 1.63-4.57) and a good response to tocilizumab with an age and sex adjusted HR of 3.64 (95% CI 2.04-6.49). Furthermore, we observed significant good responses to tofacitinib, and a significant non-response to golimumab.

Table 3. Comparative effectiveness analyses in the stratum of patients with low disease burden						
Treatment disc. due to non-response	Cross HR (95% CI)	Age and sex adjusted HR (95% CI)	20% DAS28-esr reduction	Cross HR (95% CI)	Age and sex adjusted HR (95% CI)	
TNF-inhibitor	228	Ref 1.00 *	Ref 1.00 *	140	Ref 1.00 *	Ref 1.00 *
Adalimumab	1	Ref 1.00 *	Ref 1.00 *	1	Ref 1.00 *	Ref 1.00 *
Certolizumab	7	1.41 (0.65-3.03)	1.41 (0.65-3.03)	6	2.36 (1.00-5.96)	2.31 (0.86-6.43)
Etanercept	59	0.71 (0.51-0.99)	0.71 (0.51-0.99)	51	1.21 (0.81-1.82)	1.23 (0.82-1.86)
Golimumab	42	2.51 (1.79-3.54)	2.51 (1.79-3.54)	22	2.72 (1.62-4.56)	2.72 (1.62-4.57)
Infliximab	21	0.69 (0.46-1.05)	0.69 (0.46-1.05)	19	0.92 (0.52-1.57)	0.91 (0.52-1.57)
Non-TNF-inh.	37	1.17 (0.83-1.66)	1.18 (0.86-1.67)	29	1.54 (1.06-2.36)	1.60 (1.09-2.45)
Abatacept	21	1.40 (0.86-2.26)	1.39 (0.86-2.26)	8	1.11 (0.52-2.37)	1.13 (0.52-2.42)
Rituximab	3	NA	NA	5	1.90 (0.60-5.80)	3.57 (0.63-20.88)
Tocilizumab	13	1.16 (0.65-2.09)	1.16 (0.65-2.09)	16	3.49 (1.96-6.21)	3.64 (2.04-6.49)
JAK-inhibitor	6	0.80 (0.36-1.81)	0.80 (0.36-1.81)	13	2.97 (1.68-5.25)	3.00 (1.69-5.31)
Baricitinib	0	NA	NA	2	NA	NA
Tofacitinib	6	0.80 (0.35-1.84)	0.80 (0.35-1.84)	11	3.21 (1.67-6.28)	3.22 (1.65-6.27)

CI: confidence interval; Disc.: discontinuation; esr: erythrocyte sedimentation rate; HR: hazard ratio; inh.: inhibitor; JAK: janus kinase; TNF: tumor necrosis factor alpha; \*The reference group in class effect analyses was TNF inhibitors; \*The reference group in individual b/tsDMARD analyses was adalimumab

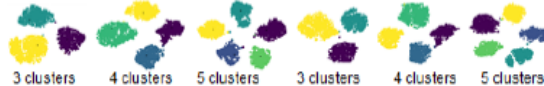


**Figure 2.** 2D latent representation of all 24 patient clusters identified through the deep embedded clustering yielding 3, 4, and 5 clusters in various clustering runs. Different colors denote the different cluster assignments.

Table 1. Comparative effectiveness analyses in strata of patients with use of at least 2 csDMARDs and prednisone						
Treatment disc. due to non-response	Cross HR (95% CI)	Age and sex adjusted HR (95% CI)	20% DAS28-esr reduction	Cross HR (95% CI)	Age and sex adjusted HR (95% CI)	
TNF-inhibitor	83	Ref 1.00 *	Ref 1.00 *	37	Ref 1.00 *	Ref 1.00 *
Adalimumab	33	Ref 1.00 *	Ref 1.00 *	8	Ref 1.00 *	Ref 1.00 *
Certolizumab	3	NA	NA	2	NA	NA
Etanercept	23	0.81 (0.46-1.39)	0.84 (0.49-1.43)	13	1.97 (0.82-4.76)	2.01 (0.80-4.96)
Golimumab	13	3.10 (1.65-5.96)	3.47 (1.83-6.68)	7	7.75 (3.80-15.46)	8.27 (3.86-18.11)
Infliximab	11	0.60 (0.31-1.20)	0.61 (0.31-1.20)	7	1.83 (0.66-5.05)	1.83 (0.66-5.04)
Non-TNF-inh.	12	0.81 (0.46-1.49)	0.79 (0.45-1.47)	10	1.62 (0.80-3.26)	1.60 (0.78-3.26)
Abatacept	5	NA	NA	3	NA	NA
Rituximab	2	NA	NA	2	NA	NA
Tocilizumab	5	1.12 (0.46-2.87)	1.17 (0.45-3.01)	5	5.36 (1.75-16.44)	5.46 (1.76-16.94)
JAK-inhibitor	4	NA	NA	5	6.33 (2.67-15.00)	6.09 (2.35-16.76)
Baricitinib	0	NA	NA	1	NA	NA
Tofacitinib	4	NA	NA	5	10.22 (3.33-31.30)	9.37 (3.02-29.31)

CI: confidence interval; Disc.: discontinuation; esr: erythrocyte sedimentation rate; HR: hazard ratio; inh.: inhibitor; JAK: janus kinase; TNF: tumor necrosis factor alpha; \*The reference group in class effect analyses was TNF inhibitors; \*The reference group in individual b/tsDMARD analyses was adalimumab

Table 2. Comparative effectiveness analyses in men stratum						
Treatment disc. due to non-response	Cross HR (95% CI)	Age and sex adjusted HR (95% CI)	20% DAS28-esr reduction	Cross HR (95% CI)	Age and sex adjusted HR (95% CI)	
TNF-inhibitor	87	Ref 1.00 *	Ref 1.00 *	53	Ref 1.00 *	Ref 1.00 *
Adalimumab	37	Ref 1.00 *	Ref 1.00 *	16	Ref 1.00 *	Ref 1.00 *
Certolizumab	1	NA	NA	1	NA	NA
Etanercept	25	0.81 (0.45-1.35)	0.81 (0.45-1.35)	18	1.45 (0.74-2.84)	1.44 (0.74-2.83)
Golimumab	13	2.24 (1.19-4.21)	2.22 (1.18-4.18)	8	2.96 (1.27-6.92)	2.83 (1.25-6.68)
Infliximab	11	0.54 (0.28-1.06)	0.54 (0.27-1.05)	10	1.23 (0.56-2.71)	1.22 (0.55-2.70)
Non-TNF-inh.	13	1.35 (0.75-2.43)	1.35 (0.75-2.43)	11	2.24 (1.06-5.08)	2.12 (1.04-4.08)
Abatacept	7	1.26 (0.56-2.82)	1.27 (0.57-2.87)	0	NA	NA
Rituximab	2	NA	NA	4	NA	NA
Tocilizumab	4	NA	NA	7	8.59 (3.52-20.94)	8.46 (3.43-20.94)
JAK-inhibitor	3	NA	NA	6	3.77 (1.65-8.71)	3.94 (1.68-9.22)
Baricitinib	0	NA	NA	0	NA	NA
Tofacitinib	3	NA	NA	5	5.03 (1.97-12.96)	5.00 (1.96-13.06)

CI: confidence interval; Disc.: discontinuation; esr: erythrocyte sedimentation rate; HR: hazard ratio; inh.: inhibitor; JAK: janus kinase; TNF: tumor necrosis factor alpha; \*The reference group in class effect analyses was TNF inhibitors; \*The reference group in individual b/tsDMARD analyses was adalimumab

Table 3. Comparative effectiveness analyses in strata of seronegative women without use of prednisone						
Treatment disc. due to non-response	Cross HR (95% CI)	Age and sex adjusted HR (95% CI)	20% DAS28-esr reduction	Cross HR (95% CI)	Age and sex adjusted HR (95% CI)	
TNF-inhibitor	56	Ref 1.00 *	Ref 1.00 *	34	Ref 1.00 *	Ref 1.00 *
Adalimumab	15	Ref 1.00 *	Ref 1.00 *	10	Ref 1.00 *	Ref 1.00 *
Certolizumab	3	NA	NA	1	NA	NA
Etanercept	20	1.02 (0.52-2.00)	1.11 (0.57-2.18)	14	1.07 (0.46-2.41)	1.06 (0.46-2.43)
Golimumab	9	2.25 (0.95-5.41)	2.36 (1.03-5.40)	2	NA	NA
Infliximab	9	1.20 (0.52-2.73)	1.17 (0.51-2.68)	7	1.34 (0.51-3.53)	1.34 (0.51-3.53)
Non-TNF-inh.	7	1.02 (0.62-1.64)	0.90 (0.42-1.94)	5	1.21 (0.47-3.10)	1.21 (0.47-3.10)
Abatacept	6	2.29 (0.89-5.90)	2.23 (0.87-5.76)	2	NA	NA
Rituximab	0	NA	NA	1	NA	NA
Tocilizumab	1	NA	NA	2	NA	NA
JAK-inhibitor	1	NA	NA	1	NA	NA
Baricitinib	0	NA	NA	0	NA	NA
Tofacitinib	1	NA	NA	0	NA	NA

CI: confidence interval; Disc.: discontinuation; esr: erythrocyte sedimentation rate; HR: hazard ratio; inh.: inhibitor; JAK: janus kinase; TNF: tumor necrosis factor alpha; \*The reference group in class effect analyses was TNF inhibitors; \*The reference group in individual b/tsDMARD analyses was adalimumab

Table 4. Comparative effectiveness analyses in the stratum of patients with seropositivity, with high disease burden and disease duration						
Treatment disc. due to non-response	Cross HR (95% CI)	Age and sex adjusted HR (95% CI)	20% DAS28-esr reduction	Cross HR (95% CI)	Age and sex adjusted HR (95% CI)	
TNF-inhibitor	62	Ref 1.00 *	Ref 1.00 *	44	Ref 1.00 *	Ref 1.00 *
Adalimumab	26	Ref 1.00 *	Ref 1.00 *	16	Ref 1.00 *	Ref 1.00 *
Certolizumab	0	NA	NA	0	NA	NA
Etanercept	18	0.59 (0.32-1.00)	0.59 (0.32-1.00)	16	0.86 (0.44-1.68)	0.82 (0.42-1.63)
Golimumab	6	3.74 (1.54-9.08)	3.79 (1.54-9.12)	2	NA	NA
Infliximab	12	0.68 (0.34-1.31)	0.68 (0.34-1.31)	9	0.81 (0.31-2.14)	0.82 (0.31-2.14)
Non-TNF-inh.	6	0.87 (0.38-2.00)	0.87 (0.37-2.05)	5	1.13 (0.45-2.94)	1.10 (0.44-2.78)
Abatacept	3	NA	NA	1	NA	NA
Rituximab	1	NA	NA	2	NA	NA
Tocilizumab	2	NA	NA	1	NA	NA
JAK-inhibitor	0	NA	NA	4	NA	NA
Baricitinib	0	NA	NA	3	NA	NA
Tofacitinib	0	NA	NA	1	NA	NA

CI: confidence interval; Disc.: discontinuation; esr: erythrocyte sedimentation rate; HR: hazard ratio; inh.: inhibitor; JAK: janus kinase; TNF: tumor necrosis factor alpha; \*The reference group in class effect analyses was TNF inhibitors; \*The reference group in individual b/tsDMARD analyses was adalimumab

## DISCUSSION & CONCLUSIONS

The deep embedded clustering identified several important characteristics by which the machine learning algorithm differentiated between clusters: sex, seropositivity, disease activity, disease duration, csDMARD, and prednisone use. Furthermore, comparative effectiveness analyses of b/tsDMARDs among groups suggests that the optimal first-line b/tsDMARD may differ based on identified phenotype. Results were validated using stratified analyses with fewer, most important features to make results applicable for clinical practice.

Non-response to golimumab among seronegative women without use of prednisone as well as seropositive patients with higher disease burden and duration may suggest to avoid this treatment in these patients. However, no other significant findings were identified in these strata to help with treatment choice. Thus, adalimumab, the reference treatment may be a suggestion; especially since a study which assessed patient characteristics associated with treatment response to adalimumab suggested also that concomitant csDMARD use as well as a high disease burden was predictive of treatment response.[1]

A study assessing drug survival of golimumab within 2 years was not able to identify predictors of response to golimumab [2]. In our study, 3 strata (patients with at least two csDMARDs and prednisone use at b/tsDMARD initiation, male patients, as well as patients with a lower disease burden) yielded a good response to golimumab. Yet, it is likely that response was not sufficient to persist on golimumab therapy given the equally increased risk of treatment discontinuation with golimumab. This may have been due to our outcome proxy for good response which was defined as a  $\geq 20\%$  reduction in DAS28-esr which only requires small improvement but yielded a sufficient number of outcomes to perform analyses.

The same 3 strata (patients with at least two csDMARDs and prednisone use at b/tsDMARD initiation, male patients, as well as patients with a lower disease burden) further yielded a good response to tofacitinib and tocilizumab. Our results are not consistent with another study suggesting that a higher disease burden is a predictor of treatment response to tocilizumab, however the outcome definition was different and the response was assessed after 6 months.[3] Nonetheless, attention should be paid to tofacitinib which was recently shown to have an early effect on pain reduction[4,5] which may work most efficiently in these 3 strata (i.e. patients with at least two csDMARDs and prednisone use at b/tsDMARD initiation, male patients, as well as patients with a lower disease burden).

To conclude, our study may suggest optimal first-line b/tsDMARD use in certain patient groups. This is a step forward towards personalizing treatment in RA patients. However, further research in other cohorts is needed to verify our results.

## REFERENCES

1. Kleinert, H.P., Tony, A., Krause et al. Impact of patient and disease characteristics on therapeutic success during adalimumab treatment of patients with rheumatoid arthritis: data from a German noninterventional observational study *Rheum Int* 2011;32:2759–2767
2. Yves-Marie Pers, Clémentine Fortunet, Elodie Constant et al. Predictors of response and remission in a large cohort of rheumatoid arthritis patients treated with tocilizumab in clinical practice. *Rheumatology* 2014;53:76–84
3. Florenzo Iannone, Leonardo Santo, Maria Grazia Anelli et al. Golimumab in real-life settings: 2 Years drug survival and predictors of clinical outcomes in rheumatoid arthritis, spondyloarthritis, and psoriatic arthritis. *Sem Arth Rheum* 2017;47:108–114
4. Karteev A, Filatova E, Pogodina E et al. THU006 A VERY EARLY (7-28 DAYS) RESPONSE ON JAK INHIBITOR TOFACITINIB IN PATIENTS WITH ACTIVE RHEUMATOID ARTHRITIS: EFFECT ON PAIN AND CENTRAL SENSITIZATION. *Ann Rheum Dis* 2020;79:327
5. Joseph C, Bilgrami SM, Ottewill L et al. THU0205 RESPONSE TO SMALL MOLECULES IS MOSTLY DRIVEN BY PATIENT GLOBAL ASSESSMENT OF DISEASE: A REAL WORLD OBSERVATION. *Ann Rheum Dis* 2020;79:327

## CONTACT INFORMATION

Dr. Theresa Burkard  
theresa.burkard@pharma.ethz.ch  
pharmacoepidemiology.ethz.ch



# Attitudes and Expectations of Patients on Home Parenteral Nutrition Towards eHealth



K. A. SCHÖNENBERGER<sup>1,2</sup>, E. REBER<sup>1</sup>, M. LEUENBERGER<sup>3</sup>, S. MÜHLEBACH<sup>2</sup>, Z. STANGA<sup>1</sup>  
<sup>1</sup> Department of Diabetes, Endocrinology, Nutritional Medicine and Metabolism, Inselspital, Bern University Hospital, University of Bern, Switzerland  
<sup>2</sup> Division of Clinical Pharmacy and Epidemiology, Department of Pharmaceutical Sciences, University of Basel, Switzerland  
<sup>3</sup> Department of Visceral Surgery and Medicine, Inselspital, Bern University Hospital, University of Bern, Switzerland

## INTRODUCTION

eHealth denotes the use of electronic tools in healthcare to improve processes and connect patients with health care personnel. We are developing an eHealth platform for home parenteral nutrition (HPN) patients, including video consultations, instructions (e.g. for patient education), and interaction with patient support groups. In addition, this platform will serve as a central repository for treatment- and care-related data for patients and medical staff.

## AIMS

For the creation and implementation of such an eHealth platform, our aim was to know the attitudes and expectations of HPN patients towards eHealth.

## METHODS

We conducted an anonymous survey on the attitudes and expectations of HPN patients towards eHealth. We interacted with patients in person or by phone. The questionnaire consisted of 18 questions on HPN care, familiarity and experience with digital devices, attitudes and expectations towards video consultations and other components of the intended platform.

## RESULTS

We included 27 HPN patients (63% females) looked after by two different HPN centers. Mean (SD) age was 56 (14) years and median (range) duration of HPN was 471 (29-5452) days. A majority of participants (n = 23, 85%) reported using a smartphone, tablet or computer and 17 (63%) rated their digital skills as proficient. Almost half of the participants (n = 11, 41%) found it cumbersome to go to the hospital for follow-up visits and 20 (74%) were open to video follow-up visits. Easy operation of the platform was important to 18 participants (67%). Few patients (6, 22%) were interested in connecting with other patients in support groups.

Table 1: Baseline characteristics

No. of participants	27
Female, n (%)	17 (63)
Age, years	mean (SD) 56 (14)
Parenteral nutrition:	median (range)
Duration, days	471 (29-5452)
Frequency, nights per week	7 (3-7)
Involved personnel:	n (%)
Physician specialized in PN	26 (96%)
General practitioner	3 (11%)
Spitex (home nurse)	18 (67%)
Possession of electronic devices:	n (%)
Cell phone	7 (26%)
Smartphone	20 (74%)
Tablet	10 (37%)
Computer	19 (70%)
None	0 (0%)

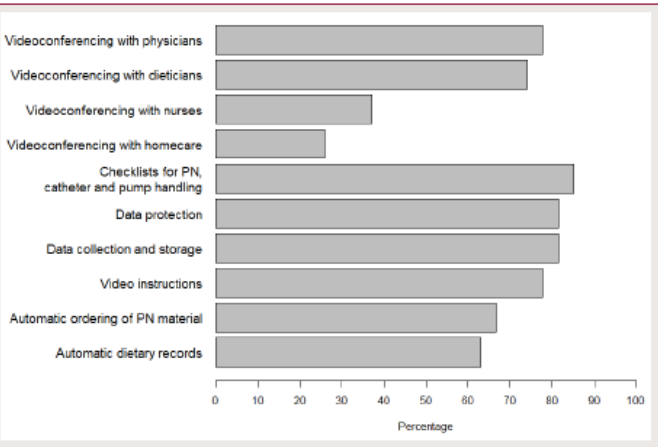


Figure 1: Percentage of participants who rated the proposed components of the platform as important

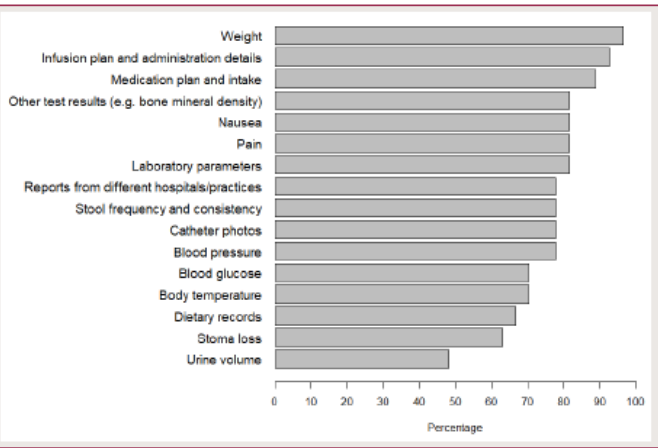


Figure 2: Percentage of participants who rated the proposed data to be stored and collected on the platform as important

## DISCUSSION & CONCLUSIONS

HPN patients are open towards an eHealth platform for care support, including video follow-up visits. Important criteria for the design of the eHealth platform were identified and confirmed by HPN patients. Such an eHealth platform has great potential for the care of HPN patients. We plan a validation study to evaluate the benefits of follow-up visits via videoconferencing versus in person usual care in those patients.

## CONTACT INFORMATION

Email: [katja.schoenenberger@extern.insel.ch](mailto:katja.schoenenberger@extern.insel.ch)



# Markers of Complement and Coagulation in Diabetes Patients treated with Dapagliflozin

SWISS  
PHARMA  
SCIENCE DAY  
2021



P - IV - 1

SAPhS  
Swiss Academy of  
Pharmaceutical  
Sciences

J. Anliker<sup>1</sup>, A. Melmer<sup>2</sup> and V. Schroeder<sup>1</sup>

<sup>1</sup> Experimental Haemostasis Group, Department for BioMedical Research (DBMR), University of Bern, 3008, Bern

<sup>2</sup> Department of Diabetes, Endocrinology, Nutritional Medicine and Metabolism, Inselspital, Bern University Hospital, University of Bern, 3010 Bern

## INTRODUCTION

Diabetes mellitus is a major cause of morbidity and mortality. It is characterised by an increase in blood glucose levels due to absolute (type 1 diabetes) or relative (type 2 diabetes) insulin deficiency.

Subjects with diabetes have an increased thrombotic tendency which can promote the development of cardiovascular diseases. This tendency is partially due to alterations in plasma levels of coagulation proteins.

Moreover, diabetes is associated with a proinflammatory state partially due to alterations in complement proteins.

## AIMS

A recent pilot study suggested that short-term dapagliflozin treatment in type 1 diabetes patients leads to a higher increase in the incretin hormone glucagon-like peptide-1 (GLP-1) following oral glucose intake than placebo treatment [1]. Since GLP-1 receptor agonists have been shown to inhibit thrombus formation, a treatment with dapagliflozin might have a beneficial impact on the thrombotic risk profile in type 1 diabetes patients. Therefore, the effects of a short-term dapagliflozin treatment for type 1 diabetes patients on the plasma levels of coagulation markers as well as complement markers were investigated in two pilot studies. It was focused on the markers known to be elevated in diabetes.

## METHODS

The participants of two cross-over intervention studies received 10 mg dapagliflozin or placebo per 7 days (Dapa01; 13 participants) and 17 days (Dapa02; 7 participants). Plasma samples were taken at baseline and after dapagliflozin and placebo treatment.

Plasma levels of complement and coagulation markers were quantified with sandwich ELISAs. Quantified complement markers were mannose-binding lectin, C3, and terminal complement complex. High-sensitivity C-reactive protein was measured as inflammatory marker. Quantified coagulation markers were tissue factor, factor VII, factor XIII, fibrinogen, DDimer, tissue plasminogen activator, and plasminogen activator inhibitor-1.

The patients' coagulation and fibrinolytic capacities were measured with a turbidimetric clot formation and lysis assay.

Statistical analysis was performed with IBM SPSS statistics 26. A dependent t-test for paired samples was performed for normally distributed markers and a paired Wilcoxon test for not normally distributed markers. An alpha-level of 0.05 was considered statistically significant.

## RESULTS

The Dapa01 study included 6 female and 7 male patients with a duration of type 1 diabetes between 7 and 36 years (average 24 years). Their ages were between 24 and 58 years with an average age of 41. Five patients had comorbidities and two had comedications. Three patients had diabetes-related complications.

The Dapa02 study included 5 female and 2 male patients with a duration of type 1 diabetes between 7 and 33 years (average 13 years). Their ages were between 21 and 47 years with an average age of 27. One patient had a comorbidity and 3 had comedications. None had diabetes-related complications.

After a week of dapagliflozin intake (Dapa01), there was no significant change in plasminogen activator inhibitor-1, fibrinogen, terminal complement complex, factor VII, tissue plasminogen activator, mannose-binding lectin, DDimer, C3 and tissue factor compared to the baseline value as well as compared to placebo intake. Factor XIII and high-sensitive C-reactive protein levels (Figure 1) after dapagliflozin intake did not differ significantly from the baseline value ( $P = 0.137$  and  $0.345$ ). However, there was a significant increase in those two markers after dapagliflozin intake compared to placebo intake ( $P = 0.012$  and  $P = 0.036$ ).

After two weeks of dapagliflozin intake (Dapa02), there was no statistically significant change in any of the measured coagulation and complement markers compared to baseline and dapagliflozin (data not shown). Tissue factor could not be measured for the Dapa02 study due to logistical problems.

In the turbidimetric clot formation and lysis assay, the area under the curve and the time from 50% clotting to 50% lysis were measured for each participant (Figure 2). After a week of dapagliflozin intake, there was no statistically significant change in the time from 50% clotting to 50% lysis and in the area under the curve compared to baseline and compared to a week placebo intake.

The turbidimetric clot formation and lysis assay was only performed for the Dapa01 study but not for the Dapa02 study.

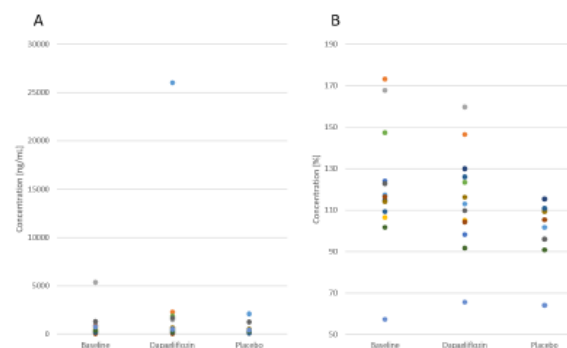


Figure 1: Scattered plots for two of the measured markers for the Dapa01 study with 13 participants; A: High-sensitive C-reactive protein; B: Factor XIII  
The plot shows the plasma levels for each individual participant at baseline, after 7 days of dapagliflozin intake and after 7 days of placebo intake

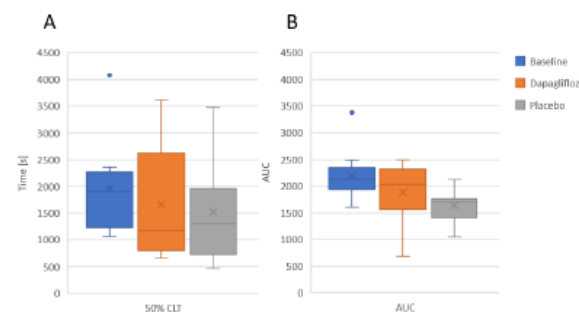


Figure 2: Box plots for the measured markers of the turbidimetric clot formation and lysis assay for the Dapa01 study with 13 participants; A: Time from 50% clotting to 50% lysis; B: Area under the curve  
The plot shows the plasma level distribution at baseline, after 7 days of dapagliflozin intake and after 7 days of placebo intake

## DISCUSSION & CONCLUSIONS

The results indicate that there is no beneficial impact of a dapagliflozin treatment on the prothrombotic state in type 1 Diabetes due to a decrease in complement and coagulation markers known to be elevated in diabetes. However, this does not have to mean that there is no beneficial impact on the cardiovascular risk, since the concentrations of coagulation and complement proteins are not the only factors influencing the cardiovascular risk.

The complement and coagulation markers do not increase with the treatment with dapagliflozin. This indicates that the prothrombotic and proinflammatory state present in diabetes is not aggravated with a dapagliflozin treatment.

However, one week respectively two weeks of treatment could be a too short intervention period to already have an impact on the expression of complement and coagulation proteins and thus their plasma levels. A longer intervention period could provide different results.

Moreover, the plasma levels of most of the markers commonly elevated in diabetes were already in the range of physiological plasma levels for most patients at baseline. For patients with elevated baseline levels, the treatment with dapagliflozin might result in an alteration of the plasma levels.

Finally, our pilot studies included only a small number of patients, so larger studies are required to confirm the result.

In conclusion, short-term dapagliflozin treatment for type one diabetes mellitus patients seems to have no effect on the levels of complement and coagulation markers which are known to be elevated in diabetes. With regard to the complement and coagulation markers, dapagliflozin (Forxiga®) could be used for the treatment of type one diabetes mellitus. This is due to the fact that it does not increase the markers commonly elevated in diabetes.

Nonetheless, further studies with a longer intervention period and including a larger number of participants are needed to confirm these results. In addition to this, patients with elevated levels at baseline should be included in those studies.

## REFERENCES

[1] Melmer A et al. Short-term effects of dapagliflozin on insulin sensitivity, postprandial glucose excursion and ketogenesis in type 1 diabetes mellitus: A randomized, placebo-controlled, double blind, cross-over pilot study. Diabetes Obes Metab 2018; 20(11): 2685–9.

## CONTACT INFORMATION

verena.schroeder@dbmr.unibe.ch

# Establishing a screening platform for the biological evaluation and modulation of complement-related integrin receptors

C. PLÜSS, E. NIKCI, C. LAMERS, R. MANCUSO, S. RABBANI, D. RICKLIN  
Molecular Pharmacy Group, Department of Pharmaceutical Sciences, University of Basel, 4056 Basel

SWISS  
PHARMA  
SCIENCE DAY  
2021

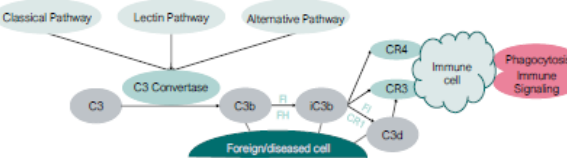


SAPhS  
Swiss Academy of  
Pharmaceutical  
Sciences

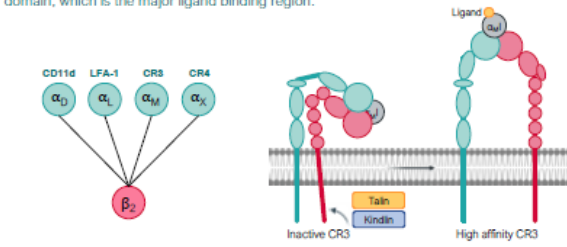
P - V - 1

## INTRODUCTION

The complement system serves as a first line of defense against pathogens and is composed of various plasma proteins and receptors. Complement can be activated via three pathways, which all lead to C3 convertase formation. They activate C3 to C3b, which covalently binds to foreign surfaces and marks them for elimination. Degradation of C3b result in the fragments iC3b and C3d that engage complement receptors 3 and/or 4 (CR3, CR4) to mediate phagocytosis. Due to its key roles in immune surveillance and inflammation, inappropriate complement activation is involved in several clinical conditions. The therapeutic modulation of immune and inflammatory signaling via complement receptors is therefore an attractive option for drug development.<sup>1,2</sup>



The  $\beta_2$  integrin family of adhesion molecules are involved in migration of leukocytes to sites of inflammation, cell adhesion to the endothelium, immune synapse formation, and the phagocytic removal of complement-opsonized particles.<sup>3</sup>  $\beta_2$  integrins form heterodimeric complexes, consisting of a distinct  $\alpha$  subunit and a shared  $\beta_2$  subunit (left). All  $\beta_2$  integrins need activation to become fully functional. In the inactive conformation, integrins form a closed, bent structure, whereas upon activation the conformation changes to an extended, open headpiece (right). This also exposes the  $\alpha$  domain, which is the major ligand binding region.



## AIMS

- Characterizing  $\beta_2$  integrin receptors as potential therapeutic targets.
- Compiling a library of major ligand-binding domains and physiological or therapeutic ligands with an emphasis on complement receptors (CR3, CR4).
- Establishing an assay platform for measuring drug-target interactions.

## METHODS

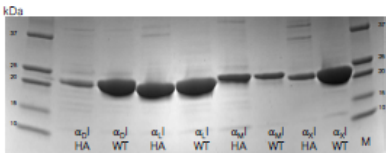
- Recombinant forms of the  $\alpha$  domain of all four  $\beta_2$  integrin family members were expressed in *E. coli* and purified by affinity chromatography.
- Surface plasmon resonance (SPR) was used to determine affinity and kinetics (direct binding) and evaluate competition between different ligands.
- Adhesion assays are currently established to determine the functional and selectivity spectra.

## RESULTS

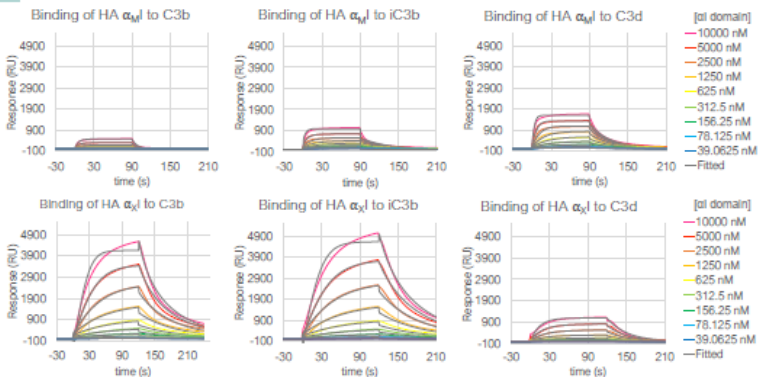
### Expression and purification of recombinant $\alpha$ domains



Recombinant forms of the  $\alpha$  domains in the wildtype (WT) and high affinity (HA) variant of all four  $\beta_2$  integrins were expressed in *E. coli* and purified by affinity chromatography using GST and/or His6 affinity tags. The 15% SDS-PAGE shows the purified  $\alpha$  domains. (Coomassie Brilliant Blue staining; non reducing conditions; M = protein marker)

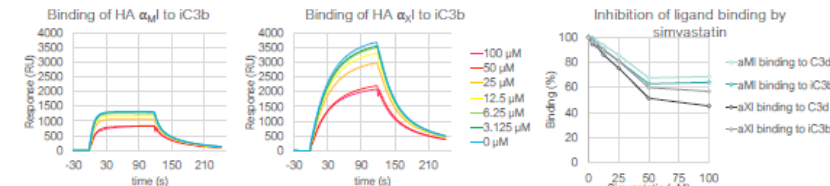


### Binding affinity to complement opsonins



The activity of recombinant CR3 and CR4  $\alpha$  domains for their biological ligands, i.e., C3-based complement opsonins, was tested by surface plasmon resonance (SPR)-based interaction analysis. For this purpose, plasma-purified C3b, iC3b, and C3d were immobilized through amine coupling on a CMD500M sensor chip in comparable levels and the purified proteins were injected at different concentrations. The assay revealed a dose-dependent interaction pattern, in which the CR3  $\alpha_M$  domain closely followed a 1:1 binding model and showed a clear preference for iC3b/C3d over C3b. Conversely, the CR4  $\alpha_X$  domain bound stronger to C3b/iC3b than C3d and showed small but notable deviations from a 1:1 model at higher concentrations.

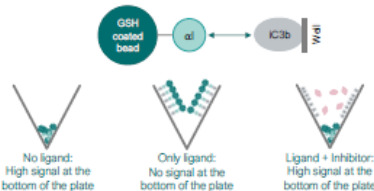
### Simvastatin as an antagonist of CR3?



Simvastatin was previously shown to allosterically inhibit LFA-1<sup>4</sup> and, more recently, was proposed to act as a competitive antagonist of opsonin binding by the CR3  $\alpha_M$  domain.<sup>5</sup> Using our SPR-based binding assay, we re-evaluated the effect of simvastatin on the CR3  $\alpha_M$ -iC3b/C3d interaction while also exploring potential effects on the CR4  $\alpha_X$ -iC3b interaction. On a iC3b/C3d-immobilized sensor chip (see above), constant concentration of CR3  $\alpha_M$  and CR4  $\alpha_X$  (5  $\mu$ M) were injected in the presence of increasing concentrations of simvastatin. While a dose-dependent inhibitory effect of simvastatin could be observed for both proteins, the plateauing at ~50-70% inhibition may suggest an allosteric rather than direct competitive interference.

### Development of an adhesion assay

We are currently developing a V-well adhesion assay<sup>6</sup> using the recombinant  $\alpha$  domains, which are bound to GSH-coated fluorescently labelled beads. The  $\alpha$  domains should adhere to ligands that are tethered to the well. Centrifugation leads to accumulation of unbound protein at the bottom of the plate. Fluorescence is measured only at this place.



## DISCUSSION & CONCLUSIONS

In this study, we established the recombinant expression of the major ligand-binding domains of CR3, CR4, LFA-1, and CD11d/CD18.

We validated the activity and selectivity profile of CR3 and CR4 by SPR and showed strong yet distinct binding to opsonins, thereby confirming the biological activity of the proteins.

Initial drug interference assays using simvastatin support the hypothesis that the activity of CR3 and CR4 can be modulated, similar to LFA-1, with small molecules.

It is anticipated to use the recombinant  $\alpha$  domains of  $\beta_2$  integrins in functional studies and for CR3/CR4-targeted drug development, with a potential expansion to the other  $\beta_2$  family members at a later stage.

## REFERENCES

- Ricklin, D., Reis, E. S. & Lambris, J. D., Complement in disease: a defence system turning offensive. *Nat. Rev. Nephrol.* 12, 383–401 (2016).
- Ricklin, D. & Lambris, J. D., New milestones ahead in complement-targeted therapy. *Semin. Immunol.* 28, 208–222 (2016).
- Lamers, C., Ploss, C.J. & Ricklin, D., The Promiscuous Profile of Complement Receptor 3 in Ligand Binding, Immune Modulation, and Pathophysiology. *Front. Immunol.* 12, 662164 (2021).
- Weitz-Schmidt et al., Statins selectively inhibit leukocyte function antigen-1 by binding to a novel regulatory integrin site. *Nat. Med.* 7, 687–692 (2001).
- Jensen et al., Structural Basis for Simvastatin Competitive Antagonism of Complement Receptor 3. *J. Biol. Chem.* 291, 16963–16976 (2016).
- Mancuso et al., Downstream effect profiles discern different mechanisms of Integrin  $\alpha_L\beta_2$  inhibition. *Biochem. Pharmacol.* 119, 42–55 (2016).

## CONTACT INFORMATION

carla.pluess@unibas.ch



# Targeting protein-protein interactions of DNA polymerase $\zeta$ to circumvent chemotherapy resistance

SWISS  
PHARMA  
SCIENCE DAY  
2021

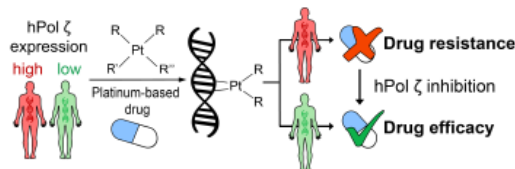


J.Z. Cresson, J.L. Held, R. Heeb, X. Xi, H.L. Gahlon

Laboratory of Toxicology, Department of Health Sciences and Technology, ETH Zürich, 8092 Zürich

## INTRODUCTION

- Platinum-based drugs are chemotherapeutic agents that form DNA adducts. These adducts impede DNA replication and evoke cell death.<sup>1</sup>
- Translesion DNA synthesis is a mechanism involving replication past DNA adducts, thus allowing cell survival and resistance to platinum-based drugs.
- The inhibition of human DNA polymerase  $\zeta$  (hPol  $\zeta$ ), an enzyme involved in TLS and whose expression increases upon platinum drug therapy, is a promising strategy to chemosensitize cells to platinum drugs.<sup>2,3,4</sup>
- The binding of Rev3 to the "seatbelt" region of Rev7 is essential for the activity of the enzyme and induces a conformational change in Rev7, from an «open» to «close» state.<sup>5</sup>
- Compound C disrupts a key protein-protein interaction between two subunits of hPol  $\zeta$ , Rev3 and Rev7.<sup>3</sup>



## AIMS

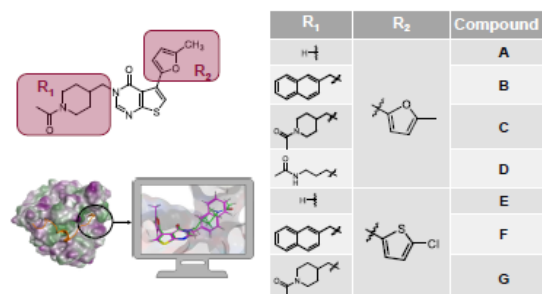
- Design and synthesize a series of analogues of compound C.
- Develop biochemical assays to evaluate their effectiveness.
- Characterize the mechanism of Rev3 displacement from Rev7.

## METHODS

- Computational modeling and chemical synthesis to generate inhibitors of the Rev7-Rev3 interaction.
- Protein expression and purification of Rev7-Rev3 complexes.
- Development of microscale thermophoresis (MST) and  $\text{Ni}^{2+}$  pull-down assays to study the structure-activity relationship of the small molecules.

## RESULTS

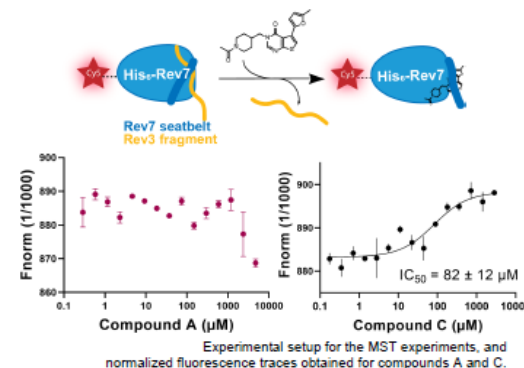
### Library of small molecule inhibitors of the Rev7/Rev3 interaction



Chemical structure of compound C, molecular modeling based on Rev7/Rev3 crystal structure (PDB 4GK0),<sup>4</sup> and small molecules synthesized.

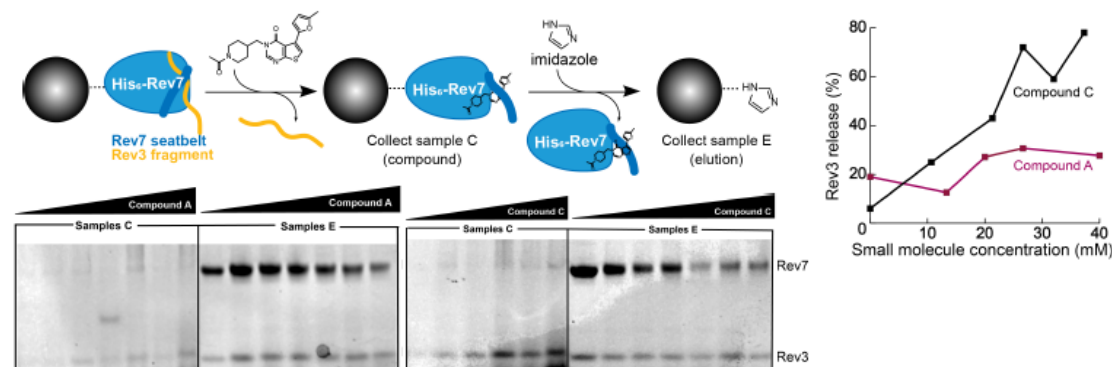
- The hypothesized binding pocket is mostly lipophilic.
- Modification of compound C will vary its lipophilicity and hydrogen bond potential in the Rev7 pocket.

### Quantification of the small molecules binding affinity to Rev7 by microscale thermophoresis



- Microscale thermophoresis (MST) measures changes in fluorescence intensity to detect binding events.
- Preliminary results indicate an  $\text{IC}_{50}$  value of  $82 \pm 12 \mu\text{M}$  for compound C binding to Rev7, while no fitting curve can be obtained for compound A.

### Development of a $\text{Ni}^{2+}$ pull-down assay to study Rev3 displacement from Rev7



- Preliminary results indicate a stronger effect of compound C in displacing Rev3 from Rev7 compared to compound A.

## DISCUSSION & CONCLUSIONS

- Six analogues of compound C have been designed and synthesized.
- Biochemical assays have been developed to evaluate the effectiveness of the small molecules. The results of these assays are expected to provide mechanistic insights into the function of hPol  $\zeta$ .
- Preliminary MST results indicate an  $\text{IC}_{50}$  value of  $82 \pm 12 \mu\text{M}$  for compound C binding to Rev7, while no  $\text{IC}_{50}$  value could be obtained for compound A in similar conditions.
- Compound C also shows a stronger effect in displacing Rev3 from Rev7 in the  $\text{Ni}^{2+}$  pull-down assay, compared to compound A.
- These preliminary results confirm that replacing the 1-acetyl-4-methylpiperidine moiety of compound C with a hydrogen strongly reduces its binding to Rev7 and its activity in disrupting Rev7/Rev3 interaction.<sup>3</sup>
- The development of new inhibitors that target the Rev7-Rev3 interaction of hPol  $\zeta$  will contribute to the development of more effective chemotherapeutic strategies aimed at combating drug resistance.

We thank Prof. Hiroshi Hashimoto and Prof. Dmitry Korzhnev for kindly sharing their Rev7/Rev3 plasmids with us.

## REFERENCES

- Nilforoushan A. *et al.* JACS (2015)
- Sharma S. *et al.* Mol. Pharmacol. (2012)
- Actis ML. *et al.* Bioorganic Med. Chem. (2016)
- Wojtaszek J.L. *et al.* Cell (2019)
- Hara K. *et al.* J. Biol. Chem (2010)

## CONTACT INFORMATION

Jeanne Cresson: [jeanne.cresson@hest.ethz.ch](mailto:jeanne.cresson@hest.ethz.ch)  
Hailey Gahlon: [hailey.gahlon@hest.ethz.ch](mailto:hailey.gahlon@hest.ethz.ch)

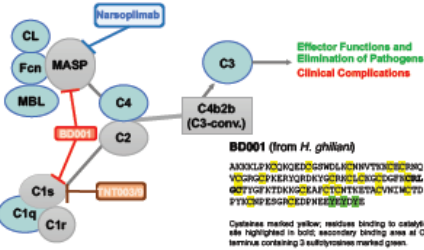
# Structure-activity assessment of the leech-derived complement inhibitor BD001

A. Blagojevic<sup>1</sup>, K. Widmer<sup>1</sup>, S. Lee<sup>2</sup>, M. Smieško<sup>2</sup>, R. Pouw<sup>1</sup>, S. Rabbani<sup>1</sup>, M. Lill<sup>2</sup>, D. Ricklin<sup>1</sup>

<sup>1</sup> Molecular Pharmacy Group, Department of Pharmaceutical Sciences, University of Basel, 4056 Basel  
<sup>2</sup> Computational Pharmacy Group, Department of Pharmaceutical Sciences, University of Basel, 4056 Basel

## INTRODUCTION

The complement system is a vital first-line-of-defense barrier against microbial intruders, yet can turn against host cells and tissues to cause clinical conditions such as hemolytic anemia or reperfusion injury (e.g., following transplantation or stroke). The interest in therapeutics that can modulate complement activation is therefore growing. Complement can be activated via the classical (CP), lectin (LP) and alternative pathway (AP). The initiation of both the CP and LP is mediated by serine proteases (i.e., C1r/C1s and MASP1/MASP2, respectively). They induce the formation of a C3 convertase with subsequent generation of potent effectors (e.g., membrane attack complex, opsonins, anaphylatoxins).<sup>1</sup>



The giant Amazon leech produces a 122 amino acid long protein, termed BD001 or Gigastatin, which is able to inhibit C1s and MASP1/2 and thereby impairs complement attack.<sup>2,3</sup> Our group explores the therapeutic value of BD001 and previously succeeded in expressing the protein in prokaryotic systems with high yield, purity and activity. Importantly, this also greatly facilitates structure-activity relationship (SAR) studies of BD001.

## AIMS

This study aimed at developing BD001 derivatives with enhanced target activity and distinct pathway selectivity profiles, based on *in silico* predictions and rational protein engineering.

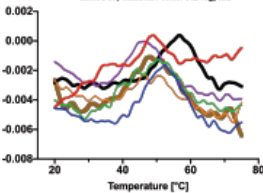
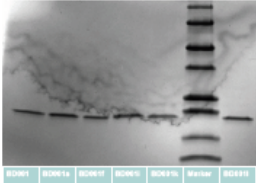
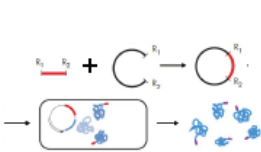
## METHODS

- Commercial/high software tools (i.e., FoldX, BioLuminate, PyRosetta) were used to predict changes in C1s affinity by performing a mutational scan of BD001.
- After visually inspecting the predictions, 16 selected mutants were expressed in *E. coli*, purified by affinity chromatography and characterized by SDS-PAGE and nanoDSF.
- The inhibitory activity of the mutants was tested in different biochemical assays, including chromogenic substrate, CP and LP ELISAs and haemolytic assays.

## RESULTS

### Expression & Purification of Recombinant BD001

Genes with the mutation of interest were amplified by PCR and, after ligation into a pET15b vector, the plasmid was transformed into *E. coli*. Proteins were expressed for 60 h at 18°C. After homogenization, proteins were purified via the His-tag using metal affinity chromatography and characterized by using SDS-PAGE and nanoDSF. Both wildtype BD001 and BD001-derived mutants were successfully obtained, and correct protein folding was shown by nanoDSF analysis.



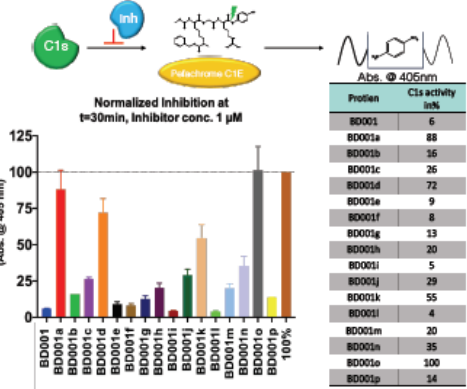
Left: The SDS-PAGE shows a selection of mutants, with BD001 derivatives being visible at the expected height of 16 kDa. Right: The nanoDSF results provide the folding of a selection of inhibitors. The graphs are mainly overlapping, leading to the conclusion that the folding of the different inhibitors is similar to the wildtype.

### Evaluation of Inhibition Profiles in Biochemical Assays

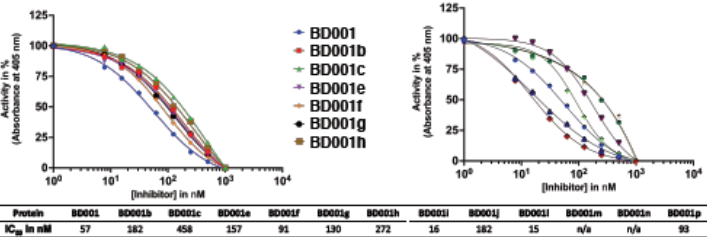
All proteins were tested in different biochemical assays like chromogenic substrate assay, ELISAs and haemolytic assays (not shown).

#### Chromogenic Substrate Assay

Target activity for C1s was measured as reduced generation of a cleavage product in the presence of BD001 mutants.



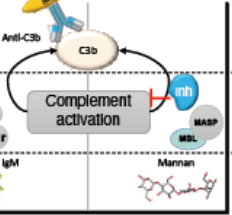
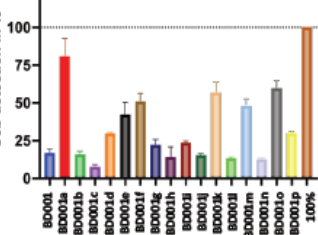
In an initial screening assay to identify the most promising inhibitors, all mutants were tested at a final concentration of 1 µM, resulting in residual C1s activities as shown in the table and graph above. Inhibitors with C1s activities below 40% were selected for a full activity assay.



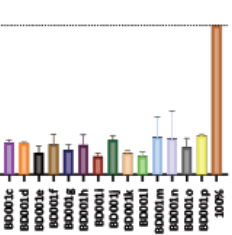
#### CP and LP ELISA

To determine the pathway-specific activity of the different mutants, CP and LP ELISAs were performed by coating assay plates with IgM or mannan, respectively. Upon addition of normal human serum, complement activation can be determined as C3b deposition. High inhibitory activities are documented by low C3b detection.

##### Classical Pathway ELISA



##### Lectin Pathway ELISA



When performing concentration-dependent chromogenic substrate assays with promising mutants, it can be observed that BD001i and BD001j have enhanced inhibitory activity for C1s when compared to the wildtype. This improvement is also shown in the CP ELISA. Additionally, these two mutants also show stronger inhibition in the LP ELISA. Intriguingly, a selectivity shift towards the LP can be observed for mutants e, f, k, m, and o. These mutants show a marked drop in CP activity while maintaining their LP inhibition capacity.

## DISCUSSION & CONCLUSIONS

Our initial SAR study already provided important insight into the molecular determinants of target activity and selectivity of the parasite-derived complement inhibitor BD001, thereby paving the way for rational protein engineering to develop the protein as drug-like entity. Our study showed that the use of off-the-shelf tools for mutant screening are of limited predictive value. We are therefore currently establishing enhanced computational methods for the next optimization steps.

Intriguingly, and despite these limitations, certain BD001 mutants showed generally enhanced activity in the biochemical assay while some even exert a notable shift in pathway selectivity. This suggests a potential for influencing the activity/selectivity of BD001 through tailored mutagenesis and support the conduction of detailed SAR studies as part of this project.

Overall, our findings establish BD001 derivatives as interesting leads for further development towards treatment options for clinical conditions such as autoimmune hemolytic anemia or ischemic-reperfusion injuries.

## REFERENCES

- Lambris JD, Ricklin D, and Geisbrecht BV. Complement evasion by human pathogens. *Nature Rev Microbiol* 2008; 6(2): 132-142
- Pang SS et al. The structural basis for complement inhibition by gigastatin, a protease inhibitor from the Giant Amazon Leech. *J Immunol* 2017; 199(11): 3883-3891
- Sheppard, P. O., Falls, G., Fox, B. A. & Us, W. A. (2 ) Patent Application Publication [10] Pub. No.: US 2002 / 0102256A1. 1, (2002).

## CONTACT INFORMATION

aleksandra.blagojevic@unibas.ch – www.pharma.unibas.ch  
Molecular Pharmacy Group, Pharmcenter, Uni Basel





# Insight into mode-of-action and structural determinants of the compstatin family of clinical complement inhibitors

C. LAMERS<sup>1</sup>, M. SMIESKO<sup>2</sup>, X. XUE<sup>3</sup>, B. WAGNER<sup>1</sup>, G. SYROERA<sup>4</sup>, N. BERGER<sup>4</sup>, P. GROS<sup>3</sup>, J. D. LAMBRIS<sup>4</sup>, D. RICKLIN<sup>1</sup>

<sup>1</sup> Molecular Pharmacy, Department of Pharmaceutical Sciences, University of Basel, 4056 Basel

<sup>2</sup> Computational Pharmacy, Department of Pharmaceutical Sciences, University of Basel, 4056 Basel

<sup>3</sup> Crystal and Structural Chemistry, Bijvoet Center for Biomolecular Research, Department of Chemistry, Faculty of Sciences, Utrecht University, 3584 CH Utrecht, The Netherlands

<sup>4</sup> Department of Pathology and Laboratory Medicine, Perelman School of Medicine, University of Pennsylvania, Philadelphia, PA 19104, USA

SWISS  
PHARMA  
SCIENCE DAY  
2021

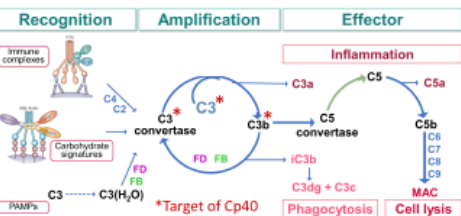


SAPhS  
Swiss Academy of  
Pharmaceutical  
Sciences

P - V - 4

## INTRODUCTION

The complement system serves as «first line of defense» against injurious stimuli and invading and leads to pathogen clearance and opsonic cell killing. Yet complement has gained increasing interest as a potential drug target, since it may be inadvertently triggered, thereby contributing to clinical complications in the pathogenesis of various autoimmune, inflammatory and age-related diseases.



The arsenal of available complement therapeutics has long been limited and it was only recently that pegcetacoplan (Empaveli, Apellis) has been approved by the FDA. Pegcetacoplan (i.e., Cp05-PEG-Cp05) is based on a second-generation analog of the peptidic C3 inhibitor compstatin (Cp05), which has been originally identified by phage display [1]. Derivatives of the compstatin family have reached clinical development for the treatment of paroxysmal nocturnal hemoglobinuria (PNH), age-related macular degeneration (AMD), periodontal disease, and COVID-19-induced acute respiratory distress syndrome.

Identified by phage display 1996:  
[ICVVQDQWGHRC]TAGHMANLTSHASAI

Compstatin	Ac-[ICVVQDQWGHRC]T	K <sub>D</sub> = 4000 nM
Cp01	Ac-[ICVVQDQWGAHRC]T	K <sub>D</sub> = 150 nM
Cp05	Ac-[ICV(1MeW)QDQWGAHRC]T	K <sub>D</sub> = 12 nM
Cp40	yl[ICV(1MeW)QDWSarAHRC]ml	K <sub>D</sub> = 0.5 nM

Empaveli™

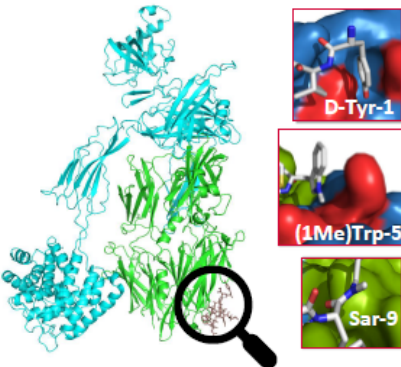
## AIMS

To provide a detailed understanding of the 3<sup>rd</sup> generation compstatin derivatives in

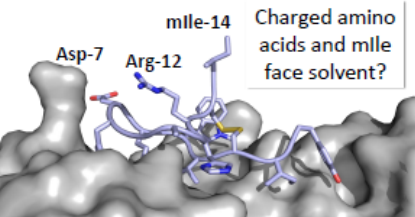
- target binding,
- target selectivity of different constructs and
- mode of action.

## RESULTS

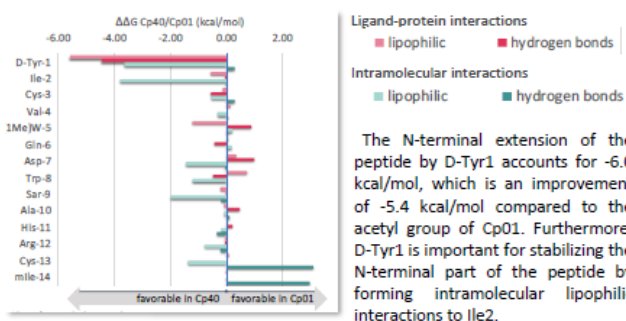
Crystal structure reveals key contacts of Cp40 to C3b



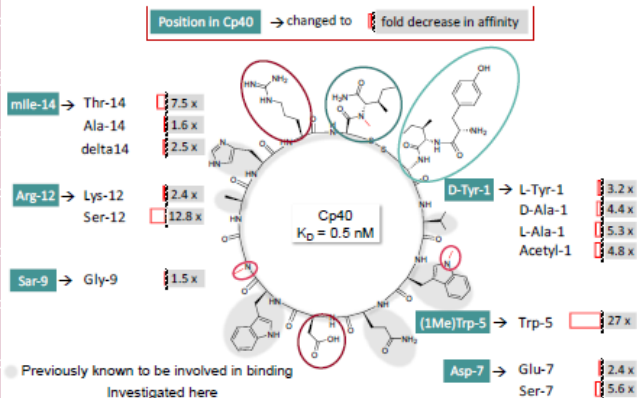
The crystal structure confirms that D-Tyr-1 interacts with a hydrophobic pocket on the MG4 domain and suggests a distinct lipophilic cavity to be filled by the methyl group of (1Me)Trp-5. Surprisingly, three of the 14 amino acids in Cp40 (Asp7, Arg12, mtle14) do not directly engage with the target in the crystal structure.



## MD confirms D-Tyr-1 forms new contacts to protein



SAR: mtle-14 and (1Me)Trp-5 increased affinity most profoundly compared to Cp01



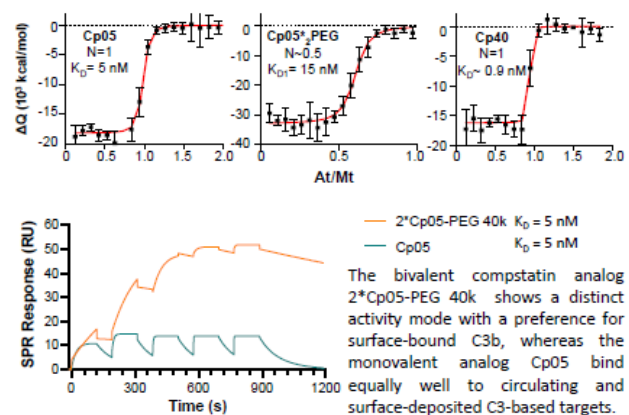
## METHODS

In this study, we combined a newly resolved co-crystal structure of Cp40 in complex with C3b with molecular dynamics simulations. Direct binding studies of compstatin derivatives yielded a detailed structure-activity-relationship profile. We compared the binding modes of mono- and bivalent compstatin derivatives concerning target binding in solution (ITC) and on surfaces (SPR) by using a surrogate of pegcetacoplan. By employing surface plasmon resonance studies we investigated the molecular mechanism of C3 inhibition by Cp40.

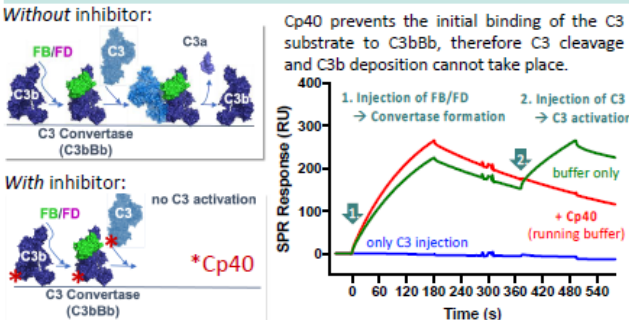
## DISCUSSION & CONCLUSIONS

- SAR : (1Me)Trp has most profound effect on affinity, Asp-7, Arg-12 and mtle-14 relevant for binding.
  - D-Tyr-1 addresses new binding site (co-crystal and MD).
  - SPR mechanistic study: Cp40 is a protein-protein inhibitor, inhibiting C3 activation, not C3 convertase assembly.
- The results of our study will guide the future development of a promising class of complement inhibitors.

## Mono- and bivalent compstatin analogs exert distinct target selectivity modes



## Cp40 is inhibiting C3 activation as PPI inhibitor



## REFERENCES

- [1] A. Sahu, J.D. Lambris et al., *J. Immunol.* 1996, 884-91.
- [2] A. Sahu, J.D. Lambris et al., *J. Immunol.* 2000, 2491-9.
- [3] B. Mallik, J.D. Lambris et al., *J. Med. Chem.* 2005, 274-86.
- [4] P. Magotti, D. Ricklin et al., *J. Mol. Recognit.* 2009, 495-505.
- [5] H. Qu, D. Ricklin et al., *Immunobiol.* 2013, 496-505.

## CONTACT INFORMATION

Christina.lamers@unibas.ch, Klingelbergstr. 50, 4056 Basel, Switzerland

# ICP-MS as a tool for *in vitro* and *in vivo* characterization of imaging probes and radioligand therapy candidates

SWISS  
PHARMA  
SCIENCE DAY  
2021



P - VI - 1

SAPhS  
Swiss Academy of  
Pharmaceutical  
Sciences

R. H. WALLIMANN<sup>1,2</sup>, H. HENSINGER<sup>1</sup>, R. BESSEY<sup>1</sup>, P. SCHINDLER<sup>1</sup>, J. REBER<sup>1</sup>, R. KNEUER<sup>1</sup>, C. MÜLLER<sup>2,3</sup>, R. SCHIBLI<sup>2,3</sup>

<sup>1</sup> Novartis Institutes for Biomedical Research, Novartis, 4056 Basel, Switzerland

<sup>2</sup> Center for Radiopharmaceutical Sciences ETH-PSI-USZ, Paul Scherrer Institute, 5232 Villigen-PSI, Switzerland

<sup>3</sup> Department of Chemistry and Applied Biosciences, ETH Zurich, 8093 Zurich, Switzerland

## INTRODUCTION

In-depth *in vitro* and *in vivo* characterization of targeting agents for molecular imaging and radioligand therapy is key for the success of the radiopharmaceutical development. So far the characterization of the targeting agents involves the handling of radioactive substances and thus can only be performed at centers that are specialized in radiopharmaceutical sciences. The extremely high sensitivity of inductively coupled plasma mass spectrometry (ICP-MS) and its wide dynamic range allow the detection of various non-radioactive metals at ultra-trace levels.

## AIMS

The goal of this study was to establish the use of ICP-MS for the characterization of the targeting agents (Figure 1a and 1b) to support the development of new candidates for radioligand therapy in a classical pharmaceutical environment. It should be tested if ICP-MS would deliver comparable results to the state-of-the-art assays that use radioconjugates for the characterization of imaging probes and RLT candidates.

## METHODS

RPC-ICP-MS Samples for quality control (QC) studies of metal-DOTA-peptide complexes were prepared in diluted rat blood extract with addition of DTPA. The formation of black carbon deposit on the cones was hindered by adding oxygen to the nebulizer argon flow (Figure 3a).

SEC-ICP-MS was used for QC studies of small proteins conjugated with a metal-chelator-complex. To hinder the formation of salt crystals on the cones (Figure 5a) and torch and to achieve separation of the [<sup>175</sup>Lu]Lu-DOTA-single domain antibody (sdAB) from the free [<sup>175</sup>Lu]Lu-DTPA on the column (Figure 5b), 20 mM ammoniumacetate buffer was used as mobile phase. Apomyoglobin (0.01 %) and DTPA (254 μM) were added to the samples.

**In Vitro Uptake and Internalization Study** For analysis of cell samples by direct infusion ICP-MS methods, samples were prepared by microwave assisted nitric acid digestion (Figure 4a). Cellular uptake and internalization studies were performed with [<sup>175</sup>Lu]Lu-DOTA-peptide (Figure 4b).

## RESULTS



Figure 1: (a) Schematic representation of [<sup>175</sup>Lu]Lu-DOTA-peptide and (b) [<sup>175</sup>Lu]Lu-DOTA-sdAB

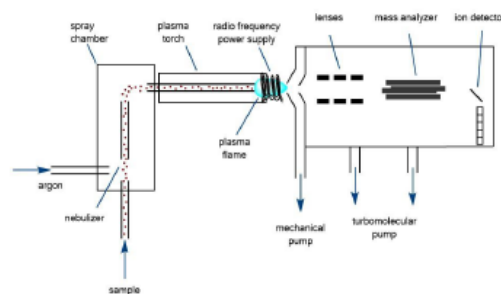


Figure 2: Systematic overview of an ICP-MS.

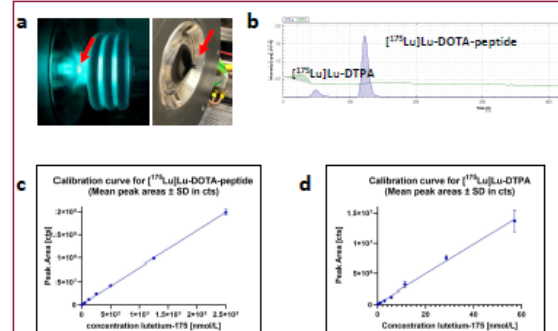


Figure 3: (a) Formation of black carbon deposit on platinum sampler cone. (b) Separation of [<sup>175</sup>Lu]Lu-DOTA-peptide spiked with free [<sup>175</sup>Lu]Lu-DTPA. (c) Linear range from 2 nM to 2.5 μM for [<sup>175</sup>Lu]Lu-DOTA-peptide ( $R^2 = 0.998$ ) and (d) from 46 pM to 57 nM for [<sup>175</sup>Lu]Lu-DTPA ( $R^2 = 0.982$ ).

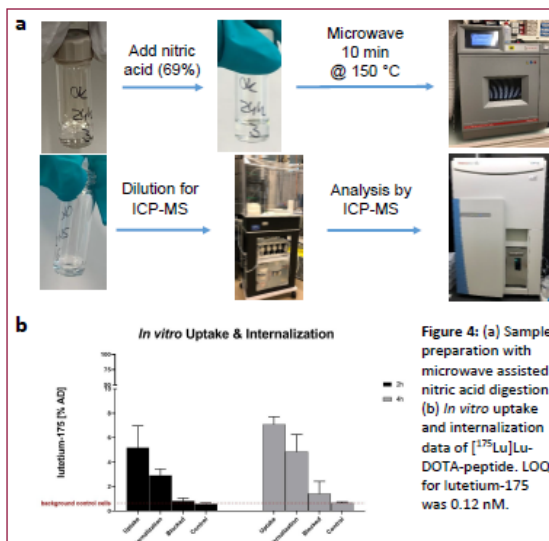


Figure 4: (a) Sample preparation with microwave assisted nitric acid digestion. (b) *In vitro* uptake and internalization data of [<sup>175</sup>Lu]Lu-DOTA-peptide. LOQ for lutetium-175 was 0.12 nM.

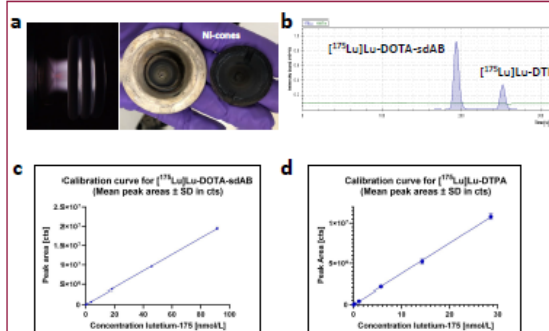


Figure 5: (a) Formation of salt crystals on the sampler and skimmer nickel cones. (b) Separation of [<sup>175</sup>Lu]Lu-DOTA-sdAB spiked with free [<sup>175</sup>Lu]Lu-DTPA. (c) Linear range from 2.5 nM to 91 nM for [<sup>175</sup>Lu]Lu-DOTA-sdAB ( $R^2 = 0.999$ ) and (d) from 1.1 nM to 57 nM for [<sup>175</sup>Lu]Lu-DTPA ( $R^2 = 1.000$ ).

## DISCUSSION & CONCLUSIONS

Various methods were successfully established to use inductively coupled plasma mass spectrometry (ICP-MS) in combination with either reversed phase chromatography (RPC), size exclusion chromatography (SEC) or in constant infusion mode for the characterization of potential candidates for nuclear imaging and radioligand therapy without the need of handling radioactivity. These characterization methods include RPC/SEC-ICP-MS for quality control of the peptide and biologics targeting agents after complexation with stable metals, such as lutetium-175, to verify the absence of free metals, free chelator and other metal containing metabolites in the probes before they go *in vitro* or *in vivo*. Direct infusion methods for ICP-MS and protocols for cell sample preparation were established to define the ligands' binding behavior with *in vitro* cellular uptake and internalization experiments. Having these applications of the ICP-MS implemented, it can be concluded that the ICP-MS has the potential to support early evaluation of new targeting agents as complementary method to the state-of-the-art methods which use radioactivity. As next steps, experiments are planned to test the applicability of ICP-MS for other *in vitro* and *in vivo* assays to examine the performance of biologics and peptide metal-conjugates. These experiments will cover *in vitro* serum stability experiments to identify metal-containing metabolites of the metal-conjugates and metal exchange with endogenous metals using the SEC/RP-ICP-MS but also the constant infusion methods for *in vivo* biodistribution experiments in tumor bearing mouse models.

## CONTACT INFORMATION

Rahel H. Wallimann, Novartis institutes for Biomedical Research, Novartis, 4056 Basel, Switzerland





# Authenticity Control of Pine Essential Oils by Chemometric Analysis and Chiral Gas Chromatography

M.D. Allenspach<sup>1</sup>, C. Valder<sup>2</sup>, C. Steuer<sup>1</sup>

<sup>1</sup> Institute of Pharmaceutical Sciences, Pharmaceutical Analytics, ETH Zurich, 8093 Zurich, Switzerland

<sup>2</sup> Systema Natura GmbH, Konrad-Zuse-Ring 8, 24220 Flintbek, Germany

## INTRODUCTION

Essential oils (EOs) defined according to the European Pharmacopoeia (Ph. Eur.) are odorless natural products obtained by steam distillation, dry distillation or a suitable mechanical process. Mono- and sesquiterpenes are the main metabolites found in pine EOs.<sup>1</sup> In order to guarantee appropriate quality of therapeutically used herbal substances the establishment of reliable and traceable qualities is a major concern. The supply chain for EOs usually involves many steps during collection of the starting material to the finished distilled product. Previously, our group investigated the chromatographic profiles of primary EOs of *Pinus (P.) sylvestris* obtained from traceable authentic plant material and developed a partial least squares discriminant analysis (PLS-DA) model for the correct taxonomic classification of closely related pine species.<sup>1</sup>

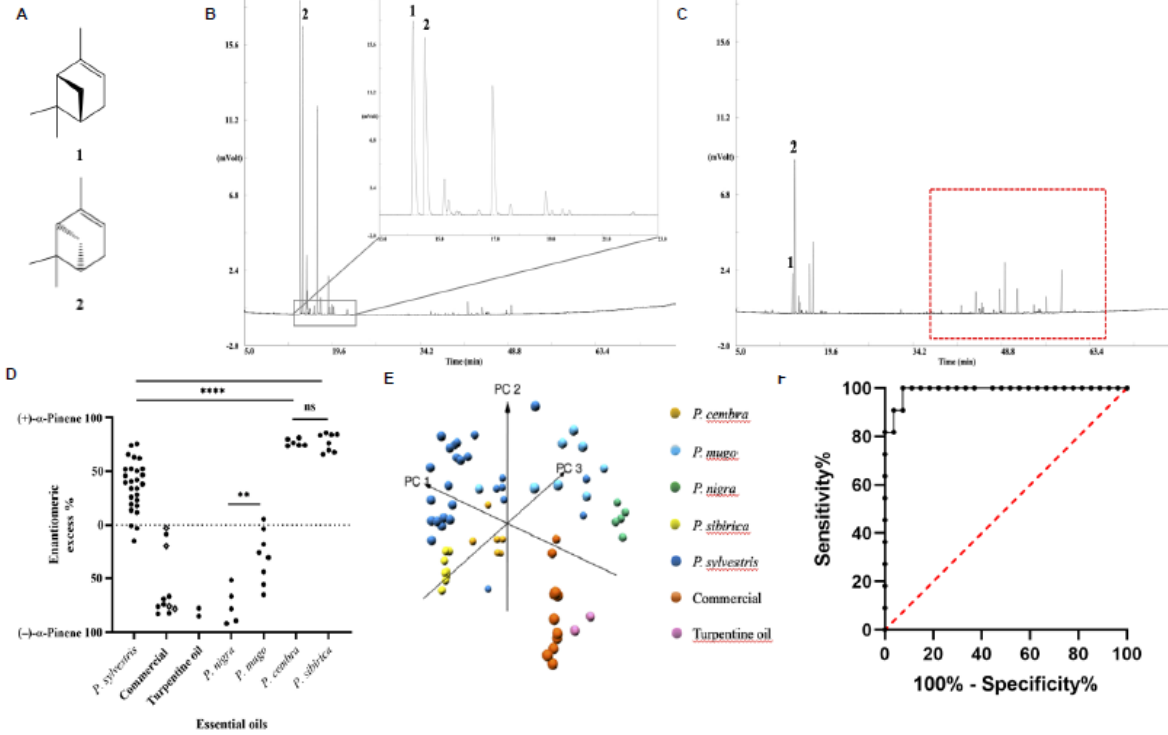
## AIMS

The present work evaluates the chiral gas chromatographic-flame ionization detector (GC-FID) profile of primary and commercially available pine EOs as additional tool for authenticity control.

## METHODS

Primary pine EOs were obtained by steam distillation from needles and twigs collected in Europe, Siberia and Canada. Commercial EOs of *P. sylvestris* were obtained from the three registered suppliers for *P. sylvestris* EO (1–4, European Chemicals Agency [ECHA] and local providers, respectively). The chiral GC-FID analysis was performed using a BGB 176 SE capillary column (30 m x 0.25 mm i.d., film thickness 0.25 µm). Helium was used as carrier gas at a constant flow rate of 2.5 ml/min. The oven temperature was kept at 50 °C for 3 min and then heated to 200 °C with 2 °C/min. Peaks were identified by comparing retention times with reference substances.<sup>3</sup> Significance of the enantiomeric excess values (%) of (+)-α-pinene and (–)-α-pinene (A) were tested using Welch's ANOVA test followed by Games-Howell's multiple comparisons post-hoc test with  $p < 0.01$  (\*\*),  $p < 0.0001$  (\*\*\*\*) and ns: not significant. Principle component analysis (PCA) was performed on fourth root calculated data. The dataset was composed of the commercial, primary pine EOs and turpentine oil characterized by 39 analytes and (+)-α-pinene. PCA was performed with Rstudio (version 1.2.5019; packages: ggbiplot, version 0.55; pca3d, version 0.10).

## RESULTS



A). Molecular structure of (–)-α-pinene (1) and (+)-α-pinene (2); B) Chromatographic profile obtained by chiral GC-FID of a commercial essential oil of *P. sylvestris*; C) Chromatographic profile of a primary essential oil of *P. sylvestris*. The red square highlight the significant sesquiterpene area. D: EE (%) of (±)-α-pinene of primary, commercial pine EOs and turpentine oil; E) The 3D score plot of the first three principal components PC1 (45.5%), PC2 (15.2%) and PC3 (9.5%) for turpentine oil, primary pine and commercial EOs based on their chemical composition obtained by the conventional and chiral GC-FID. F) ROC curve for primary and commercial pine EOs.

Table 1: EE (%) of (±)-α-pinene of commercial pine EOs (1–11), turpentine oil (12,13) and primary EOs of *P. sylvestris* (14–32), *P. cembra* (34–38), *P. mugo* (39–54), *P. nigra* (47–51) and *P. sibirica* (52–56).

EO	1	2	3	4	5	6	7	8	9	10	11	12	13	14
(+)-α-Pinene	15	16	17	18	19	20	21	22	23	24	25	26	27	28
(–)-α-Pinene	3.1 ± 0.0	19.8 ± 0.0	78.4 ± 0.1	76.0 ± 0.0	74.3 ± 0.0	82.4 ± 0.0	69.1 ± 0.0	76.1 ± 0.1	66.7 ± 0.1	8.6 ± 0.1	83.0 ± 0.0	77.9 ± 0.0	85.3 ± 0.0	34.0 ± 1.4
EO	29	30	31	32	33	34	35	36	37	38	39	40	41	42
(+)-α-Pinene	27.9 ± 0.0	13.6 ± 0.1	46.6 ± 0.2	-	74.3 ± 0.1	73.6 ± 0.1	81.2 ± 0.0	74.3 ± 0.0	79.6 ± 0.1	76.4 ± 0.2	-	-	-	-
(–)-α-Pinene	-	-	-	15.1 ± 0.1	-	-	-	-	-	-	65.2 ± 0.4	3.8 ± 1.9	55.8 ± 0.4	25.8 ± 0.1
EO	43	44	45	46	47	48	49	50	51	52	53	54	55	56
(+)-α-Pinene	-	-	-	5.2 ± 0.1	-	-	-	-	-	85.7 ± 0.1	83.4 ± 0.1	84.0 ± 0.1	84.2 ± 0.1	76.1 ± 0.1
(–)-α-Pinene	18.2 ± 1.0	30.4 ± 0.4	43.9 ± 0.5	-	66.5 ± 0.3	89.5 ± 0.0	91.9 ± 0.2	51.6 ± 0.1	78.4 ± 0.2	-	-	-	-	-

## DISCUSSION & CONCLUSIONS

In general, the chromatographic profile of a primary pine EOs from assigned and traceable pine trees consists of monoterpenes, sesquiterpenes and their oxygenated derivatives (B and C).<sup>1-3</sup> Our results clearly indicated, that commercial EOs were predominantly composed of monoterpene hydrocarbons with α-pinene as dominant analyte. However, commercial EOs of *P. sylvestris* showed significant different sesquiterpene patterns compared to primary EOs of the corresponding species. A possible reason for the reduced sesquiterpene profile could have been allowed modification of primary EOs e.g. by rectification. The dominant enantiomer of the main analyte in *P. sylvestris* of different origin was (+)-α-pinene (D and Table 1). The majority of the commercial EOs showed the opposite enantiomeric excess of (–)-α-pinene compared to primary EOs of *P. sylvestris*. Our data showed, that the commercial EOs were distinguished into two groups. Most of the commercial EOs belonged to group 1 (ee 65.0–85.0%) whereas the ee of the second group ranged from 0.0–20.0%. Although the second group showed similar ee values as observed for some primary EOs the main part of all commercial oils is significant different regarding the ee. A clear taxonomic separation in-between primary EOs but also to commercial oils was obtained by applying a 3D-PCA. Based on the first three principal components (PC1, PC2 and PC3) 70.2% of the total variance was explained. Interestingly, PCA revealed chemical similarity of commercial EOs and turpentine oils (E). According to our data, a threshold of e.g. 17.5% ee for (–)-α-pinene would allow identification of a commercial essential oil (F: specificity: 1.0; sensitivity: 0.82).

For the evaluation of the correct herbal substance, the unique chromatographic profile including chiral analytical markers is crucial. Our results clearly demonstrate that for comprehensive quality control the enantiomeric ratio of at least the major terpenes in pine EOs is of high importance to uncover possible mislabeling, the use of wrong herbal substances and/or adulteration within the supply chain.

## REFERENCES

- [1] Allenspach M. D. et al., Verification of Chromatographic Profile of Primary Essential Oil of *Pinus sylvestris* L. Combined with Chemometric Analysis. *Molecules*, 2020, 25, 13
- [2] Allenspach M. and Steuer C., Alpha-pinene: a never ending story, *Phytochemistry*, 2021, 190, 112857
- [3] Allenspach et al., Authenticity control of pine sylvestris essential oil by chiral gas chromatographic analysis of α-pinene, *Scientific reports*, 2021, accepted

## CONTACT INFORMATION

Email: christian.steuer@pharma.ethz.ch

# Determination of Ammonia in Different Matrices Using LC-MS

D. Hyseni<sup>1</sup>, C. Steuer<sup>1</sup>  
Institute of Pharmaceutical Sciences, Pharmaceutical Analytics, ETH Zurich, 8093 Zurich, Switzerland

## INTRODUCTION

Ammonia plays a key role in the nitrogen cycle among aquatic life, and humans. The human microbiome contributes to over 50% of ammonia production in mammals. Dysfunction of ammonia metabolism results in many diseases, for example, hepatic encephalopathy, cancer, urea cycle disorders and cerebral dysfunction [1,2]. The quantitative determination of ammonia attracts a wide range of research topics. Currently, colorimetric, enzyme-based assays or ion-selective electrodes can be used for quantification. However, these methods show some limitations like sensitivity, selectivity, cross reactivity and the use of toxic solvents. Therefore, a sensitive and selective LC-MS method is needed for the determination of ammonia in complex matrices, like urine and surface waters [3].

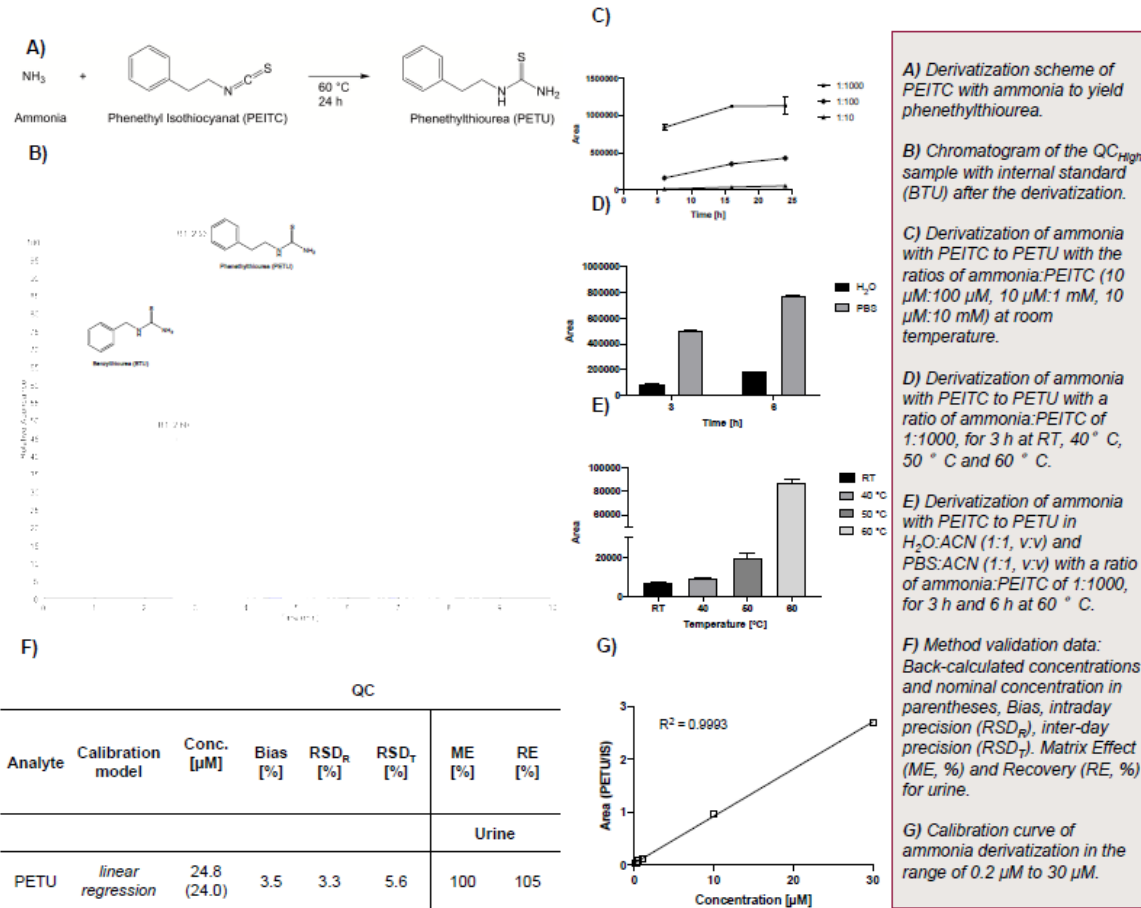
## AIMS

The aim of our study is the development of a new and highly selective LC-MS method to detect and quantify ammonia in different aqueous matrices. For clinical routine analysis, fast, simple and safe LC-MS based analysis are of high interest.

## METHODS

Ammonia was derivatized with phenethyl isothiocyanate (PEITC) to phenethylthiourea (PETU) in PBS/MeCN [4]. Benzylthiourea (BTU) was used as an internal standard (IS). PETU was quantified against reference substance by LC-MS comparing peak areas and normalized to the IS. Analysis was performed using an LTQ-XL linear ion trap (Thermo Scientific, San Jose, USA) mass spectrometer coupled to a Waters Acquity™ UPLC system (Milford, USA). Detection of PETU and BTU was done in ESI positive mode. Chromatographic separation was performed on an ACE Excel 2 C-8 column (30 x 2.1 mm, 2 µm, 100Å) at 30 °C. Gradient elution was done with water and acetonitrile containing 0.1% formic acid as mobile phase, respectively. Flow rate was set to 0.4 mL/min and injection volume was 5 µL.

## RESULTS



## DISCUSSION & CONCLUSIONS

After derivatization ammonia can sensitively be detected as PETU by LC-MS in ESI positive mode within 10 minutes. Various parameters were optimized for derivatization efficiency, duration and applicability in clinical laboratories. Optimal derivatization conditions were found at a higher PEITC:Ammonia ratio, a temperature of 60 °C and in PBS:ACN (1:1, v:v) (C-E), respectively (C-D). Subsequently, linearity for PETU was given in a range of 0.07 µM to 30 µM, with a calculated LoQ of 0.03 µM determined according to the ICH Q2 (R1) guideline [6]. Accordingly, the working range was set from 0.2 µM to 30 µM and covered well the physiological range of ammonia concentration found in different human body fluids. E.g., for urine 4-107 mM is reported [3] and a 500-fold predilution with water before analysis is even necessary. The predilution further lowers matrix effects which are often observed in LC-ESI-MS analysis. Compared to previously published methods who offered LoDs of 500 nM and a quantification range of 25 µM to 500 µM respectively [2, 5], the presented method is much more sensitive. Bias, intra- and inter-day precision, matrix effect and recovery for selected QC fulfilled our preset criteria of less than 15%.

In here we present a fast and sensitive method for the detection of ammonia in different matrices. Compared to previously published methods, the described LC-MS method is faster less, expensive and more ecologically friendly. It represents a valuable starting point for ammonia detection in further clinical studies and upcoming research projects.

## REFERENCES

- [1] Barsotti RJ. Measurement of ammonia in blood. J Pediatrics 2001; 138, 1: S11-S20.
- [2] Spinelli JB, Kelley LP, and Halgis MC. An LC-MS approach to quantitative measurement of ammonia isotopologues. Sci Rep 2017; 7, 1: 1-8.
- [3] Hutzenga JR, Tangerman A, and Glips CH. Determination of ammonia in biological fluids. Ann Clin Biochem 1994; 31, 6: S29-S43.
- [4] Y. Ji and M. E. Morris, "Determination of phenethyl isothiocyanate in human plasma and urine by ammonia derivatization and liquid chromatography-tandem mass spectrometry," Analytical biochemistry, vol. 323, no. 1, pp. 39-47, 2003.
- [5] Ayub, Omar B., et al. "Simple and inexpensive quantification of ammonia in whole blood." Molecular genetics and metabolism 115:2-3 (2015): 95-100.
- [6] ICH Q2 (R1) Validation of Analytical Procedures: Text and Methodology, p. 15, 2006.

## CONTACT INFORMATION

Email: christian.steuer@pharma.ethz.ch



# Fluorescence-based detection method for the separation and quantification of hydrolysis products in oil-in-water emulsions

G. HOLTZHAUER<sup>1</sup>, M. TADDIO<sup>1</sup>, J. RADONJIC<sup>1</sup>, E. LUCCHINETTI<sup>2</sup>, G. ROGLER<sup>3</sup>, M. HERSBERGER<sup>4</sup>, M. ZAUGG<sup>2,5</sup>, S. D. KRÄMER<sup>1</sup>

<sup>1</sup>Center for Radiopharmaceutical Sciences, Department of Chemistry and Applied Biosciences, ETH Zürich, Zürich, Switzerland

<sup>2</sup>Department of Anesthesiology and Pain Medicine and Cardiovascular Research Centre, University of Alberta, Edmonton, Canada

<sup>3</sup>Division of Gastroenterology and Hepatology, University Hospital Zurich, Zurich, Switzerland

<sup>4</sup>Division of Clinical Chemistry and Biochemistry, University Children's Hospital Zurich, Zurich, Switzerland

<sup>5</sup>Department of Pharmacology, University of Alberta, Edmonton, Canada



SWISS  
PHARMA  
SCIENCE DAY  
2021



P - VII - 3

SAPhS  
Swiss Academy of  
Pharmaceutical  
Sciences

## INTRODUCTION

Parenteral nutrition (PN) serves to provide essential nutrients especially in preterm infants when oral ingestion is not possible yet. PN mixtures contain lipid emulsions and the triglycerides can be hydrolyzed to free fatty acids (FFA). Released FFA can bind to albumin and compete with bilirubin [1]. Excess FFA pose the risk of developing hyperbilirubinemia, leading to jaundice and in severe cases to neurotoxicity. An improved HPLC method was thus developed to accurately quantify the amount of individual FFA species in oil-in-water emulsions for PN. Insights into different ratios between individual FFA species in contrast to simply assessing the level of total FFA can further enhance our understanding of underlying degradation mechanisms.

## METHOD OVERVIEW

Extracted FFAs from as little as 7.5  $\mu$ L emulsion were activated with 13.3  $\mu$ M DMT-MM as coupling agent and subsequently labelled with 1.25 mM of the fluorescent dye DBD-PZ. The non-natural FFAs pentadecanoic acid (C15:0) and heptadecanoic acid (C17:0) were used as internal standards. The one-pot labelling reaction was performed at room temperature. After incubation for 2 h, aliquots were quenched with 1% formic acid and analysed by HPLC with fluorescence detection. Acetonitrile was used as solvent for all reagents. Calibration curves were prepared from pure FFA standards. Commercially available reference emulsions Intralipid (20% soy bean oil, SO), Omegaven (10% fish oil, FO) and SMOFlipid (20% SO/FO/MCT (medium-chain triglycerides), all from Fresenius Kabi) were used to develop the method. Subsequently, emulsions mimicking the composition of these reference emulsions were manufactured and analysed in comparison to the respective original formulations.

Key facts HPLC method:

Column: Waters XBridge C18, 5  $\mu$ m, 4.6 x 150 mm  
FL-Detection:  $\lambda_{ex}$  = 444 nm /  $\lambda_{em}$  = 557 nm  
Solvent system: Acetonitrile and 0.1% TFA in H<sub>2</sub>O, gradient from 15% to 5% aqueous

Flow rate: 1 ml/min  
Injection volume: 10  $\mu$ L  
Total run time: 25 min

## RESULTS

We were able to detect 10 different natural fatty acids (FA) commonly present in the studied oil sources as well as 2 non-natural FFAs as internal standards over a 25 min time course. The identity of the peaks was confirmed by spiking with the respective standards. Distinct FA profiles were obtained depending on the type of oil used in the manufacturing process. The use of internal standards as well as calibration curves for each FFA species also allowed the quantification of the individual FFAs.

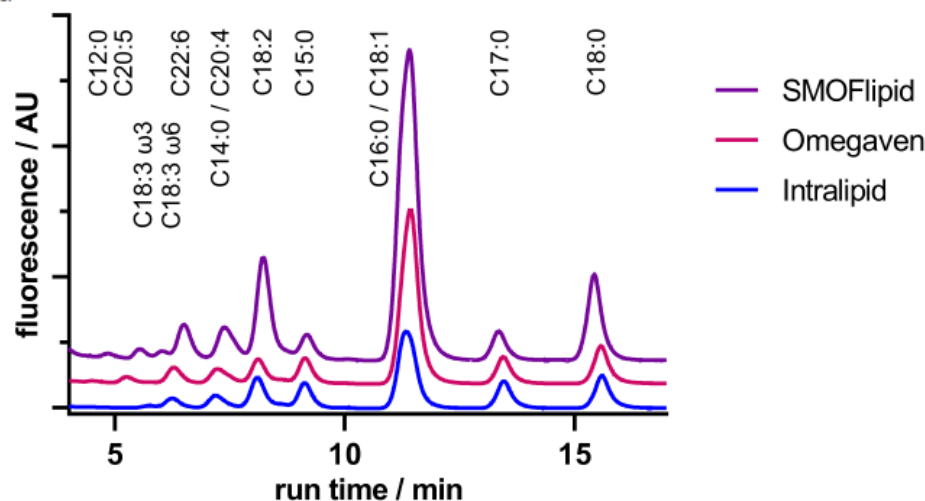


Fig. 1: Stacked chromatograms of commercial references Intralipid, Omegaven and SMOFlipid, normalized to internal standards C15:0 and C17:0, with annotated peaks. View from 4-17 min.

Tab. 1: Limit of detection for all studied fatty acids

Fatty acid	Limit of quantification
lauric acid (C12:0)	5 pmol
myristic acid (C14:0)	1 pmol
palmitic acid (C16:0)	0.25 pmol
stearic acid (C18:0)	1 pmol
oleic acid (C18:1)	1 pmol
linoleic acid (C18:2)	1 pmol
$\alpha$ -linolenic acid (C18:3 $\omega$ 3)	2.5 pmol
$\gamma$ -linolenic acid (C18:3 $\omega$ 6)	1 pmol
arachidonic acid (C20:4)	1.5 pmol
eicosapentaenoic acid (C20:5)	2.5 pmol
docosahexaenoic acid (C22:6)	1 pmol

Tab. 2: Total free fatty acids of commercially available lipid emulsions and in-house manufactured references.

Emulsion	Total FFA
Intralipid	20.8 $\mu$ mol/ml
Omegaven	46.9 $\mu$ mol/ml
SMOFlipid	97.5 $\mu$ mol/ml
20% Soy bean oil (SO)-based emulsion	2.6 $\mu$ mol/ml
10% Fish-oil (FO)-based emulsion	3.1 $\mu$ mol/ml
20% SO/FO/MCT-based lipid emulsion	4.6 $\mu$ mol/ml

Values are given as total FFA concentrations per emulsion volumes, since the United States Pharmacopeia does not specify threshold values for specific FFAs, but only stipulates the upper limit of 0.07 mEq/g for total amounts of FFAs. Also, the different oil contents (10% vs. 20% lipid emulsion) are not considered.

## ASSAY OPTIMIZATION

Compared to previous reports [2], highly toxic reagents were replaced, the assay time was reduced by a factor of 2.9 to increase sample throughput, sample consumption was successfully minimized by a factor of 133.3 and the use of the costly fluorescent dye was lowered by a factor of 4. Increasing the concentration of the coupling reagent allowed to shorten the reaction time for labelling. The concentration of the fluorophore had no impact on the reaction speed. Common excipients in lipid emulsions like phospholipids and antioxidants did not interfere with the analysis. Sucrose esters of inferior quality used as co-surfactants however were hydrolyzed as well and contributed to the signal.

## DISCUSSION & CONCLUSIONS

The presented method allows the simultaneous identification and quantification of various hydrolytic degradation products in lipid emulsions with minimal sample requirement. The limit of quantification was determined in the single-digit pmol range for all studied fatty acids. Like this, the quality of the emulsion can be controlled prior to administration and severe complications prevented. Emulsions with oil sources rich in polyunsaturated fatty acids show higher total FFA values and thus seem to be more prone to hydrolytic degradation. Freshly produced in-house references showed lower values right after manufacturing than corresponding original formulations in the second half of their shelf life.

## REFERENCES

- [1] Amin SB, J. Parenter. Enter. Nutr. 2010; 34 (4): 414-420.
- [2] Ueno Y et al. Chem. Pharm. Bull. 1999; 47 (10): 1375-1379.

## ACKNOWLEDGEMENT

This project is funded by a Sinergia team grant by the Swiss National Science Foundation SNF (project CRSII5\_177225).



SWISS NATIONAL SCIENCE FOUNDATION

## CONTACT INFORMATION

G. HOLTZHAUER: gregoryh@ethz.ch

R. TILÉN<sup>1,2</sup>, A. N. GOETSCH<sup>3</sup>, P. PAIONI<sup>1</sup>, C. BERGER<sup>1</sup>, S. D. KRÄMER<sup>3</sup> and H. E. MEYER ZU SCHWABEDISSEN<sup>1</sup>  
<sup>1</sup>University Children's Hospital Zurich, Department of Infectious Diseases and Hospital Epidemiology, Zurich, Switzerland  
<sup>2</sup>University Basel, Department of Pharmaceutical Science, Biopharmacy, Basel, Switzerland  
<sup>3</sup>ETH Zurich, Department of Chemistry and Applied Biosciences, Biopharmacy, Zurich, Switzerland

## Introduction

Invasive fungal infections (IFIs) are a serious complication and a major cause of morbidity and mortality in immunocompromised children [1]. Voriconazole is among the first-line antifungal drugs to treat IFIs in children is voriconazole [2]. This drug is known for its narrow therapeutic range and its non-linear pharmacokinetic profile with pronounced inter- and intra-individual variability [3]. Due to the high risk for therapy failure if the therapeutic range is not reached, therapeutic drug monitoring (TDM) is strongly recommended [4]. Drug-drug interactions and patient specific characteristics as age, weight, liver function, and also the phenotype of the metabolizing enzyme cytochrome P450 2C19 are known factors to influence the *in vivo* behaviour of voriconazole [5]. In addition to CYP2C19 genetic variants, single nucleotide polymorphisms (SNPs) in other genes are involved in the metabolism and transport of voriconazole and are thought to influence serum concentrations and eventually the therapeutic outcome [6]. Accordingly, understanding how genetics affect pharmacokinetic, efficacy and safety of voriconazole in children is essential to optimize dosage and thus treatment success.

## Aims

Our aim was to investigate the impact of genetic variants on voriconazole serum levels in order to allow future optimization of voriconazole dosage and improve the therapeutic outcome in children with IFIs.

## Methods

We performed a retrospective data analysis, where we used data on medication including trough levels, health-related personal data, co-medication and biological material from 36 children aged 10 (0-17) years, suffering from IFI, and treated with voriconazole between 2014 and 2019 in two different children's hospitals. Data were extracted from the clinical and laboratory information systems of the hospitals with the recently built Swiss Personalized Health Network infrastructure *SwissPK<sup>cdw</sup>*. We analysed a total of 395 voriconazole trough levels. Among 23 individuals with samples available for DNA extraction, 12 selected SNPs within the voriconazole metabolizing enzymes CYP2C19, CYP3A4, and CYP3A5 and transporters ABCG2, ABCG2, and SLCO1B3 were genotyped using commercially available TaqMan® real-time PCR assays.

## Results

All children were initially treated with clinically recommended dose, followed by individual dose adjustments according to TDM. 195 (49%) of the 395 voriconazole trough levels measured were outside the recommended therapeutic target trough concentration of 1-5.5 mg/L, of which 169 (87%) were at sub-therapeutic level (Figure 1). Analysis of trough levels with genotyping revealed statistically significant differences in mean voriconazole serum concentrations associated with 5 of 12 genetic variants tested. SNPs within ABCG2 (rs2273697,  $P = 0.005$  and rs177620,  $P < 0.001$ ), ABCG2 (rs2231142,  $P = 0.001$ ), CYP2C19 (rs4244285,  $P < 0.001$ ), and SLCO1B3 (rs4149117,  $P = 0.001$ ) influenced dose-corrected trough levels (Figure 2). No association was observed for the ABCG2 (rs1320400), CYP2C19 (rs12248560 and rs4986893), CYP3A4 (rs35599367), and CYP3A5 (rs776746) genotype. None of the patients harboured the variants CYP2C19 (rs28399504) and CYP3A5 (rs10264272).

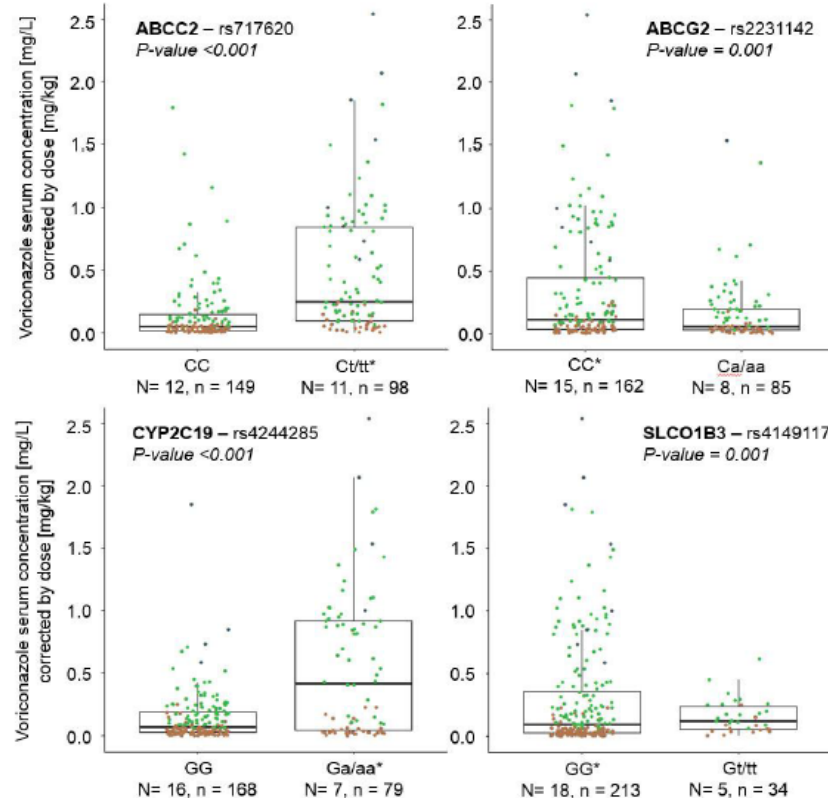


Figure 2 Association of mean voriconazole serum concentrations [mg/L] and 4 examples of genetic variants tested. N = Number of patients. n = Total number of subtherapeutic (red), therapeutic (green), and supratherapeutic (grey) trough levels. GG/CC: reference genotypes. Ca/aa/Ct/tt/Ga/aa/Gt/tt: variant genotypes. \*A data point at 7.897 kg/L was omitted for clarity.

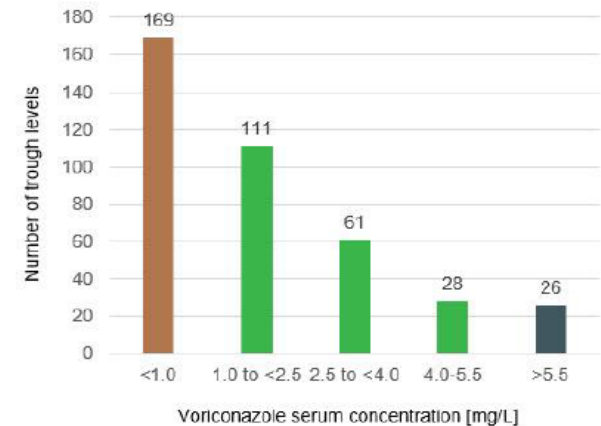


Figure 1 Results of therapeutic drug monitoring of voriconazole

## Discussion & Conclusions

Our results suggest that voriconazole serum concentrations in children are affected by several genetic polymorphisms. In order to prescribe an optimal drug dosage, pre-emptive pharmacogenetic (PGx) testing in addition to therapeutic drug monitoring might be helpful for patients treated with voriconazole. The results of this retrospective study need to be confirmed prospectively in order to guide voriconazole dosing in critically ill children.

## References

- [1] Lehmbecher, T. & A.H. Groll. Expert Rev Anti Infect Ther 2011;9(3):275-8
- [2] Warris, A., et al. Clin Microbiol Infect 2019;25(9):1096-1113
- [3] Pfizer. Vfend® SmPC 2017
- [4] Kang, H.M., et al. Pediatr Hematol Oncol 2015;32(8):557-67
- [5] Kadam, R.S. & J.N. Van Den Anker. Clin Pharmacokinet 2016;55(9):1031-43
- [6] Allegra, S., et al. Pharmacogenomics 2018;19(11):913-925

## Contact information

Email: romy.tilen@kispi.uzh.ch, Tel.: +41 (0) 244 266 80 90



# Inflammasome activation increases with age and positively correlates with the high risk of CMML

L. DE MEURON<sup>1,2</sup>, N. ANDINA<sup>1,2</sup> and R. ALLAM<sup>1,2</sup>

<sup>1</sup>Departement of Hematology and Central Hematology Laboratory, Inselspital, Bern University Hospital, University of Bern, Bern, Switzerland  
<sup>2</sup>Departement for BioMedical Research, University of Bern, Bern, Switzerland

SWISS  
PHARMA  
SCIENCE DAY  
2021

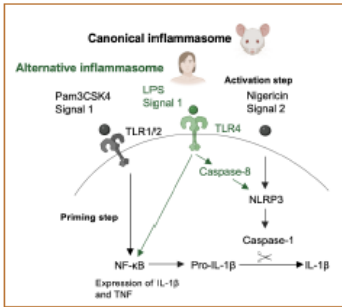


SAPhS  
Swiss Academy of  
Pharmaceutical  
Sciences

P - VIII - 2

## INTRODUCTION

As the human life span increases, chronic as well as age related health problems have become a major issue in health care. Age related chronic low-grade inflammation is known as inflammaging and is a risk factor for several non-communicable chronic disorders like arthritis, diabetes, and cardiovascular diseases including myeloid leukemias, such as Chronic Myelomonocytic Leukemia (CMML). Recent studies suggest that NLRP3 Inflammasome activation plays a critical role in the development of inflammaging [1]. NLRP3 inflammasome is a multiprotein signaling platform formed in the cytosol of stimulated immune cells such as monocytes. The canonical NLRP3 inflammasome activation is a two-step mechanism established in mice. The initial priming step involves an NF- $\kappa$ B-activating stimulus, such as LPS binding to TLR4, that induces transcription and translation of the IL-1 $\beta$  precursor as well as increased expression of NLRP3 protein. The second step results in an activation of caspase-1 which cleaves pro-IL-1 $\beta$  into its mature form IL-1 $\beta$ . An alternative inflammasome pathway had previously been discovered specifically arising in human monocytes. Herein LPS directly activates this inflammasome via TLR4 and caspase-8 without requiring a second signal [2].



## AIMS

- This project can be subdivided into two parts:
- I. Investigation of age-dependent changes in NLRP3 inflammasome activation arising in CD14<sup>+</sup> monocytes derived from old healthy donors.
  - II. To see whether NLRP3 inflammasome signaling contributes to the age dependent disease CMML.
- It is known that aging causes chronic low-grade inflammation. However, molecular mechanisms and cell intrinsic changes that contribute to low grade inflammation are not entirely understood.

## METHODS

Human CD14<sup>+</sup> monocytes were isolated using Ficoll-Paque Tm sterile solution. The PBMCs were collected with magnetic Anti-CD14<sup>+</sup> Micro beads after centrifugation. CD14<sup>+</sup> monocytes were stimulated for inflammasome activation. TLR4 agonist LPS was used to address the alternative inflammasome. TLR1/2 agonist Pam3CSK4 and Nigericin were used to target the canonical inflammasome, since this pathway requires two signals. ELISA and Western blot analysis were performed to check IL-1 $\beta$  levels and caspase-1 activation in cell lysates and supernatants. In addition, a diverse set of pharmacological inhibitors were used to gain a greater insight into the molecular mechanism of inflammasome signaling during the aging process.

## RESULTS

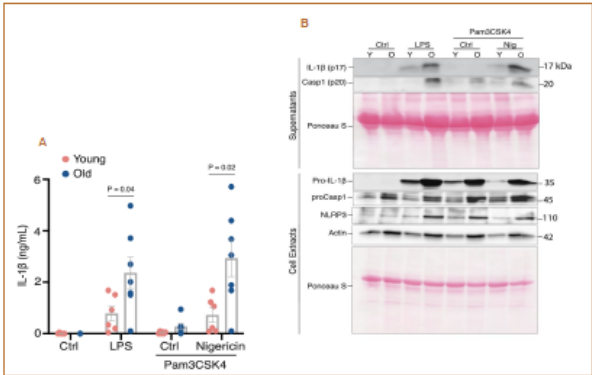


Figure 1: Old healthy donors show increased NLRP3 inflammasome signaling. (A) Monocytes obtained from old healthy donors produce higher levels of IL-1 $\beta$  compared to monocytes from young healthy donors. (B) Caspase-1, NLRP3 and pro-IL-1 $\beta$  are present in a higher amount in monocytes derived from old healthy donors. Due to elevated expression of pro-IL-1 $\beta$ , the priming step (signal 1) could be enhanced in monocytes derived from old healthy donors.

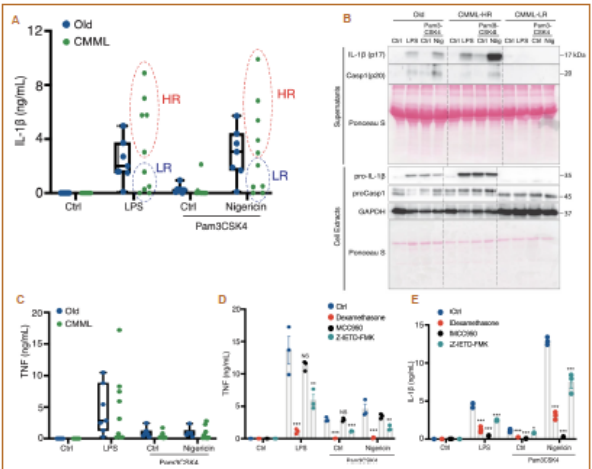


Figure 3: Inflammasome signaling divides CMML patients into two groups. (A) CMML patients have more variable inflammasome activation compared to old healthy donors and can be divided into CMML high reactive (CMML HR) and CMML low reactive (CMML LR). Monocytes from CMML patients show some IL-1 $\beta$  secretion in absence of signal 2. This is reasonable since CMML patients are old. (B) The priming step is enhanced in CMML HR due to elevated levels of pro-IL-1 $\beta$ . (C) TNF levels are variable in CMML patients but did not show significant increase compared to old healthy donors. (D and E) Z-IETD-FMK (caspase-8 inhibitor) is able to reduce IL-1 $\beta$  secretion. This shows that monocytes obtained from CMML patients exhibit an enhanced susceptibility to TLR1/2 receptor signaling similar to monocytes obtained from old healthy donors.

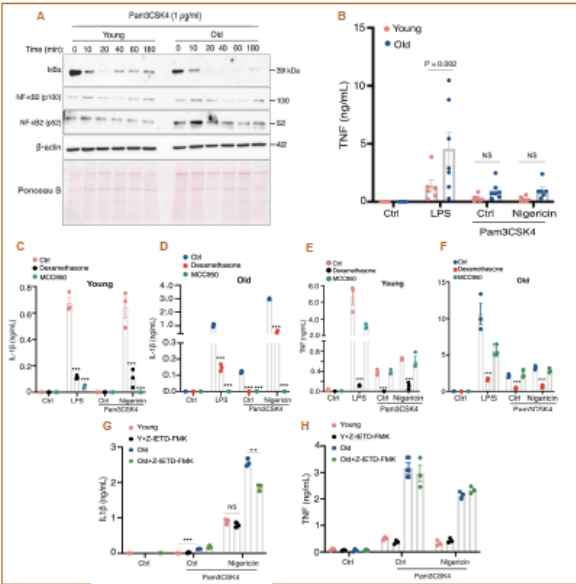


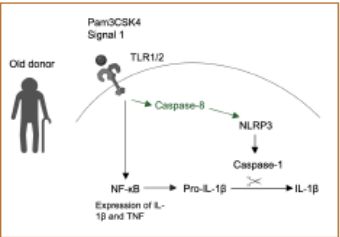
Figure 2: Enhanced priming and alternative inflammasome signaling via TLR1/2 in monocytes derived from old healthy donors. (A) NF- $\kappa$ B is activated in a higher extent in monocytes derived from old healthy donors compared to monocytes obtained from young healthy donors. (B) Besides IL-1 $\beta$ , NF- $\kappa$ B is inducing the expression of TNF. An increased priming step results in elevated levels of TNF. (C-F) Devamethasone (NF- $\kappa$ B inhibitor) is able to reduce IL-1 $\beta$  and TNF levels. MCC950 (NLRP3 inhibitor) is able to block IL-1 $\beta$ , but not TNF secretion significantly. IL-1 $\beta$  production is dependent on NLRP3 and NF- $\kappa$ B, whereas TNF secretion is specifically regulated by NF- $\kappa$ B. (G) Interestingly, monocytes stimulated with Pam3CSK4 derived from old healthy donors are able to produce IL-1 $\beta$  in the absence of signal 2. (H and I) IL-1 $\beta$  levels are clearly decreased in monocytes derived from old healthy donors treated with Z-IETD-FMK (caspase-8 inhibitor, denominator of the alternative inflammasome pathway). While Z-IETD-FMK has no impact on TNF levels.

Patient ID	NLRP3 inflammasome response	Sex	Diagnosis (WHO 2016)	IPSS	IPSS-R	Splenomegaly	Time to therapy (d)	Time to death (d)	Age at diagnosis (years)
PD04	LR	M	CMML-0	low	low	NO	1188	alive	72.9
PD08	LR	F	CMML-0	low	very low	NO	NA	alive	77.4
PD09	LR	M	CMML-0	low	low	YES	NA	alive	56.3
PD12	LR	F	CMML-0	low	very low	NO	NA	1069	64.9
PD13	LR	M	CMML-0	low	very low	NO	NA	alive	69.7
PD02	HR	M	CMML-1	intermediate 2	high	YES	0	733	68.3
PD03	HR	F	CMML-0	low	very low	NO	1051	1379	69.8
PD05	HR	M	CMML-1	intermediate 1	low	YES	3602	dead	70.6
PD07	HR	M	CMML-1	low	low	YES	642	1002	78.1
PD01	HR	M	CMML-2	high	very high	YES	0	35	67.2

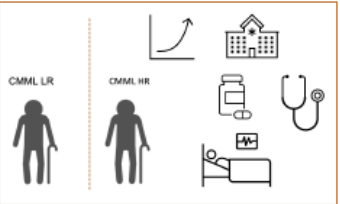
Table 1: Positive association between inflammasome reactivity and sensitivity of CMML. Clinical data from CMML patients was collected and analysed. Low reactive patients had low grade CMML (CMML-0), whereas higher grade CMML (CMML-1/2) was only found in high reactive CMML patients. The risk scores, namely International Prognostic Scoring System (IPSS) and Revised International Prognostic Scoring System (IPSS-R), are more likely to be increased in high reactive patients. Splenomegaly was more frequently to be found in high reactive patients. Additionally, time to treatment and time to death were shorter in high reactive patients.

## DISCUSSION & CONCLUSIONS

Collectively, our results suggest that aging causes dysregulation and increase sensitivity to NLRP3 inflammasome activation at the cellular level, which may explain increased inflammation and immunopathology in the elderly.



Our results identified a new age dependent pathway exclusively arising in old people via TLR1/2 caspase-8 alternative inflammasome activation. Taken together, aging increases sensitivity for inflammasome activation in human monocytes and positively correlates with disease severity in CMML.



The proinflammatory cytokine IL-1 $\beta$  could possibly be used as a prognostic factor or as a basis for a future drug target for CMML patients. However, further studies are needed to explore the role of IL-1 $\beta$  in the human aging process and in the pathogenesis of CMML.

## REFERENCES

- [1] Allison K Meyers and Xuewei Zhu. Cells 2020
- [2] Moritz M Gaidt et al. Immunity 2016

## CONTACT INFORMATION

Hematology Department/Inselspital  
Department for BioMedical Research, University of Bern  
Murtensstrasse 40, CH-3008 Bern  
Switzerland.

Email: loulise.demeuron@students.unibe.ch



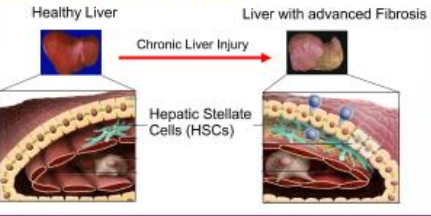


# Extracellular Vesicles from Human Hepatic Stellate Cells Provide Insights into Liver Fibrosis Treatments using Proteomic Data

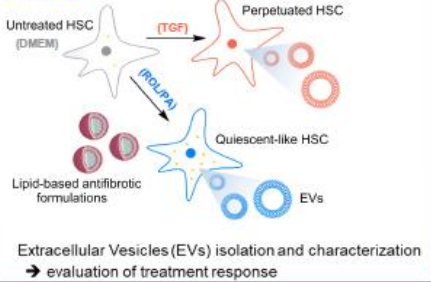
C. Zivko<sup>1,2</sup>, K. Fuhrmann<sup>2</sup>, G. Fuhrmann<sup>2</sup>, P. Luciani<sup>1</sup>

<sup>1</sup>Department of Chemistry, Biochemistry and Pharmaceutical Sciences, University of Bern, Switzerland  
<sup>2</sup>Helmholtz Institute for Pharmaceutical Research Saarland, Saarland University, Germany

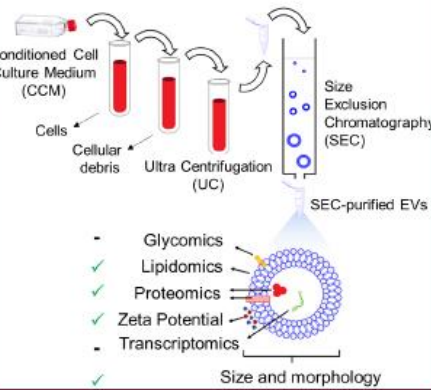
## INTRODUCTION



## AIMS



## METHODS



## RESULTS

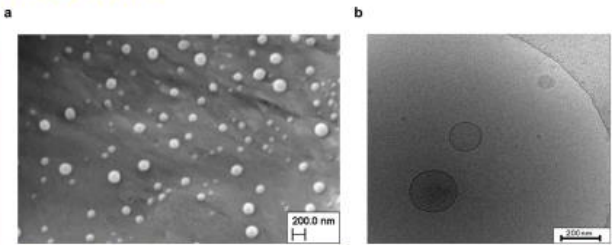


Figure 1: SEM (a) and cryo-TEM (b) images of EVs isolated from untreated cells.

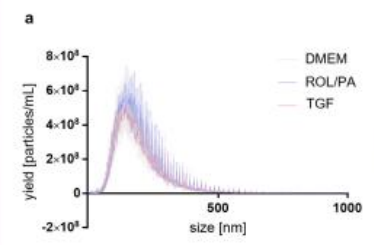
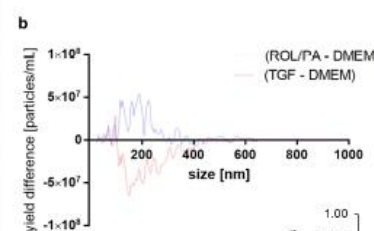
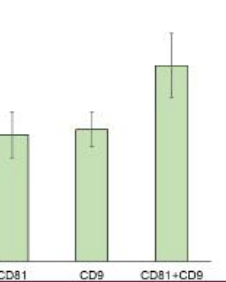


Figure 2: Size distribution profiles of the isolated EVs from the differently treated HSCs (a).



Quantile differences in the yielded EV populations (b).  
(n = 3, software: ZetaView 8.05.05 SP2).

Figure 3: Presence of exosomal markers CD81 and CD9 on untreated cells (mean ± SD, n = 3).



Treatment discriminating 44-proteins panel

DMEM	ROL/PA	TGF	Additional treatments		
			1	2	3
0.131041	0.143962	0.097731	0.049667	0.219253	0.358346
0.23759	0.184593	0.177327	0.194043	0.103549	0.102899
0.082487	0.119659	0.121999	0.070899	0.068961	0.535995
0.046227	0.047696	0.048711	0.032097	0.05194	0.773329
0.132741	0.102134	0.099212	0.176996	0.155226	0.333691
0.053309	0.082517	0.098608	0.042519	0.033504	0.689543
0.146318	0.105381	0.127021	0.079414	0.130328	0.411537
0.125187	0.104815	0.067602	0.094452	0.132509	0.475436
0.149243	0.118704	0.487867	0.101843	0.033909	0.108434
0.265088	0.242945	0.218848	0.178426	0.082204	0.012489
0.15099	0.135041	0.46714	0.065352	0.051406	0.13007
0.055054	0.087459	0.063442	0.045598	0.038399	0.710047
0.146998	0.106521	0.649987	0.047058	0.040746	0.00869
0.114099	0.141511	0.067861	0.159889	0.19972	0.316921
0.117776	0.11104	0.061021	0.19661	0.188027	0.325526
0.054038	0.087652	0.116629	0.061325	0.074734	0.605621
0.213238	0.182828	0.103304	0.240878	0.149222	0.11053
0.041618	0.149059	0.039669	0.057754	0.121367	0.590471
0.080863	0.127724	0.047015	0.035018	0.092004	0.617377
0.134111	0.161602	0.183152	0.116089	0.186171	0.218876
0.126516	0.115533	0.092473	0.089154	0.087846	0.488681
0.067079	0.10073	0.050706	0.027333	0.1696	0.584553
0.354338	0.158485	0.211064	0.117706	0.07429	0.084116
0.101897	0.091388	0.057368	0.032657	0.18909	0.5276
0.111775	0.152392	0.181405	0.107127	0.120196	0.327104
0.089273	0.109141	0.032178	0.087862	0.151277	0.530269
0.096081	0.189733	0.03494	0.048668	0.165154	0.465423
0.187691	0.270953	0.354989	0.098817	0.064021	0.023529
0.081366	0.094164	0.085096	0.068951	0.083833	0.586589
0.132783	0.163698	0.038042	0.121133	0.158974	0.38537
0.116219	0.115527	0.062519	0.08052	0.055472	0.569742
0.130536	0.140481	0.080074	0.173069	0.177018	0.298822
0.062216	0.068583	0.066066	0.079212	0.130432	0.593492
0.035262	0.086115	0.060899	0.043234	0.056064	0.718427
0.190427	0.246698	0.18235	0.101399	0.190035	0.089091
0.078538	0.085823	0.071195	0.072456	0.081349	0.610638
0.178892	0.241125	0.089596	0.071678	0.132973	0.285736
0.135858	0.118225	0.077794	0.257036	0.197343	0.213743
0.143909	0.190258	0.081586	0.1846	0.203068	0.196579
0.146503	0.190384	0.174792	0.07894	0.126025	0.283356
0.106136	0.123526	0.12567	0.059337	0.139446	0.445885

Figure 4: Treatment-discriminating proteomic panel. Expression levels for each protein were scored to generate a heat map.

## DISCUSSION & CONCLUSIONS

### Discussion

EVs were found to play an active role in affecting neighboring cells' status.  
  
Differently treated HSCs produced EVs in similar yields ( $10^{10}$  particles/mL), sizes ( $180 \pm 90$  nm) and zeta potential values ( $-36 \pm 3$  mV), generated by ca.  $10^7$  cells (>96% cell viability).  
  
Successful purifications revealed EV subpopulations with different physico-chemical behaviors.

Electron microscopy imaging corroborated the size polydispersity and EV-morphology.

Peptide analysis by nano-LC-MS/MS revealed EV-associated proteins whose expression correlated with HSCs treatment.  
Complex proteomic datasets were mined to develop a screening panel that can be used to effectively distinguish between treatments and cell status.

For the first time, we could measurably correlate the cellular response to lipid-based antifibrotic treatment to the relative presence of candidate protein markers on the released EVs.

### Conclusions

Our results confirmed differences in EV populations originating from the same cells in either healthy or diseased state, paving the way for more precise and less invasive diagnostic analyses.

## REFERENCES

- [1] Bataller et al., J Clin Invest. 2005
- [2] Valentino et al. Pharmaceuticals. 2019
- [3] Zivko et al., Biochim Biophys Acta Gen Subj., 2020
- [4] Frank J et al. Sci Rep. 2018
- [5] Zivko et al., manuscripts in preparation 2021

## CONTACT INFORMATION

cristina.zivko@unibe.ch  
@CristinaZivko, @Luciani\_Jab & @FuhrmannGregor





A. Ferro<sup>1,2</sup>, D.G. Graikioti<sup>3</sup>, C.M. Athanassopoulos<sup>3</sup>, M. Cuendet<sup>1,2</sup>

<sup>1</sup>School of Pharmaceutical Sciences, University of Geneva, 1211 Geneva 4, Switzerland

<sup>2</sup>Institute of Pharmaceutical Sciences of Western Switzerland, University of Geneva, 1211 Geneva 4, Switzerland

<sup>3</sup>Synthetic Organic Chemistry Laboratory, Department of Chemistry, University of Patras, 26504 Patras, Greece

## INTRODUCTION

Despite enormous advances among therapeutic strategies, multiple myeloma (MM) remains an incurable disease with MM patients often not responding to standard treatments [1]. Proteasome inhibitors (PI), with the first in class bortezomib (BTZ), are one of the backbones of the anti-MM regimens [2]. Unfortunately, MM cells often develop resistance to PI by using the alternative aggresome pathway for protein degradation in which histone deacetylase 6 (HDAC6) is one of the main player [3]. In the past decade, HDAC inhibitors such as panobinostat (Pan), vorinostat, entinostat, ricolinostat and others have been considered in combination with conventional regimens [4]. Multiple targeted therapies have proven to be more beneficial compared to monotherapy approaches, leading to overcome drug resistance and improving median patient overall survival [4]. Beside the drug combination approach, another strategy consists of designing dual-target agents with the added advantage of achieving inhibition of multiple pathways through a single molecular entity [5]. Thus, dual HDAC-PI inhibitors could be a promising strategy to decrease resistance and to minimize the administered therapeutic doses [5].

## AIM

Evaluation of synthetic dual HDAC-PI hybrid inhibitors against MM.

## METHODS

- For the synthesis of the dual HDAC-PI hybrid inhibitors, standard liquid phase peptide chemistry procedures were used, starting from (*R*)-borelucine (1*S*,2*S*,3*R*,5*S*)-(+)-2,3-pinanediol ester trifluoroacetate.
- The antiproliferative activity of the compounds was measured through XTT assay in RPMI 8226 cells and RPMI 8226 cells resistant to PI (RPMI 8226-R).
- The HDAC inhibitory activity was measured in RPMI 8226 cells treated for 8 h using a UHPLC-MS-based method [6].

## RESULTS

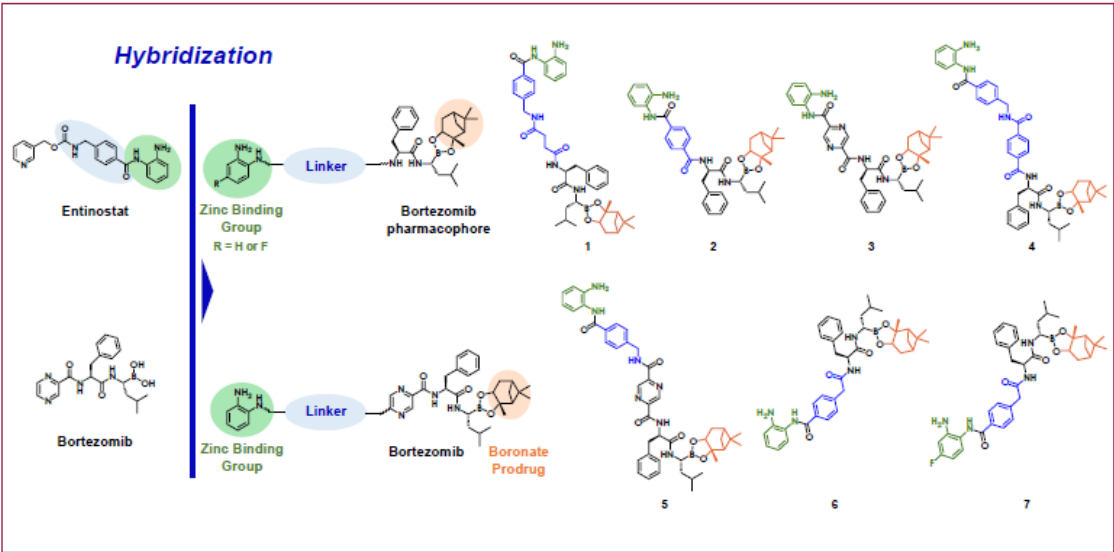


Figure 1. Chemical structures of the synthetic dual HDAC-PI hybrid inhibitors.

Table 1. Antiproliferative activity (IC<sub>50</sub> values  $\pm$  SD in nM, n = 3) of compounds 1-7 in RPMI 8226 cells and in RPMI 8226-R cells.

Compound	IC <sub>50</sub> RPMI 8226 (nM)	IC <sub>50</sub> RPMI 8226-R (nM)
1	677.7 $\pm$ 42.5	ND <sup>a</sup>
2	37.1 $\pm$ 2.9	63.6 $\pm$ 6.3
3	9.5 $\pm$ 1.4	18.9 $\pm$ 0.5
4	802.4 $\pm$ 72.7	ND
5	215.8 $\pm$ 13.8	ND
6	336.6 $\pm$ 49.4	729.7 $\pm$ 57.7
7	3098.6 $\pm$ 232.2	ND
BTZ <sup>b</sup>	2.1 $\pm$ 0.4	6.0 $\pm$ 1.2
Entinostat <sup>b</sup>	328.9 $\pm$ 25.7	524.1 $\pm$ 46.4

<sup>a</sup>ND: not determined

<sup>b</sup>positive controls

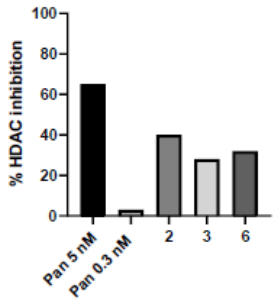


Figure 2. HDAC inhibitory activity of compounds 2, 3 and 6 measured after 8 h treatment at 10  $\mu$ M.

## DISCUSSION & CONCLUSIONS

Seven dual HDAC-PI hybrid inhibitors were synthesized based on entinostat and BTZ (Figure 1), and tested in RPMI 8226 cells for their antiproliferative activity. Those that showed an IC<sub>50</sub> lower than 500 nM were screened in RPMI 8226-R (Table 1). Compound 3 displayed the strongest antiproliferative activity due to the structural modification to the boronic acid of BTZ as pinanediol ester and the presence of the arylamide zinc binding group of entinostat. It showed low nM antiproliferative activity both in RPMI 8226 cells and in RPMI 8226-R cells of 9.5 nM and 18.9 nM, respectively. It exhibited slightly less activity than BTZ but with the advantage of targeting multiple pathways. The HDAC inhibitory activity in RPMI 8226 cells was measured after 8 h at a concentration of 10  $\mu$ M. Preliminary results reported that compounds 1 and 4 did not have activity while compounds 2, 3 and 6 demonstrated 40%, 28% and 32% HDAC inhibition, respectively (Figure 2). Further experiments are on going to assess the IC<sub>50</sub> values of the compounds that showed HDAC inhibitory activity. Since the derivatives are made of BTZ, the 26S proteasome chymotrypsin-like inhibitory activity of the compounds will also be evaluated. Previous studies have shown that HDAC6 selective inhibitors can be as efficient as pan-HDAC with the profit of improving the safety profile [7]. In MM, HDAC6 plays a significant role in the progression of the malignancy. Thus, the substitution of entinostat with a selective HDAC6 inhibitor is currently being pursued and it may reduce unfavorable side effects.

## REFERENCES

- [1] Kyle RA and Rajkumar SV. Multiple myeloma. Blood 2008; 111: 2962-72.
- [2] Gandolfi S et al. The proteasome and proteasome inhibitors in multiple myeloma. Cancer Metastasis Rev 2017; 36: 561-584.
- [3] Simms-Waldrip T et al. The aggresome pathway as a target for therapy in hematologic malignancies. Mol Genet Metab 2008; 94: 283-6.
- [4] Imai Y et al. HDAC inhibitors exert anti-multiple myeloma effects through multiple modes of action. Cancers 2019; 11:475.
- [5] Zhou Y et al. Discovery of peptide boronate derivatives as histone deacetylase and proteasome dual inhibitors for overcoming bortezomib resistance of multiple myeloma. J Med Chem 2020; 63: 4701-4715.
- [6] Zwick V et al. UHPLC-MS-based HDAC Assay Applied to Bio-guided Microfractionation of Fungal Extracts. Phytochemical Analysis 2017; 28: 93-100.
- [7] Vogl DT et al. Ricolinostat, the first selective histone deacetylase 6 inhibitor, in combination with bortezomib and dexamethasone for relapsed or refractory multiple myeloma. Clin Cancer Res 2017; 23: 3307-3315.

## CONTACT INFORMATION

angelica.ferro@unige.ch



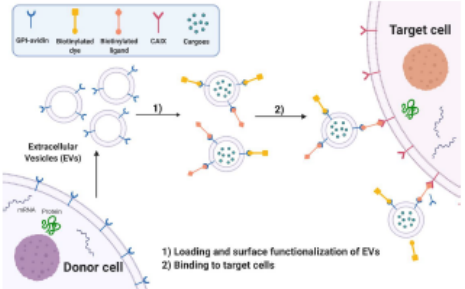
# A Novel and Flexible Strategy to Functionalize Extracellular Vesicles for Targeted Tumor Therapy

**B. SABANI<sup>1</sup>, M. Brand<sup>1</sup>, M. Nedic<sup>1</sup>, I. ALBERT<sup>1</sup>, R. Riedl<sup>1</sup>, S. LEHMANN<sup>1</sup>**  
<sup>1</sup> Institute of Chemistry and Biotechnology, Zürich University of Applied Sciences

**INTRODUCTION**

Extracellular vesicles (EVs) are cell-derived, membrane vesicles, which efficiently shuttle biological cargo including proteins between cells.<sup>[1]</sup> EVs are therefore considered as novel **nanocarriers** for drug delivery.<sup>[2]</sup> However, EVs exhibit a low targeting specificity and an unfavorable pharmacokinetic profile. To overcome these limitations, surface functionalization with ligands directing EVs to specific tissues is essential.<sup>[3]</sup> In this project, a novel and flexible strategy for **surface functionalization of EVs with small molecule ligands** to target them to tumor cells was established. The novel functionalization method is based on a simple "building block" approach involving the **avidin-biotin system** (see figure 1).

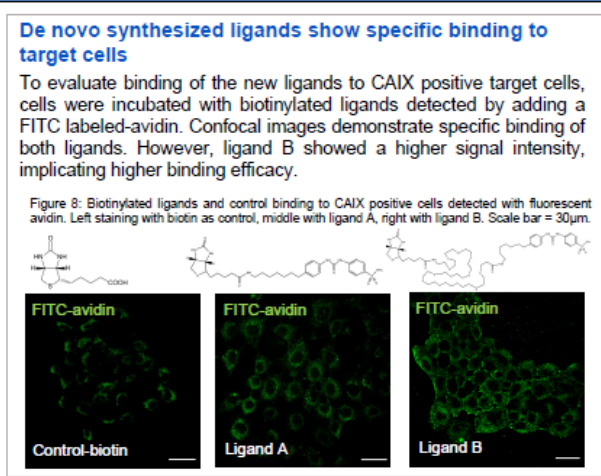
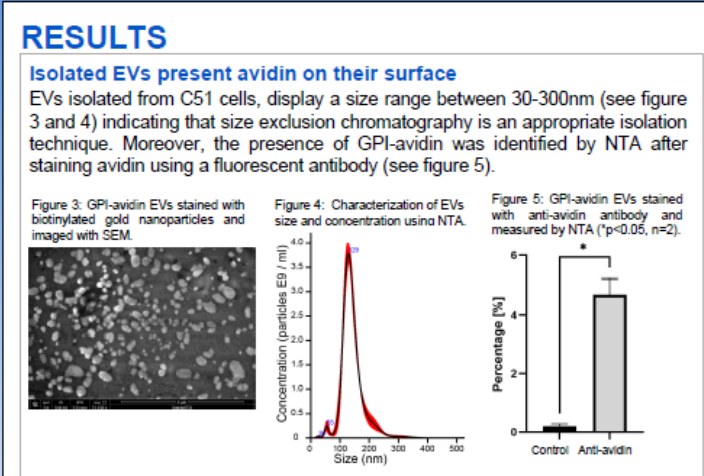
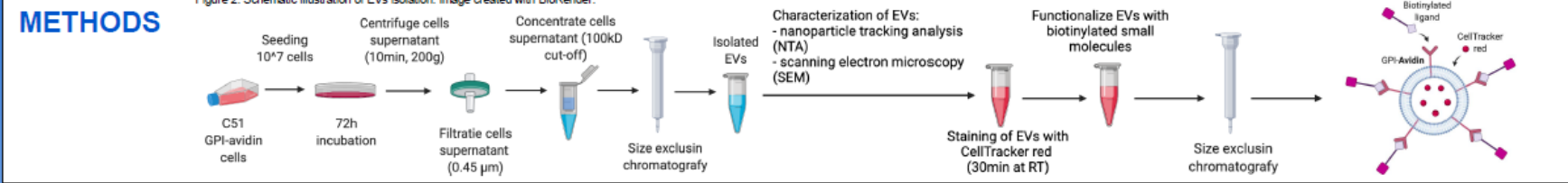
Figure 1: Surface functionalization of GPI-Avidin-EVs with biotinylated dyes. Image created with BioRender.



1) Loading and surface functionalization of EVs  
2) Binding to target cells

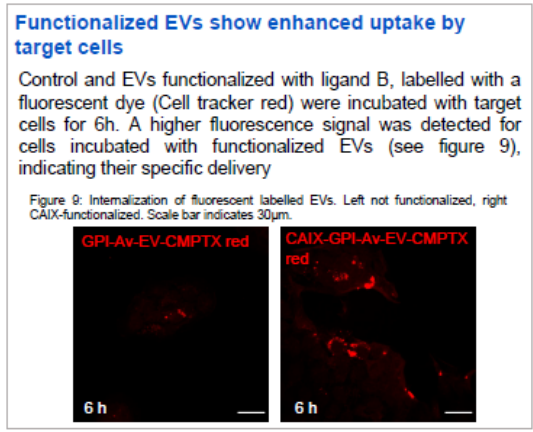
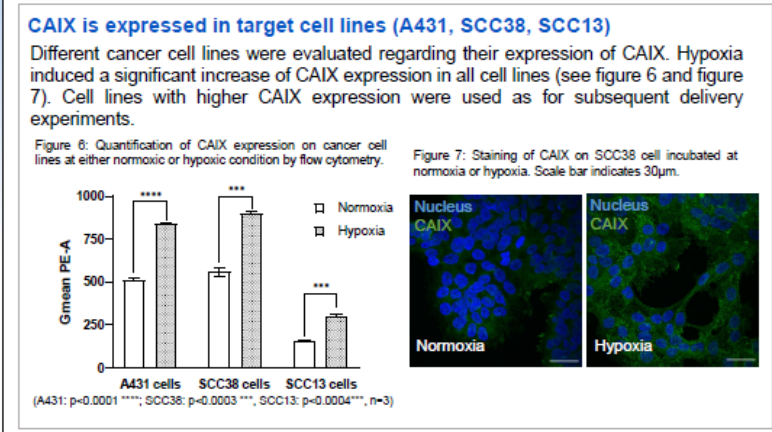
**AIMS**

- I. Establish a protocol for efficient EV isolation
- II. Confirm the presence of GPI-avidin on EVs
- III. Assess the expression of CAIX on cancer cells and characterize the binding affinity of *de novo* synthesized biotinylated CAIX ligands
- IV. Investigate the binding and internalization of functionalized EVs by target cells



**DISCUSSION & OUTLOOK**

Overall, this project provides first evidence that EVs can be flexibly functionalized using the GPI-Avidin system. GPI-Avidin EVs functionalized with ligands targeting CAIX specifically bound to and were internalized by CAIX expressing cancer cells within 6 hours, revealing the appropriateness of EVs as drug delivery system. However, for the translation into the clinic and for the application of precision and personalized medicine, EVs will have to be characterized with regard to their biodistribution and targeting capacity in preclinical animal models. Furthermore, EVs from human mesenchymal stem cells, associated with minimal immunogenicity according to first clinical studies or autologous patient cells will have to be stably transfected to express GPI-Avidin and used for further experiments.



**REFERENCES**

- [1] EL Andaloussi et al., 2013
- [2] Colombo et al., 2014
- [3] Wiklander et al., 2019.

**CONTACT INFORMATION**

leht@zhaw.ch (S.L.); sabn@zhaw.ch (B.S.)





# FOLFOXIRI-resistance induction in colorectal carcinoma in vitro models

G. M. Ramzy<sup>1,2,3</sup>, S. Boss<sup>1,2,3</sup>, P. Nowak-Sliwinski<sup>1,2,3</sup>

<sup>1</sup> Molecular Pharmacology Group, School of Pharmaceutical Sciences, University of Geneva, 1211 Geneva, Switzerland;

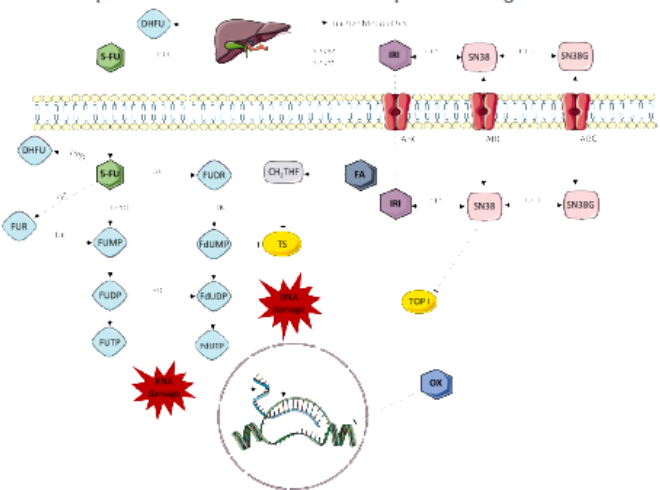
<sup>2</sup> Institute of Pharmaceutical Sciences of Western Switzerland, University of Geneva, 1211 Geneva, Switzerland

<sup>3</sup> Translational Research Center in Oncohaematology, 1211 Geneva, Switzerland.

## INTRODUCTION & AIMS

FOLFOXIRI (folinic acid, 5-fluorouracil, oxaliplatin and/or irinotecan) is a standard of care for colorectal cancer (CRC), yet an aggressive and non-personalized treatment option [1]. The treatment efficacy remains low due to patient-intolerance and induced resistance.

We aimed to generate CRC cells that would reflect the clinical situation of stage IV CRC patients long term treated with FOLFOXIRI. This would serve as a platform to study how an induced drug resistance to this chemotherapeutic mixture could alter the response to targeted treatment.



## METHODS

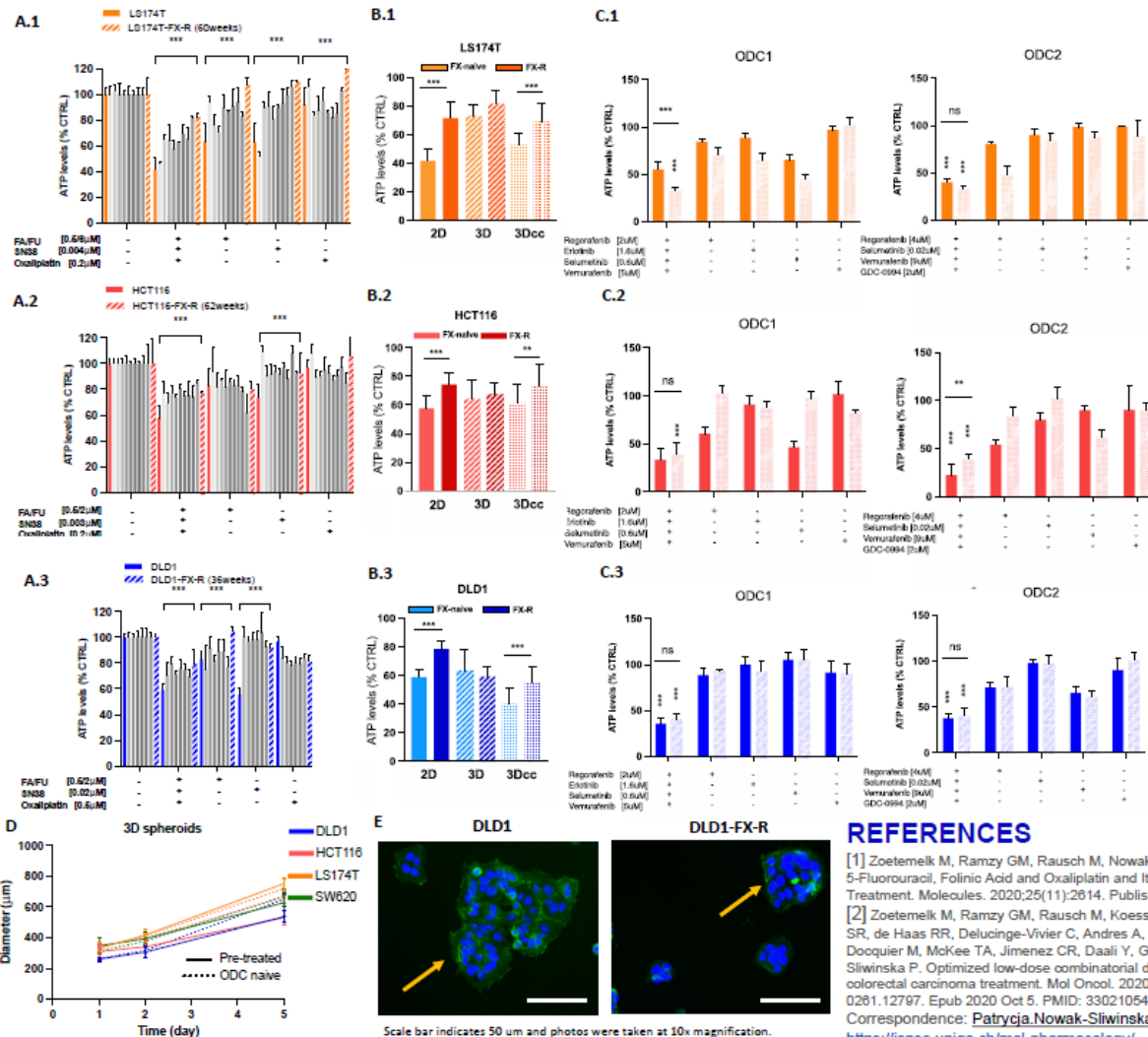
Four human CRC cell lines

Cell line	Mutations/Deregulations
DLD1	metastatic APC, KRAS, PIK3CA, TP53
SW620	metastatic APC, KRAS, TP53
LS174T	primary KRAS, PIK3CA, BRAF
HCT116	primary KRAS, PIK3CA

were chronically treated with their corresponding optimized FOLFOXIRI mixture, once weekly.

Drug [μM]	CUD	DLD1	HCT116	SW620	LS174T
Folinic acid	0.5	0.5	0.5	0.25	0.5
5-Fluorouracil	10	2	2	6	6
SN-38	0.1	0.02	0.003	0.004	0.004
Oxaliplatin	0.6	0.5	0.2	0.3	0.2

## RESULTS & DISCUSSION



A. Significant loss in sensitivity to FOLFOXIRI was observed in all four chronically treated CRC cell lines, with up to 40% in LS174T cell line.

B. Resistance induction was observed compared to the parental treatment-naïve cell lines, in both 2D, 3D and 3D co-cultures of the pre-treated cell lines together with endothelial cells and fibroblasts.

C. Previously optimized synergistic drug combinations (ODC) [2] maintain their activity and overcome resistance to FOLFOXIRI.

D. Pre-treated cell lines have similar growth over time compared to their naïve counterpart.

E. Induced morphometric changes are also observed in the pre-treated cells

## CONCLUSIONS

By chronically exposing human CRC cell lines to a cell line specific FOLFOXIRI mixture, resistance is obtained over time. The latter can be overcome using ODC. RNA sequencing analysis is being conducted to highlight the different signaling pathways implicated in the

## REFERENCES

- [1] Zoetemelk M, Ramzy GM, Rausch M, Nowak-Sliwinski P. Drug-Drug Interactions of Irinotecan, 5-Fluorouracil, Folinic Acid and Oxaliplatin and Its Activity in Colorectal Carcinoma Treatment. *Molecules*. 2020;25(11):2614. Published 2020 Jun 4. doi:10.3390/molecules25112614
- [2] Zoetemelk M, Ramzy GM, Rausch M, Koessler T, van Beijnum JR, Weiss A, Merville V, Piersma SR, de Haas RR, Delucinge-Vivier C, Andres A, Toso C, Henneman AA, Ragusa S, Petrova TV, Docquier M, McKee TA, Jimenez CR, Daali Y, Griffioen AW, Rubbia-Brandt L, Dietrich PY, Nowak-Sliwinski P. Optimized low-dose combinational drug treatment boosts selectivity and efficacy of colorectal carcinoma treatment. *Mol Oncol*. 2020 Nov;14(11):2894-2919. doi: 10.1002/1878-0261.12797. Epub 2020 Oct 5. PMID: 33021054; PMCID: PMC7607171.

Correspondence: [Patrycja.Nowak-Sliwinski@unige.ch](mailto:Patrycja.Nowak-Sliwinski@unige.ch), [George.ramzy@unige.ch](mailto:George.ramzy@unige.ch)  
<https://isps.unige.ch/mol-pharmacology/>

# Development of a complex organoid platform to evaluate the impact of synergistic drug combinations for colorectal cancer treatment

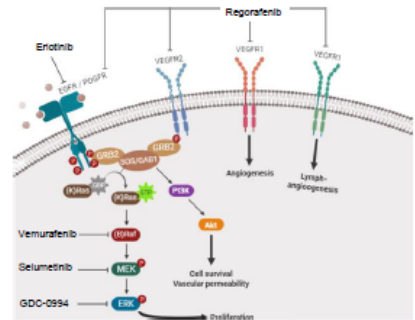
Y.J. PETERMANN<sup>1,2,3</sup>, G.M. RAMZY<sup>1,2,3</sup>, P. NOWAK-SLIWINSKA<sup>1,2,3</sup>

1 School of Pharmaceutical Sciences, Faculty of Science, University of Geneva, Switzerland;  
2 Institute of Pharmaceutical Sciences of Western Switzerland, University of Geneva, Geneva, Switzerland;  
3 Translational Research Center in Oncohaematology, Geneva, Switzerland

## INTRODUCTION

Colorectal cancer (CRC) is one of the three most commonly occurring cancer types with 1.8 million new cases in 2018 while its incidence is expected to rise by 60% until 2030. Current standard therapies for CRC consisting of combined chemotherapeutics are facing some limitations, especially in the late stage of the disease, and, therefore, novel drug-based therapies are urgently required.

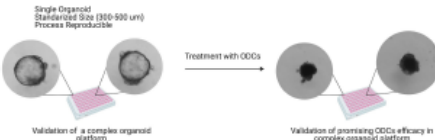
In our previous studies<sup>(1)</sup> we have identified promising synergistic low-dose four drug mixtures for treatment of human CRC. The optimization was performed using our validated phenotypic Therapeutically Guided Multidrug Optimization (TGMO) platform, a technology that allows rapid identification of synergistic multidrug combination at low doses. Validation of the optimized drug combinations (ODCs) efficacy is expected to give important insights into their potency in a representative model of CRC.



## METHODS

- Organoids generated from a genetically modified C57 Black 6 Mouse (Apcfl/fl;Krasfl-LSL-G12D-fl/+;p53fl/fl; villin-CreERT2) (AKP Organoids), were cultivated on 96 well plate<sup>(2)</sup>
- Imaging of AKP Organoids and size measurement overtime to monitor their growth and morphology
- ATP Levels of AKP Organoids were assessed overtime in order to establish the viability of the platform and the efficacy of ODCs previously validated in human CRC cell line, SW620 and DLD1<sup>(1)</sup>

## AIMS



- Establishment of a complex organoid platform (A)
- Validation of the efficacy of previously identified ODCs in the newly created organoid platform (B)

## DISCUSSION & CONCLUSIONS

The organoid platform was successfully established with high reproducibility and a 95% success rate of single organoid formation. Moreover, the previously identified ODCs maintained their cytotoxic effect in the newly created organoid model, despite the species change. We are currently enriching the platform with immune cells to evaluate the effect of ODCs on the immune system.

## REFERENCES & ACKNOWLEDGEMENT

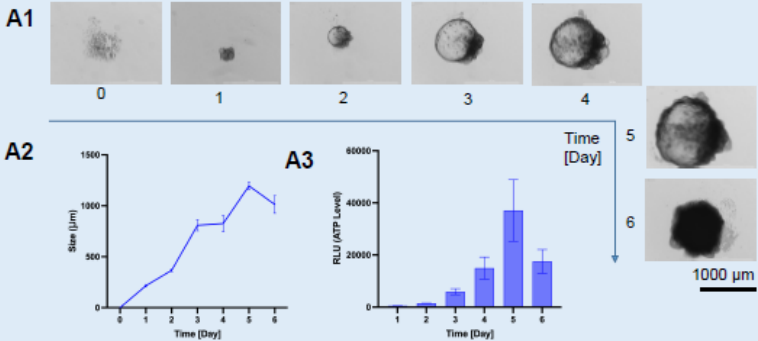
[1] Zoelmeik M et al. Optimized low-dose combinatorial drug treatment boosts selectivity and efficacy of colorectal carcinoma treatment. Mol Oncol. 2020;14(11):2894-2919.  
[2] Ragusa S, Prati-Luri B, Gonzalez-Loyola A, Nassiri S, Squadrini ML, Guichard A, Cavin S, Gjorevski N, Barras D, Marm G, Lutorf MP, Perentes J, Corse E, Bianchi R, Wettstein L, Kim J, Oliver G, De Lorenzi M, De Palma M, Petrova TV. Antitumorigenic immunotherapy suppresses desmoplastic and chemoresistant intestinal tumors in mice. J Clin Invest. 2020 Mar 2;130(3):1199-1216. doi: 10.1172/JCI129558. PMID: 32015230; PMCID: PMC7269598.

We would like to thank Prof. Tatiana Petrova's group from the Vascular and Tumor Biology Laboratory of the University of Lausanne for kindly providing us the AKP organoids, thus allowing the establishment of the organoid platform.

## CONTACT INFORMATION

<https://ispso.unige.ch/moi-pharmacology/>  
Correspondence: [Patrycja.Nowak-Sliwinska@unige.ch](mailto:Patrycja.Nowak-Sliwinska@unige.ch), [Yuan.Petermann@unige.ch](mailto:Yuan.Petermann@unige.ch)

## RESULTS

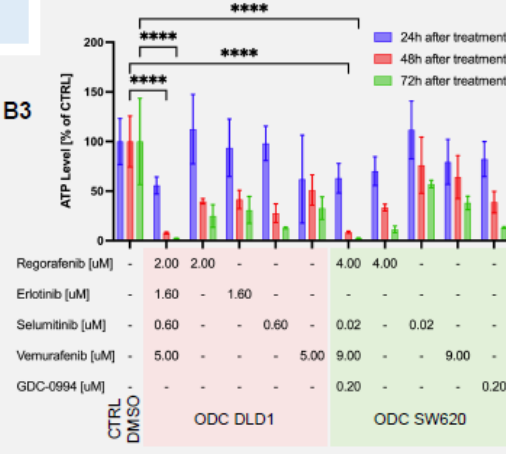
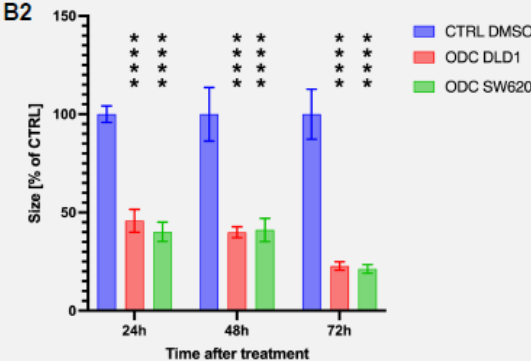
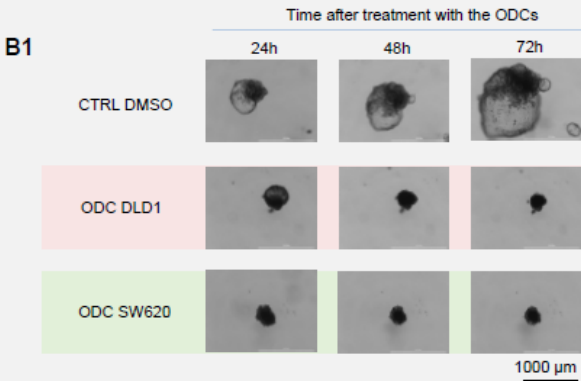


### ESTABLISHMENT OF THE ORGANOID PLATFORM (A)

A1. Overtime monitoring of the AKP organoids by live cell imaging showing successful formation of single organoids. A2. Size measurement overtime of the AKP organoids, displaying a growth until day 5 and an ideal size (300 to 500 µm) for treatment at day 2. A3. ATP levels of the single AKP Organoids overtime suggesting a timeframe for treatment readout at day 3, 4 and 5. Lower ATP levels at day 6 in comparison to day 5 indicate cell death 6 days after the formation of the organoids.

### VALIDATION OF THE ODCs IN THE ORGANOID PLATFORM (B)

B1. Imaging comparison of the control AKP organoids (CTRL DMSO) vs the organoids treated with the ODCs (ODC DLD1 and ODC SW620) shows morphological changes with the combination. B2. Size in percentage to control of the treated organoids. Both combinations display a significant size inhibition (P<0.0001) in comparison to control at 24h, 48h and 72h after treatment. B3. ATP level in percentage to control (CTRL DMSO) of the DLD1 and SW620 combination and their respective monotherapies. The ODCs display significant (P<0.0001) cell viability inhibition, validating them in the newly created platform.





# Squalene-NIR dye nanoassemblies for treatment of cancer by phototherapy

S.ADRIOUACH<sup>1,2</sup> and E.ALLEMANN<sup>1,2</sup>

<sup>1</sup> School of Pharmaceutical Sciences, University of Geneva, 1211 Geneva

<sup>2</sup> Institute of Pharmaceutical Sciences of Western Switzerland, University of Geneva, 1211 Geneva 4



UNIVERSITÉ  
DE GENÈVE



SWISS  
PHARMA  
SCIENCE DAY  
2021



SAPhS  
Swiss Academy of  
Pharmaceutical  
Sciences

P - VIII - 8

## INTRODUCTION

Squalene (Sq) is a natural precursor of cholesterol (1). The conjugation of Sq to a drug produces bioconjugates that self-assemble in water to give nanoassemblies (NAs) (2). Near-infrared (NIR) fluorescence has great potential for in vivo tumour imaging. NIR dyes such as the recently synthesized IR-774 (3) are lipophilic cations with preferential accumulation in the mitochondria of cancer cells. They also have photosensitizing properties inducing tumour cell death after NIR light irradiation.

## AIMS

This study aims to develop Sq-IR-774 NAs targeting mitochondria, with imaging and photosensitizing properties and to assess their capacity to induce tumour cell death by phototherapy after NIR light irradiation. Here, we report the in vitro fluorescence imaging, specific mitochondrial localization and antitumour effect of Sq-IR-774 NAs after NIR light irradiation.

## METHODS

### Cell culture

MCF7 human breast cancer cells and MCF-10A non-tumorigenic human breast cells were used to assess the specific localization of Sq-IR-774 NAs in the mitochondria of cancer cells.

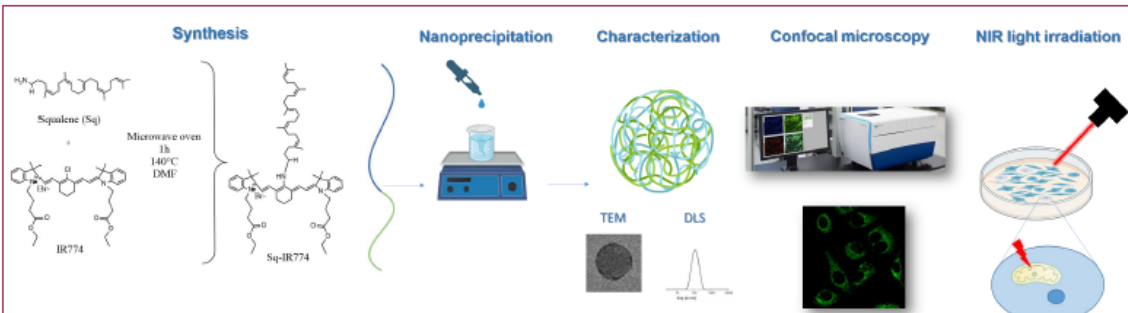
### Cellular uptake

MCF7 and MCF-10A were incubated with 10  $\mu$ M of IR-774 or Sq-IR-774 NAs for 1 h. Mitochondria were stained with MitoTracker® Orange and nuclei with Hoechst®. Cells were observed by live-cell imaging using the automated IXM-XL microscope (Molecular devices, 1 x 40).

### Phototherapy

To study the photosensitizing properties of our product, we incubated MCF7 cells with 20  $\mu$ M of IR-774 and Sq-IR-774 NAs for 1 h. The cells were washed and irradiated with a NIR LED lamp at 660 nm, at 100mW/cm<sup>2</sup> for 10 min. We performed the cytotoxicity assay after 24h using WST-1 cell proliferation assay.

## RESULTS



**Scheme 1 :** Synthesis, nanoprecipitation, imaging and NIR light irradiation of Sq-IR-774 NAs

### NAs preparation and characterization

The Sq-IR-774 is obtained by the covalent conjugation of squalene-amine and IR-774 (Scheme 1). The Sq-IR-774 NAs are obtained by the nanoprecipitation of Sq-IR-774. Briefly, 1mg of Sq-IR-774 are dissolved in 300  $\mu$ L of acetone/ethanol (1:1) and added dropwise into 1.2 ml of MilliQwater. The organic solvent is evaporated under reduced pressure using a rotavapor (Buchi) and the obtained nanoassemblies were characterized by size using dynamic light scattering (DLS) and morphology (TEM). The average size of the NAs obtained by DLS measurement was at 104 nm with a low polydispersity (PDI : 0.144). TEM analysis indicated that Sq-IR-774 had a spherical shape.

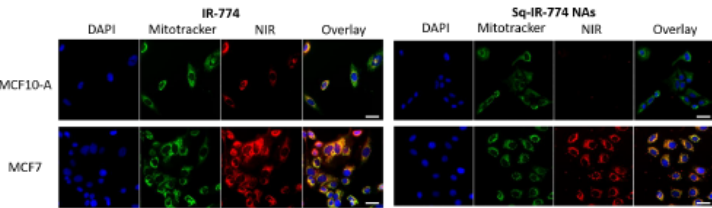


**Figure 1 :** Subcellular localization of IR-774 (10  $\mu$ M) and Sq-IR-774 NAs (10  $\mu$ M) in MCF-10A non-tumorigenic human breast cells and MCF7 human breast cancer cells (scale bar, 10  $\mu$ m).

### Subcellular localization

Fluorescence imaging of MCF-7 cells demonstrated effective localization of both IR-774 and Sq-IR-774 NAs in mitochondria of cancer cells by the co-staining with MitoTracker® Orange. The comparison with MCF-10A non-tumorigenic breast cells demonstrated the preferential accumulation of our product in cancer cells.

### Light toxicity

Light toxicity assay indicated that both IR-774 and Sq-IR-774 induced tumour cell death after NIR light irradiation compared to the control (dark condition).

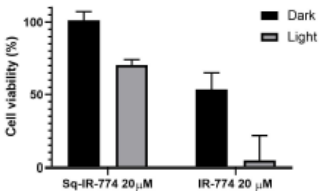


**Figure 2 :** Cytotoxicity assay on MCF7-cells incubated with 20  $\mu$ M of IR-774 or Sq-IR-774 NAs and irradiated with NIR light at 660 nm vs dark.

## DISCUSSION & CONCLUSIONS

To study the subcellular localization of our compounds, MCF-10A human breast non-tumorigenic cells and MCF7 breast cancer cells were incubated with IR-774 and Sq-IR-774 NAs at 10  $\mu$ M for 1h and imaged with IXM-XL confocal microscope. Live-cell imaging of MCF-10A and MCF7 cells demonstrated preferential localization of both IR-774 and Sq-IR-774 NAs in the mitochondria of cancer cells by the co-staining with MitoTracker®Orange (Figure 1).

IR-774 is a lipophilic cation known to accumulate preferentially in the mitochondria of cancer cells (3) because of the high negative potential of the inner mitochondrial membrane. The conjugation of squalene to IR-774 and the following nanoprecipitation provided NAs that targeted preferentially the mitochondria of cancer cells.

NIR light irradiation of MCF7 cells at 660 nm after incubation with 20  $\mu$ M of Sq-IR-774 NAs, demonstrated enhanced antitumour activity compared to dark condition.

Furthermore, the squalenoylation of IR-774 improve the pharmacokinetics and decrease the toxicity towards healthy cells.

The squalenoylation of IR-774 provides several benefits including reduced toxicity without radiation and potential enhancement of antitumour efficacy due to high local retention of the NAs inside the tumour cells compared to IR-774 alone.

Finally, the photothermal properties of our NAs will induce the tumour cell death only upon the activation Sq-IR-774 NAs by NIR light irradiation.

This study demonstrated the preferential accumulation of Sq-IR-774 in the mitochondria of cancer cells by comparison to healthy cells. Sq-IR-774 showed enhanced antitumour activity upon NIR light irradiation and no toxicity towards healthy cells.

The fluorescence and photosensitizing properties of the Sq-IR-774 NAs suggest their potential use as a nanotheranostic agent for imaging and treatment of cancer by phototherapy.

## REFERENCES

- Desmaële D, Gref R, Couvreur P. Squalenoylation: A generic platform for nanoparticulate drug delivery. J Control Release. 2012;161(2): 609-18
- Adriouach S et al. Squalene-PEG: Pyropheophorbide-a nanoconstructs for tumor theranostics. Nanomedicine: NBM 2019;15(1): 243-51
- Vorobiev V et al. Vascular-targeted micelles as a specific MRI contrast agent for molecular imaging of fibrin clots and cancer cells. Eur J Pharm Biopharm 2021; 158: 347-58.

## CONTACT INFORMATION

[Souad.adriouach@unige.ch](mailto:Souad.adriouach@unige.ch)

# Investigating the effects of targeted drug combinations on colorectal cancer

V. MIÉVILLE<sup>1,2</sup>, M. ZOETEMELK and P. NOWAK-SLIWINSKA<sup>1,2</sup>

<sup>1</sup> School of Pharmaceutical Sciences, Faculty of Science, University of Geneva, 1211 Geneva 4  
<sup>2</sup> Institute of Pharmaceutical Sciences of Western Switzerland, University of Geneva, 1211 Geneva 4

## INTRODUCTION

Current therapies used in the clinic for the treatment of colorectal carcinoma (CRC) are composed mostly of chemotherapeutic drugs, which have a less-than-optimal therapeutic window and induce side effects. An interesting alternative is the use of targeted drugs instead. Used as monotherapies, those targeted drugs are however often rapidly followed by the apparition of resistance in the tumors. To challenge these issues, we identified from the large spectrum of possibilities a low-dose synergistic targeted drug combinations (ODC), which are both selective and effective in *in vitro* and *in vivo* models of human CRC [1].

## AIMS

We aimed to characterize at the histological level the activity of two cell subtype specific ODCs, composed of Regorafenib, Selumetinib, Vemurafenib and either Erlotinib or GDC-0994, on human CRC types, DLD1 and SW620 grown in mice..

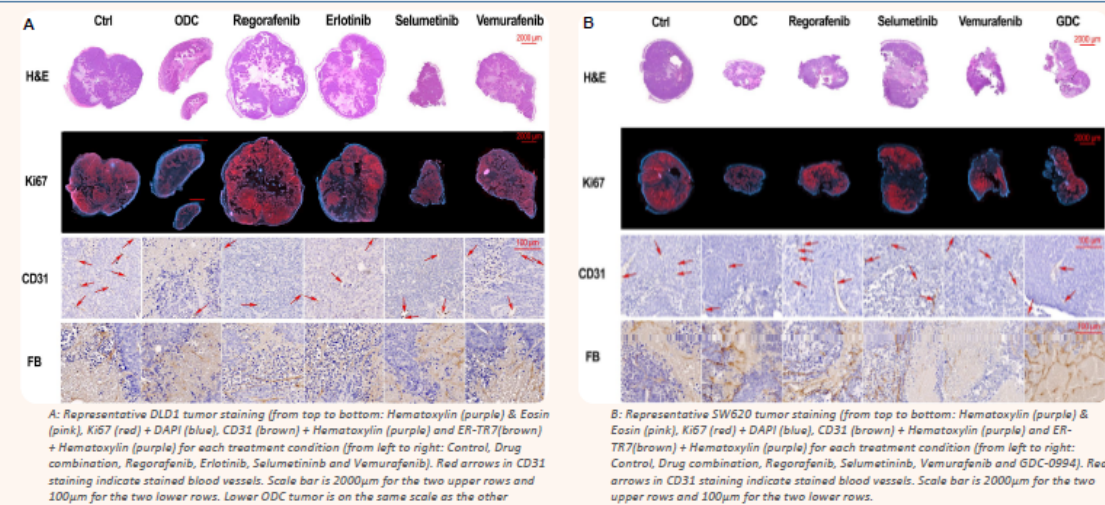
## METHODS

In a previous study we treated mice subcutaneously injected with colorectal cancer cell lines with our ODCs. Mice injected with DLD1 cells were treated with Regorafenib (1,0 mg/day), Erlotinib (6,3 mg/day), Selumetinib (0,27 mg/day) and Vemurafenib (0,3 mg/day). Mice injected with SW620 cells were treated with Regorafenib (1,9 mg/day), GDC-0994 (0,09 mg/day), Selumetinib (0,009 mg/day) and Vemurafenib (4,4 mg/day). The mice were treated with either one drug, the whole combination or solution without any of the drug. Fixed tumors were fixated in paraformaldehyde, dehydrated with ethanol, embedded into paraffin, sliced at 5µm and mounted on glass slides.

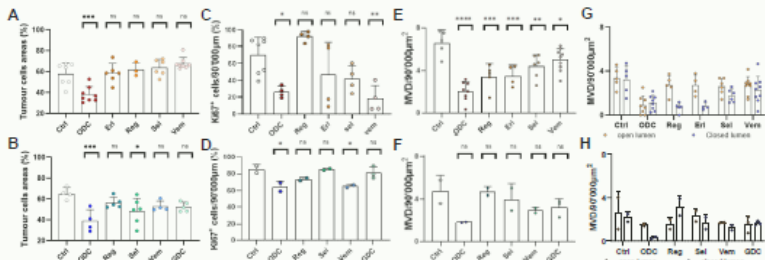
Histological staining were used as follows:

- Hematoxylin + Eosin staining for comprehensive micro-anatomy picture.
- Ki67 + DAPI immunofluorescent staining for proliferation.
- CD31 + Hematoxylin immunohistochemistry staining for blood vessels density and morphology..
- ER-TR7 + Hematoxylin immunohistochemistry staining fibroblast distribution.

## RESULTS



Tumors treated with the respective ODC showed significantly reduced cell and vessel density (minus 17.6% and 26% for cell density and minus 69.7% and 61.7% for vessel density), as well as reduced cell proliferation (minus 42.8% and 20.7%) when compared to control and respective monotherapy treated tumors. Qualitative test for other characteristics could also hint for a fibroblast density reduction effect in SW620 ODC-treated tumors and an apoptosis induction in DLD1 ODC-treated tumors (not displayed here).



Percentage of A) DLD1 and B) SW620 tumor areas containing tumor cells as opposed to stroma (here defined the extracellular matrix and necrotic areas) quantified from n=6 and n=2 tumors, respectively.  
Percentage of C) DLD1 and D) SW620 cells positive to Ki67 staining quantified from 300µm x 300µm areas of n=4 and n=2 tumors, respectively.  
Micro vessels density quantified in 90'000 µm² areas of E) DLD1 and F) SW620 tumors.  
Micro vessels density quantified in 90'000 µm² areas split based on lumen aperture in G) DLD1 and H) SW620 tumors.  
Results from A, B, C, D, E and F were compared to control using Dunnett's multiple comparisons test. \*\*\*\*p<0,0001; \*\*\*p<0,01; \*\*p<0,001; \*p<0,05. Error bars represent standard deviation.

### Key points:

- On top of being smaller, cell density in ODC treated tumors are actually significantly lower than in other treated tumors and control
- ODC significantly decrease proliferation in the tumors
- The ODC reduce the number of blood vessels in the tumors
- Observed effects on blood vessels physiognomy differ between the ODC and the monotherapies

## DISCUSSION

Overall, most of the monotherapies showed, in term of tumor growth inhibition, greater activity *in vivo* as they did *in vitro* but stayed mostly less active than the drug combinations. In DLD1 tumors, the ODC was the treatment that led to the strongest reduction in blood vessel density. We could have attributed this feat to an accumulation of the monotherapies' activities but when observing other parameters such as the effects on the blood vessels physiognomy we can see significant differences with the ODC. Same observation regarding the antiproliferative effect in SW620 tumors. Vemurafenib decreased the expression of Ki67 in a way that is comparable to the ODC. We could have attributed the antiproliferative effect of the ODC solely to this drug, however, when comparing the proliferation spatially in the tumors we observed that the activity of the Vemurafenib was only significant in the edges of the tissue while the ODC decreased the proliferation all over the tumor. As a result, the ODC was the only condition having a significant impact on the cell density in the tumor (i.e., the percentage of the tissue (epidermal cells excluded) covered by cells) for DLD1 and was the one that reduced it the most significantly for SW620. As the tumor treated with the ODC were measured to be the smallest out of all conditions, we know that this is the result of a decrease in tumor cell population in the tissue and not just an increase in stroma production. The source of this better efficacy might partially come from an apoptosis induction in DLD1 or be mediated by an increase in fibroblast in the tumor microenvironment. We could not quantify these parameters, but observations suggest these hypothesis to be possible. They would also match with some of the drug mechanism as Erlotinib and Regorafenib can influence the PI3K-Akt pathway and ERK1/2, the target of GDC-0994, is known to play a role in fibroblast DNA synthesis [2].

## CONCLUSION

The ODCs identified *in vitro* were proven to be effective on various tumor hallmark *in vivo*. The treatment with ODC improved antitumor activity showing encouraging results toward the use of personalized drug combinations in the clinic.

## REFERENCES

- [1] Optimized low-dose combinational drug treatment boosts selectivity and efficacy of colorectal carcinoma treatment - Zoetemelk - 2020 - Molecular Oncology - Wiley Online Library.
- [2] Rosenfeldt, H., and Grinnell, F. (2000). Fibroblast Quiescence and the Disruption of ERK Signaling in Mechanically Unloaded Collagen Matrices'. Journal of Biological Chemistry 275, 3088–3092

## CONTACT INFORMATION

Valentin Miéville: [Valentin.Mievill@unige.ch](mailto:Valentin.Mievill@unige.ch).  
Patrycja Nowak-Sliwinska: [Patrycja.Nowak-Sliwinska@unige.ch](mailto:Patrycja.Nowak-Sliwinska@unige.ch)  
<https://isps.unige.ch/mol-pharmacology/>



# Low-dose multidrug combination preventing spindle pole clustering in dividing cancer cells

E. DUCREY<sup>1,2,3</sup>, G.M. RAMZY<sup>1,2,3</sup>, C. CASTROGIOVANNI<sup>3,4</sup>, P. MERALDI<sup>3,4</sup>, P. NOWAK-SLIWINSKA<sup>1,2,3</sup>

<sup>1</sup>Molecular Pharmacology Group, School of Pharmaceutical Sciences, University of Geneva, Geneva, Switzerland

<sup>2</sup>Institute of Pharmaceutical Sciences of Western Switzerland, University of Geneva, Geneva, Switzerland

<sup>3</sup>Translational Research Center in Oncohaematology, Geneva, Switzerland

<sup>4</sup>Department of Cell Physiology and Metabolism, Faculty of Medicine, University of Geneva, Geneva, Switzerland

SWISS  
PHARMA  
SCIENCE DAY  
2021



P - VIII - 10

SAPhS  
Swiss Academy of  
Pharmaceutical  
Sciences

## INTRODUCTION

Synergistic low-dose multidrug combinations are a promising anti-cancer strategy to achieve high treatment efficacy and decrease the occurrence of dose-related toxicities and acquired resistance.

Our validated phenotypic Therapeutically Guided Multidrug Optimization platform [1] allowed for the identification of an optimized 4-drug combination (ODC) highly effective in renal cell carcinoma, colorectal carcinoma (CRC) and melanoma, while maintaining negligible toxicity towards non-malignant organ-specific epithelial cells.

ODC consists of two tyrosine kinase inhibitors (dasatinib, erlotinib) and two histone deacetylase (HDAC) inhibitors (tacedinaline, tubacin).

## AIMS

- Identify the full **mechanism of action of ODC** and causally link ODC efficacy to spindle pole clustering inhibition
- Evaluate **ODC efficacy in CRC ex vivo models**, highly relevant to human physiopathology

## METHODS

- Selection of CRC cell lines with various mutational status, according to their tendency to present multipolar spindles (**A1**)
- Cell metabolic activity assay (ATP levels) on CRC cell lines (**A2**) and patient-derived organoids (PDO) (**A3**) to evaluate ODC efficacy on cell viability inhibition
- Immunofluorescence microscopy to quantify multipolar spindles and centriole amplification frequencies in cells treated with ODC (**B1**)
- Live cell imaging to monitor mitotic progression (**B2**)

## RESULTS

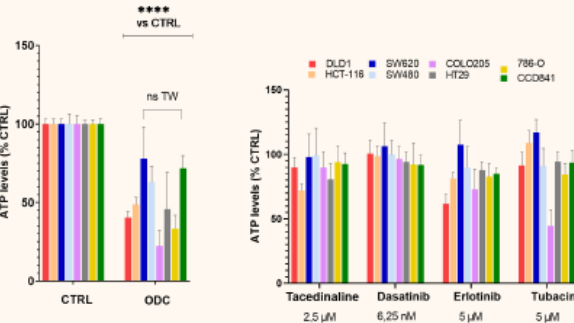
The six CRC cell lines (**A1**), selected according to their tendency to form multipolar spindle, significantly respond to ODC, while maintaining a favorable therapeutic window (TW) with non-malignant colon cells CCD841 (except for SW620). ODC shows strongest efficacy in COLO205 (78% cell viability inhibition vs. control), the cell line displaying highest centriole amplification frequency (**A2**)

**A1**

CRC cell lines	MSI	CIN	Mutation status	Origin	Centriole amplification frequency (%)
DLD1	MSI	-	APC, KRAS, PIK3CA, TP53	Metastatic	No data
HCT116	MSI	-	KRAS, PIK3CA	Primary	7,0
COLO205	MSS	+	APC, BRAF, TP53	Metastatic	57,1
SW480	MSS	+	APC, KRAS, TP53	Primary	No data
SW620	MSS	+	APC, KRAS, TP53	Metastatic	10,3
HT29	MSS	+	APC, BRAF, TP53	Primary	5,8

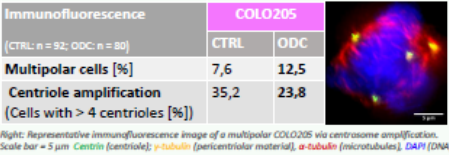
Control cell lines	Centriole amplification frequency (%)
CCD841 Non-malignant epithelial colon cells	No data
786-O Renal cell carcinoma - ODC efficacy positive control	7,4

**A2**



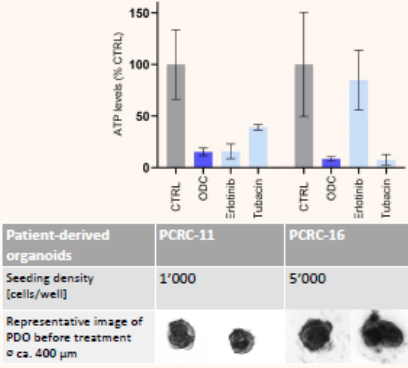
COLO205 display an increased number of multipolar cells (12,5% vs. 7,6% in control) and a decreased proportion of cells presenting centriole amplification after ODC treatment (**B1**). Using live cell imaging reveals, we measured a significant increase in mitotic timing and a 2-fold reduction of mitotic index (**B2**).

**B1**



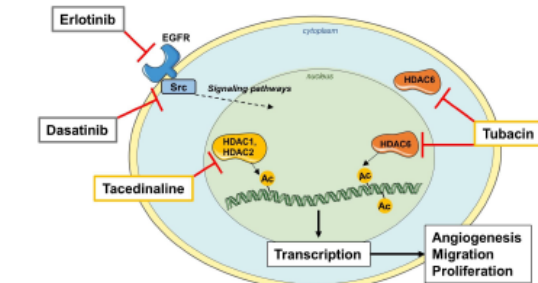
**A3 PRELIMINARY DATA**

ODC shows promising activity (> 80% cell viability inhibition vs. control) in CRC patient-derived organoids isolated from freshly resected primary CRC patient tumors (PCRC-11 and PCRC-16). Optimization of PDO establishment protocol and personalization of drugs doses are still needed.

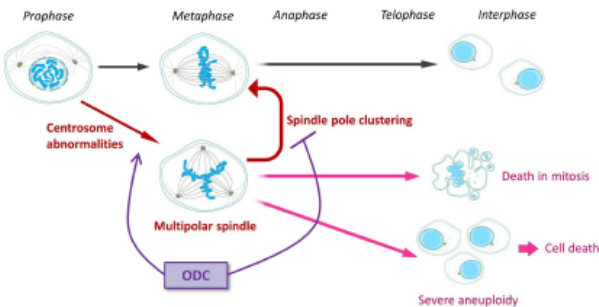


## DISCUSSION & CONCLUSIONS

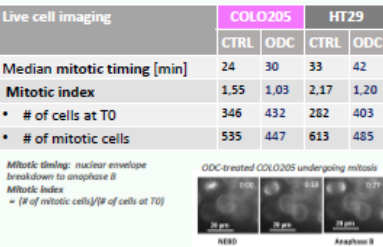
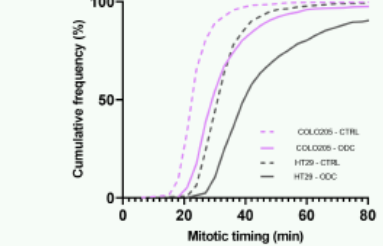
ODC significantly inhibits cell viability in six CRC cell lines, while maintaining a favorable therapeutic window. Strongest ODC efficacy is observed in COLO205, the cell line in our panel displaying highest frequency of centriole amplification. ODC treatment increases the number of multipolar COLO205 cells and reduces proportion of COLO205 cells displaying centriole amplification. This supports the hypothesis ODC targets cells prone to form multipolar spindles. Live cell imaging reveals an increase in mitotic timing, indicating a mitotic mode of action of ODC. However, a 2-fold reduction of mitotic index suggests additional mitosis-independent mechanisms of action need to be investigated. ODC selectively targets dividing cancer cells prone to form multipolar spindles. Its activity in CRC patient-derived organoids reveals potential for clinical translation.



ODC efficacy was strongly correlated with the induction of multipolar spindles and the inhibition of spindle pole clustering, a survival mechanism cancer cells with centrosome abnormalities or mitotic spindle defects use to avoid death via multipolar divisions [1,2].



**B2**



## REFERENCES

- [1] Weiss A et al. Identification of a Synergistic Multi-Drug Combination Active in Cancer Cells via the Prevention of Spindle Pole Clustering. *Cancers (Basel)* 2019; 11 (10). doi:10.3390/cancers11101612
- [2] Ducrey E et al. Forcing dividing cancer cells to die: low-dose drug combinations to prevent spindle pole clustering. *Apoptosis* 2021; .doi:10.1007/s10495-021-01671-3

## CONTACT INFORMATION

Eloise.Ducrey@unige.ch <https://isps.unige.ch/mol-pharmacology/>  
Correspondence: Patrycja.Nowak-Sliwinska@unige.ch; Patrick.Meraldi@unige.ch

# Oatp2b1 influences coproporphyrin serum levels as determined in a novel *Slco2b1*<sup>-/-</sup> rat model

J. Kinzi<sup>1</sup>, J. Hussner<sup>1</sup>, A.M. Schäfer<sup>1</sup>, A. Treyer<sup>2</sup>, I. Seibert<sup>1</sup>, M. Hamburger<sup>2</sup>, H.E. Meyer zu Schwabedissen<sup>1</sup>

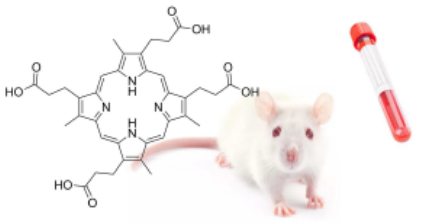
<sup>1</sup> Biopharmacy, Department of Pharmaceutical Sciences, University of Basel, 4001 Basel

<sup>2</sup> Pharmaceutical Biology, Department of Pharmaceutical Sciences, University of Basel, 4001 Basel

SWISS  
PHARMA  
SCIENCE DAY  
2021



P - VIII - 11  
SAPhS  
Swiss Academy of  
Pharmaceutical  
Sciences



## INTRODUCTION

Coproporphyrin (CP) I and III are isomeric byproducts of the heme metabolism. They are handled as potential biomarkers to indicate drug-drug interactions involving hepatic Organic Anion Transporting Polypeptide (OATP) 1B. Another hepatically expressed transporter which is a member of the OATP family is OATP2B1. Literature shows that OATP2B1 specifically transports CP-III and not CP-I.

## AIMS

It was aim of this study to test, whether CP-III could be applied as an endogenous biomarker for OATP2B1-involving interactions by investigating CPs in a novel *Slco2b1*-knockout rat model.

## METHODS

- Handling of CP-III by transport proteins was assessed *in vitro* in single of the human and rat orthologues of rOatp2b1/OATP2B1. Accumulation was determined in double-transfected HeLa cells with Oatp2b1/OATP2B1 (with Mrp3/MRP3 or Mrp2/MRP2). In this cell model expression is driven by the T7 RNA polymerase from the vTF7-virus.
- The novel *Slco2b1*-knockout rat model was characterized for the expression of the transporters assumed to modify the organic anion transporter route in liver and kidney applying Real-time PCR, Western blot analysis and immunohistochemistry.
- CP-I and CP-III plasma levels were determined applying LC-MS analytics.

## CONTACT INFORMATION

Contact: [jonnyhanna.kinzi@unibas.ch](mailto:jonnyhanna.kinzi@unibas.ch)

## RESULTS

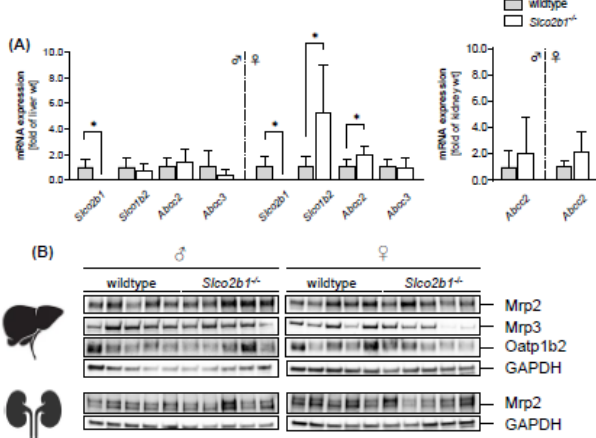


Figure 1: Protein and mRNA expression analysis of genes assumed to be involved in the cellular handling of CP-III in liver and kidney of wildtype and *Slco2b1*<sup>-/-</sup> Wistar rats (age 11 weeks). (A) Relative gene expression of rat *Slco2b1*, *Slco1b2*, *Abcc2*, *Abcc3*, *Mrp2*, *Mrp3*, *Oatp1b2*, *Abcc2*, *Mrp2*, *Abcc3*, *Mrp3*. Levels were quantified by real-time PCR. (B) Western Blot analysis of tissue samples detecting the presence of drug transporters that are assumed to be involved in cellular handling of CP-III. Data shown as mean  $\pm$  SD (n = 5-7; \* p < 0.05, unpaired t-test).

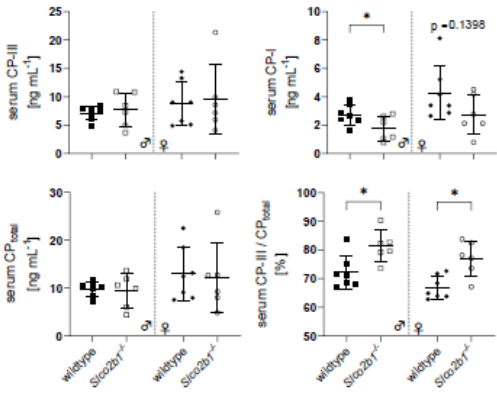


Figure 2: Bioanalysis of serum of wildtype and *Slco2b1*<sup>-/-</sup> rats using LC-MS based quantification of the isomers CP-I and CP-III. Reduction was observed for CP-I levels while CP-III levels are mainly unaffected by the absence of rOatp2b1. The CP ratio shifts towards CP-III due to the lower CP-I and unaltered total CP levels. Data shown as mean  $\pm$  SD (n = 6-7; \* p < 0.05, unpaired t-test).

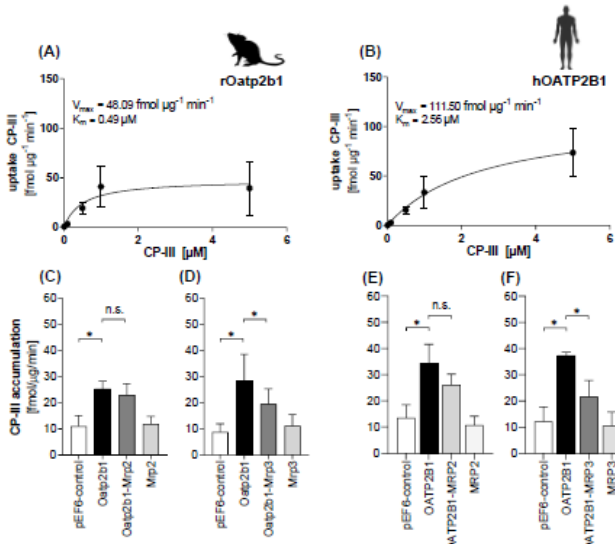


Figure 3: Validation of CP-III transport by rOatp2b1 (A) and OATP2B1 (B) and in effect on cellular accumulation in presence of efflux transporters Mrp2/MRP2 and Mrp3/MRP3 in transiently transfected HeLa cells. (C-F) Double-transfected HeLa cells show significant reduction in CP-III accumulation in the presence of Mrp3 (D) / MRP3 (F), but not in the presence of Mrp2 (C) / MRP2 (E). Data shown as mean  $\pm$  SD (n = 5; \* p < 0.05, one-way ANOVA).

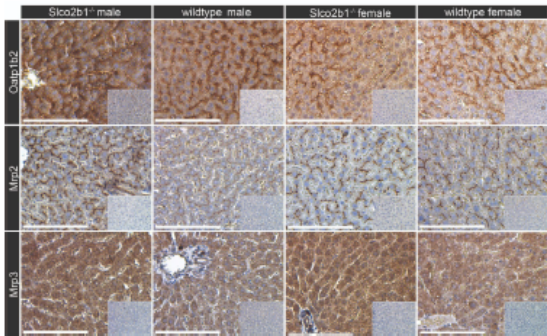


Figure 4: Immunohistochemistry of liver sections of male and female wildtype and *Slco2b1*<sup>-/-</sup> rats. The staining showed distinctive expression of Oatp1b2 on sinusoidal and Mrp2 on canalicular membrane, while for Mrp3 no difference across liver lobules were observed. Nuclei were counterstained using Mayer's hemalum solution. (White bar scale = 100 µm).

## DISCUSSION & CONCLUSIONS

Expression analysis of genes and proteins assumed to be involved in the CP handling revealed significantly higher expression levels in *Slco1b2* and *Abcc2* and *Mrp2* in female rats while in male rats no differences were observed. Quantification of CP in serum using a validated LC-MS/MS bioanalytical method showed lower levels of CP-I in *Slco2b1*<sup>-/-</sup> compared to wildtype rats. Furthermore, we investigated *in vitro* transport of CP-III using overexpressing HeLa cells and showed that human and rat orthologues transport OATP2B1 with differences in transport kinetics. In order to understand the cellular handling of CP-III, we identified an interplay between OATP2B1/rOatp2b1 and MRP3/Mrp3. Further studies are warranted to validate CPs as biomarkers of OATP-mediated interactions.

## REFERENCES

1. Bezençon et Al. 2020. DOI: 10.1016/j.xphs.2020.10.017
  2. Ediage et Al. 2018. DOI: 10.1007/s40262-018-0648-3
  3. Bednarczyk et Al. 2016. DOI: 10.3109/00498254.2015.1085111
- Graphics: shutterstock.com, biorender.com